GSI Report
2020-2
December 2020

News and Reports from

High **E**nergy **D**ensity generated by Heavy Ion and Laser Beams

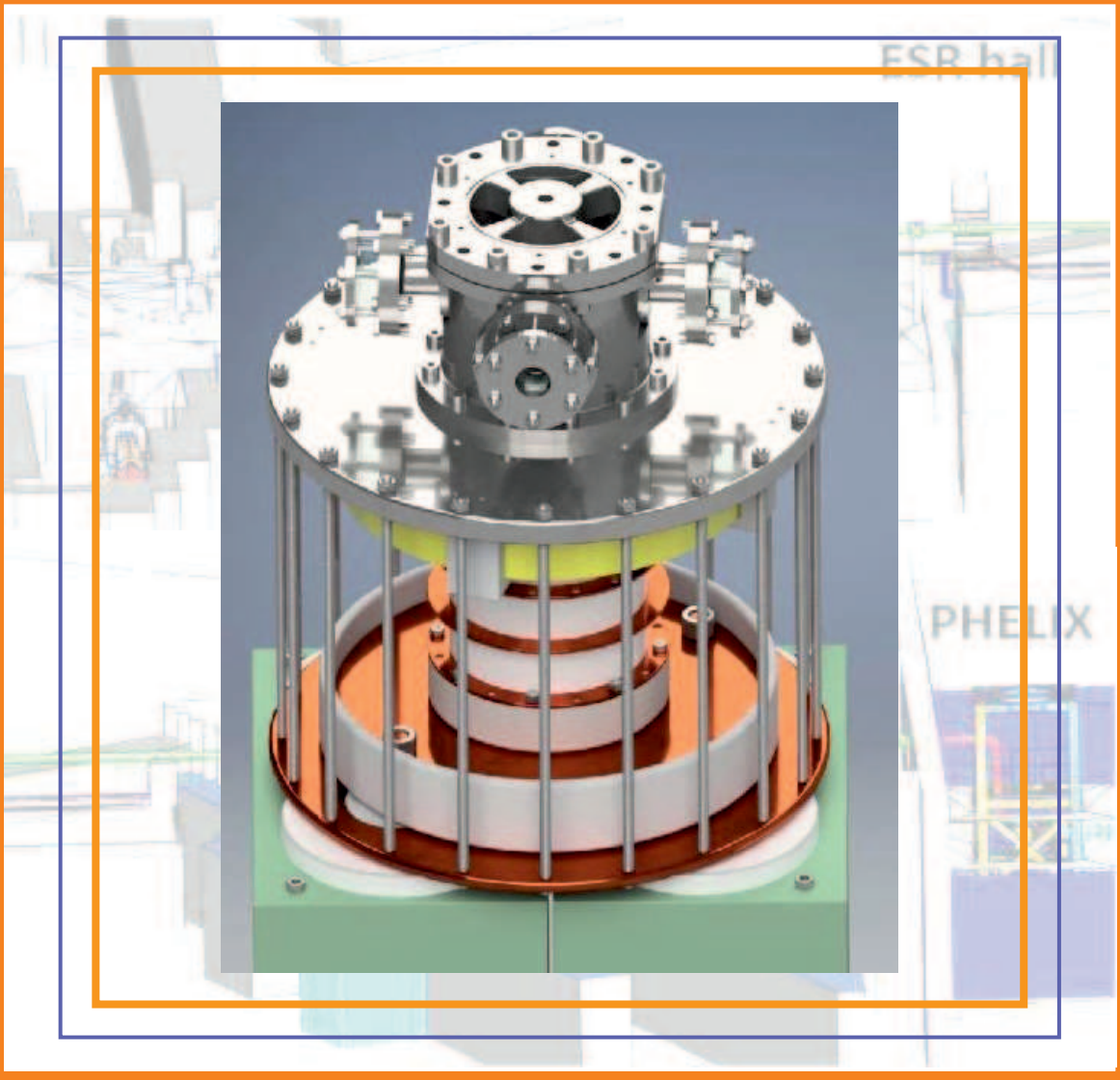

The HED@FAIR Collaboration - Report 2019

The cover picture shows the pulsed-power UEWE device and as background a faded scheme of the new PHELIX laser beamline to HHT.

With this issue of the 'High Energy Density Physics Report' the 40th anniversary of the report series can be celebrated. The first report was published in 1980 in the research program 'Studies on the Feasibility of Heavy Ions Beams for Inertial Confinement Fusion', which was started in 1979 and so also can be considerd as the launching of HEDP research at GSI.

In this report a contribution is included about the history of the report series and the development of HEDP research at GSI in these 40 years, starting with accelerator physics and plasma physics and later extending to laser physics.

With the cover picture of the issue of this report a symbolic bridge shall be spanned from the historical past over the present research in 2019 to the future with the Phase-0 experiments for HEDP at FAIR beginning in 2021. The UEWE pulsed power device (UEWE = Underwater exploding wire experiment) for the PRIOR experimental campaign at HHT in 2021 was built at the university of Frankfurt and was upgraded and improved at GSI in 2019 (find details on the set-up and the planned experiments in the contribution on page 3). The background of the picture is the scheme of the PHELIX laser beamline built to the experimental area HHT for the HIHEX (Heavy Ion Heating and Expansion) experimental campaign, which will start also in 2021. The construction of the beamline began in 2019. Information on the planned experiments can be found on page 1, while the original picture can be found in the HEDP-Report, GSI-Report 2019-2 on page 21. (For the background picture the original picture was folded, so that the beginning of the beamline is shown in the upper left corner and the end at HHT in the lower right corner.)

News and Reports from

High Energy Density generated by Heavy Ion and Laser Beams

2019

December 2020

Imprint

Publishers:

HED@FAIR Collaboration
(https://www.gsi.de/work/forschung/appamml/plasmaphysikphelix/hed_at_fair.htm)

GSI Helmholtzzentrum für Schwerionenforschung GmbH, Darmstadt, Germany (http://www.gsi.de)

GSI is member of the Helmholtz association of national research centers
(http://www.helmholtz.de)

Editors:

Karin Weyrich (k.weyrich@gsi.de)

Dieter H.H. Hoffmann (dhoffmann@ikp.tu-darmstadt.de)

DOI:10.15120/GSI-2020-01321

Contents

Editorial I

Four Decades of the HEDP Annual Report Series and History of 40 Years HEDP at GSI III

1 New Diagnostic Methods and Diagnostic Tools

Laser-driven x-ray diagnostics for heavy-ion heated dense plasmas 1
Zs. Major, L. Geiger, C. Hyland, H. Karadas, M. Metternich, H. Nazary , D. Schumacher, D. Riley, P. Neumayer

Hard X-ray and Proton Radiography of Underwater Electrical Wire Explosion 3
A. *Müller-Münster, C. Hock, M. Iberler, J. Jacoby, P. Neumayer, D. Varentsov*

Time-resolved interferometric diagnostics on a theta-pinch plasma 4
P. Christ , K. Cistakov, M. Fröhlich, R. Gavrilin, F. Heppner, M. Iberler, A. Khurchiev, L. Laghchioua, D. Mann, O. Rosmej, S. Savin, J. Jacoby

Spectroscopic Analysis of Cu X-ray Emission from High Intensity Laser Interaction 5
S. Sander, T. Abel , T. Eberl, D. Hartnagel, M. Hesse, G. Schaumann, M. Šmíd, A. Tebartz, K. Falk, M. Roth

Investigation of shocked water by combination of VISAR and PDV methods 6
K. Gubskiy, T. Kazieva, A. Mikhaylyuk, A. Kuznetsov, V. Pirog, S. Ananiev

Study of Shock Compressibility of Anisotropic Materials Based on Aramid Fibers for Experiments at PRIOR 7
V. Mochalova, A. Utkin

Spectroscopic observation of isolated dense plasma generated through laser driven gold hohlraum radiation 8
Bubo Ma, Jieru Ren, Yongtao Zhao, Zhigang Deng, Wei Qi, Rui Cheng, Xing Wang, Wei Liu, Shuai Yin, Benzheng Chen, Jianhua Feng, Shaoyi Wang, Quanping Fang, Bo Cui, Xingming Zhou, Weimin Zhou, Leifeng Cao

Calibration of Radiochromic Films for Laser-Ion Acceleration Experiments 9
P. Neumayer, A. Blazevic, C. Brabetz, A. Denker, G. Kourkafas

Measurement of magnetic field compression by imploding plasma 10
M. Cvejic, D. Mikitchuk, E. Kroupp, R. Doron, Y.Maron

In-situ imaging and control of intense hard X-ray FEL beams with submicron spatial resolution by means of LiF fluorescence detector 11
T.A. Pikuz, A,Ya. Faenov, S.S. Makarov, N. Ozaki, T. Matsuoka, K. Katagiri, K. Miyanishi, S.A. Pikuz, M. Nishikino, M. Ishino, T. Kawachi, T. Yabuuchi, Y. Inubushi, T. Togashi, Y. Tange, K. Tono, M. Yabashi, A. Grum-Grzhimailo, K.A.Tanaka, I. Skobelev, R. Kodama

2 FAIR related Issues of HED/WDM - Research for Phase-0 and Day-1

Preparations for high energy density experiments at FAIR 13
S. Neff, A. Blazevic

Test Facility for FFS Quadrupoles 14
A. Ageev, A. Kalchuk, A. Kharchenko, E. Kashtanov, S. Kozub, A. Orlov, M. Stoliarov, L. Tkachenko, A. Vlasov

Hydrodynamic Simulation of the Future HED Matter Properties Research Experiments at FAIR 16
V. Kim, D. Nikolaev, I. Lomonosov, V. Mintsev

Construction, characterization and optimization of a plasma window for FAIR, status update 17
A. Michel, B. F. Bohlender, M. Iberler, J. Jacoby

X-Ray Fluorescence Imaging of the Heavy-Ion Beam Distribution on Target at Experiments in Phase-0 and at FAIR 18
S. Zähter, M. Gyrdymov, J. Jacoby, O. Rosmej

The SIS100 laser cooling facility 19
S. Klammes, M. Bussmann, V. Hannen, D. Kiefer, Th. Kühl, X. Ma, P. Spiller, U. Schramm, M. Siebold, Th. Stöhlker, Th. Walther, W. Wen, D. Winters

Temporal coupling of nanometric inhomogeneities in an excited target at the initial stage of a FAIR bunch 20
S. A. Gorbunov, A. E. Volkov

Prototype Quadrupole Chamber with Cryogenic Components 21
S. Aumüller, L. Bozyk, K. Blaum, P. Spiller

3 Interaction of Ion- and Laser Beams with Matter

Contribution of recombination processes to ion beam induced light emission 23
R. Hampf, J. Wieser, A. Ulrich

Research activities at 400 kV High-voltage Ion Beam Platform of Xi'an Jiaotong University 24
Shuai Yin, Wei Liu, Jieru Ren, Bubo Ma, Xing Wang, Benzheng Chen, Jianhua Feng, Yongtao Zhao, Dieter H.H. Hoffmann

Z-Pinch Study with Discharge Initiation by an Electron Beam 25
A. Drozdovsky, P. Sasorov, A. Bogdanov, S. Drozdovsky, R. Gavrilin, A. Kantsyrev, V. Panyushkin, I. Roudskoy, S.Savin

Ablation mode of polymers by nanosecond intense pulsed ion beam 26
X. Yu, S. Zhang, S. Yan, G.E. Remnev, X. Le

Development of Ion Stopping Models for HED Plasmas Using Unified SelfConsistent Field Models and Self-Consistent Electron Distributions 27
T.A. Mehlhorn, I.E. Golovkin

.
New unified model for fast charged particle cross sections, mean free paths, and stopping powers in solids 28
N. Medvedev, A.E. Volkov

Monte Carlo simulation of the energy distribution in laser-irradiated solids under the influence of a magnetic field 29
X. del Arco, J. Amann, M. Schäfer, F. G. Keabou, G. Torosyan, J. A. L'huillier, P. N. Terekhin, B. Rethfeld

Transport of intense particle beams in large scale plasmas 30
B.Z. Chen, D. Wu, J.R. Ren, D.H.H. Hoffmann, Y.T. Zhao

Effects of an additional current on laser heating of silicon 31
S. Hirtle, Y. Kang, G. Torosyan, M. Schäfer, J. A. L'huillier, P. N. Terekhin, B. Rethfeld

Monte-Carlo Simulation of Bremsstrahlung Photon Spectra from 10 µm Au Target Induced by Laser-driven Electron Beams 30
N. Zahn, O. Rosmej, A. Sokolov, M. Gordimov, F. Horst, E. Kozlova, T. Radon, N. Borisenko, J. Jacoby

PIC Simulation of the Directionality of Proton Acceleration in Laser irradiated Micro-Plasma 33
V. Pauw, P. Hilz, H. Ruhl

Studies on Spin Polarization in High Density Degenerate Plasma 34
Punit Kumar, Shiv Singh, Nafees Ahmad

Amplification of a surface electromagnetic wave by running over plasma surface ultrarelativistic electron bunch as a new scheme for generation of Teraherz radiation 37
S. P. Sadykova, A. A. Rukhadze

4 Particle-, Radiation- and Plasma Sources

Improved laser-to-proton conversion efficiency utilizing p-polarization at PHELIX 39
J*. Hornung, Y. Zobus, P. Boller, C. Brabetz, T. Kühl, Zs. Major, M. Zepf, V. Bagnoud*

Recovery of Nanodiamonds Produced by Laser-Induced Shock-Compression of Polystyrene 40
A.K. Schuster, N. J. Hartley, J. Lütgert, K. Voigt, J. Vorberge , M. Zhang, A. Benad, A. Eychmüller, B. Klemmed, D. O. Gericke, A. Rack, V. Bagnoud, A. Blazevic, C. Brabetz, U. Eisenbarth, S. Götte, D. Reemts, D. Schumacher, M. E. Toimil Molares, M. Tomut, D. Kraus

On-line detection of radioactive fission isotopes produced by laser-accelerated protons 41
P. Boller, A.Zylstra, P. Neumayer, L. Bernstein, Ch. Brabetz, J. Despotopulos, J. Glorius, J. Hellmund, E. A. Henry, J. Hornung, J. Jeet, J.Khuyagbaatar, L. Lens, S.

Röder, Th.Stoehlker, A.Yakushev, Y. A. Litvinov, D. Shaughnessy, V. Bagnoud, Th. Kuehl, D.H.G. Schneider
.

Wigner crystals in the bubble regime of wakefield acceleration 42
Lars Reichwein, Alexander Pukhov, Johannes Thomas

Nanostructuring and plasmonics governed by surface plasmon polaritons 43
P. N. Terekhin, P. D. Ndione, S. T. Weber, B. Rethfeld

Application of Geant4 toolkit for modeling of experiments on laser-driven neutron and gamma generation. 44
A. Skobliakov, O. N. Rosmej, M. Gyrdymov, M. M. Günther, P. Tavana, A. Golubev, A. Kantsyrev

Superionic states produced by nonthermal melting in laser spots 45
R.A. Voronkov, N. Medvedev, A.E. Volkov

5 Fusion related Issues of Plasma Physics

A new approach to inertial fusion energy 47
M. Roth, G. Korn, M. von der Linden, P. Shabalin, K.-G. Schlesinger

Experimental scheme for investigation of stopping and fusion reactions initiated by laser-accelerated proton beams in a dense boron plasma 48
Jieru Ren, Yongtao Zhao, Wenqing Wei, Xing Xu, Zhigang Deng, Shaoyi Wang, Quanping Fang, Bubo Ma, Shuai Yin, Xing Wang, Benzheng Chen, Jianhua Feng, Rui Cheng, Dieter H.H. Hoffmann, Weimin Zhou, Leifeng Cao

About Thermal and Non-thermal Ignition of Nuclear Fusion Reactions 49
H. Hora, J. Krasa, D.H.H. Hoffmann, S. Eliezer6 , N. Nissim, J. Kirchhoff, W. McKenzie, G. Kirchhoff, P. Lalousis, G.H. Miley, D. Margarone, A. Picciott , L. Giuffrida, P.G.A. Cirrone, G. Korn, B. Liu, M. Ho

Possible explanations of PXTD-measured reaction histories 51
Zixiang Yan, Wei Kang

Inner screening corrections to the Debye interaction in hot/dense plasmas in the vicinity of the bound - free transitions 52
C. Deutsch, G. Naouri, N.A. Tahir

Author Index 55
List of Participating Institutes 59

Editorial

Dear Colleagues,

this year our traditional annual report starts with a contribution to outline the history of 40 years of this report series and High Energy Density Physics at GSI and the collaborating institutes compiled by Karin Weyrich.

Our last meeting before the Pandemic also reached Europe was in January 2020. After this date personal meetings were hardly possible and also slowed down the preparation of our report and other activities as well. Progress in science is only possible through unlimited exchange of ideas and discussions. To some extent this can be achieved by online meetings. We made the experience, that those who know each other quite well can very well communicate for some time by internet meetings. However, it is extremely difficult to establish new contacts. We all hope that in the near future we will have the opportunity to meet again in Hirschegg and at other conferences. The next conference to come up with possible personal participation is the Physics of Non-ideal Plasma (PNP-17, Dresden 20-24 September).

In the current report, which in a preliminary version is online since the end of December 2020, we have 10 contributions in the first chapter "**New Diagnostic Methods and Diagnostic Tools**". The combination of new facilities – lasers and accelerators – and the development of novel diagnostic techniques are the driving forces of progress in our field. The contributions in this topic show the collaborative results of research teams from Russia, Japan, the UK and Germany.

The second chapter of this report deals with **FAIR related Issues**. While the construction of FAIR shows progress, scientific review committees continuously ask the active collaborations to define the ideas for Phase-0 and Day-One experiments. Over the years the final beam parameters become clearer and the experiments have to adapt accordingly. Phase-0 of HEDP with ion and laser beams at GSI will be carried out mainly at the HHT experimental area (HIHEX, PRIOR). The second chapter also provides information on the status of the preparations for first High Energy Density Experiments at FAIR. Good news we hear about the final test for the superconducting wide-aperture high-gradient quadrupoles, which are an essential part of the final focusing system for HED experiments at FAIR. For the future SIS-100 laser cooling techniques based on a device to cool accelerated heavy-ion beams is described and the SIS-100 will be the first facility to be equipped with. This is a collaboration between a number of institutions in Germany and also the Institute of Modern Physics in Lanzhou, China, which is also the lead institute for the construction of the High Intensity Accelerator Facility in China.

The third chapter of the report deals with the traditional topic of **Interaction of Ion- and Laser Beams with Matter**. - The topic was part of this report series since the early beginning and is still an area of wide activities in experimental and theoretical research. This is also evident from the contributions spread geographically nearly world-wide, reaching from the US over Europe, Russia, India to China.

The fourth chapter deals with **Particle-, Radiation- and Plasma Sources.** High Energy Density Physics depends on reliable and intense sources of radiation and particles. Laser accelerated particle beams have contributed significantly to the progress of this field. Therefore, an improvement of the efficiency to generate intense particle beams is of utmost importance. Significant progress in this aspect has been achieved at the GSI PHELIX facility. These high intensity proton beams also produce radioactive isotopes in sample materials and a detection method for them is described. The production and recovery of nano-diamonds created in laser-induced shock compression was carried in collaboration of institutes from France, the UK and Germany, and is a topic of laboratory astrophysics.

The final chapter of this report deals with **Fusion Related Issues**. In recent years an interest in proton boron fusion came up again. Non-equilibrium processes generated by intense laser radiation give rise to expectations that this fusion reaction may be a promising possible candidate to obtain fusion energy.

We wish all readers and authors of this report a healthy 2021 and hope to meet several of you again in Hirschegg in January 2022.

Dieter H.H. Hoffmann and Karin Weyrich (June 2021)

Four Decades of the HEDP Annual Report Series and History of 40 Years HEDP at GSI

With this issue of the HEDP-Report the 40th anniversary of the report series can be celebrated. The various research fields and the change of the main topics also represent the evolution and the broad spectrum of scientific research in this scientific area at GSI.

1979 - 1989

In 1979 a scientific program for a 'Feasibility Study for Inertial Confinement Fusion' (ICF/IFE) with heavy ion beams was established and funded by the Bundesministerium für Forschung and Technologie (BMFT). Involved in this program were 10 working groups at German research centers and universities, including MPQ Garching, Karlsruhe University and in the state of Hesse the Universities of Frankfurt and Gießen and GSI Darmstadt. The research topics concerned the fields of accelerator research for ICF like beam transport and ion sources, pellet physics and atomic physics of ion-beam-matter interaction. - In 1980 first results at GSI were published in a report under the name 'Studies on the Feasibilty of Heavy Ion Beams for Inertial Confinement Fusion' which was initiated by Prof. Rudolf Bock as scientific editor, summarizing the results of the first year of the research program.

This BMFT-program ended in 1984 and from 1985 on the annual reports in this research field were published under the new name 'High Energy Density in Matter produced by Heavy Ion Beams', presenting results in the three chapters 'Experimental Program', 'Accelerator Research and Development' and 'Target Theory'. Besides accelerator issues, also atomic physics data on energy deposition of ion beams were part of the program but were first only studied with cold matter and ion beams up to 10 MeV/u at the UNILAC. - In the new funding period - starting from 1985 - the research field was labelled under the more general name 'matter at high energy density and its basic research problems` (later called 'high energy density or warm dense matter physics', HED/WDM). Due to the initiative of Prof. R. Bock (Nucl. Phys. I depart. , GSI) in this funding period in a collaboration between the GSI departments Nuclear Physics I and Atomic Physics together with MPQ/Garching research on the interaction of ions with plasmas as new research field was initiated, inspired by first experimental results reported in the USA for protons and deuterons interacting with plasmas. This resulted in the foundation of a plasma physics group and later the new plasma physics department at GSI. A first task was to define and identify possible plasma targets (for example linear discharges with free electron densities in the plasma up to $2\text{-}3*10^{17}$ cm^{-3} and Z-pinchs up to $1.5*10^{19}$ cm^{-3}).

In the second part of the 1980es the topics of the annual report included the research field of IFE driver physics by the RFQ MAXILAC at GSI and ion beam physics and transport accompanying beam interaction experiments with (external) plasma targets. With the new SIS-18/ESR facility at the horizon, completion expected in 1989, with much higher beam-intensities as possible as at the UNILAC the idea of creating plasmas/HED-matter with an intense ion-beam and new diagnostic methods for such plasma states were discussed and developed as well as a plasma lens to focus intense beams. Parallel to this electron cooling of ion beams after pre-studies at the UNILAC, connected to high current injection at IFE drivers, became possible.

And at the ESR first cooled beams enabled high phase-space density and fully stripped ions became possible.

1989- 1999

With the completion of the SIS-18 and the UNILAC-Upgrade after 1990 new research opportunities opened up in plasma/HED physics. Also accelerator issues still connected partly to IFE, like the transfer of energy between SIS-18 and ESR and beam stacking became possible. – The new HED topics explored in the 1990s in the plasma physics department were:

- Creating first samples of HED-Matter with 300 MeV/u ion beams which heated solid targets. This was successfully realized first in 1991 at the new 'High Intensity, High Temperature experimental area' called HHT and was accompanied by the development of diagnostics for beam-induced plasmas. Accumulation of beam pulses in the ESR, which was available after 1991 helped to increase the intensity at HHT.
- Plasma lenses (wall-stabilized discharges for example) to focus ion beams to small focal spots, to deposit high energy in small volumes, were developed and employed at HHT as final focusing system, operating with 300 MeV/u ion beams, and focal spots of 2 mm could be realized.
- Another new research field entered the report from the mid-1990s on, laser-matter-interaction, with the installation of a Nd:glass laser system at the UNILAC at Z6, which was completed in 1996. The nhelix laser could deliver beam pulses up to 100 J in 15 ns producing high-power, high-density plasmas around 10^{20} free electrons/cm^{-3} by irradiating thin foils. -

A stronger laser system, called PHELIX, was already discussed in the last three years before the year 2000 and supposed to be realized and deliver first beams after 2001.

- Capillary discharge plasmas were also a new research topic and installed at the at Z4 experimental area beside the Z6 experimental area.
- Converter targets for indirect drive were investigated, which demanded higher energy deposition in the target to produce homogenous X-ray radiation in the converter for the compression of the target by increased beam energies and transfer efficiency of the driver systems.

In the second half of the 1990s a new accelerator facility with very intense ion beams appeared already at the horizon and new experimental schemes started to be discussed. In 1996 a study group of six working groups was founded to investigate and discuss the long-range perspectives of GSI. As a result a paper on a new research facility (later called FAIR) was published and reported on in the 1997 issue of the HEDP-report, and soon research dedicated to these new topics became part of the report series. The impact of the new accelerator facility in the research field of 'Dense Plasmas and Inertial Fusion' was emphasized. It was also recommended to include a high-intensity femtosecond laser facility (a petawatt laser) in the new accelerator facility. In 1998 the decision to build such a laser facility was made and a laser named PHELIX was supposed to deliver first beams in the next years (2001).

1999-2009

With the beginning of the new millennium new aspects and research topics became part of the annual HEDP report series. Now D.H.H. Hoffmann took over the responsibility as scientific editor of the report from Rudolf Bock.

And as already emphasized in the report issues after 1997, the aspect of energy generation by inertial fusion retreated behind the aspects of basic research. Laboratory planetary- and astrophysics, atomic physics or solid-state physics became more important in this research field and were reflected in the issues from 2000 on with new topics and a growing community of contributing institutes to the report with new authors from Russia, Japan, Spain, Italy, which was also supported by the process of declassification in the middle of the 1990s and a following exchange of information between Russia and the USA.

With the decision to build the new petawatt laser system PHELIX the number of contributions with topics in laser physics increased strongly in the next years, and lead to a change of the title of the report into 'High Energy Density Physics with Heavy Ion and Laser Beams' from the 2002 issue on. Chapter 1 'The Experimental Program' was extended by a section 'Laser Plasma Physics' including contributions on the PHELIX laser project. With the good progress in the next years a new chapter on 'Laser Physics with PHELIX' was added, reporting on commissioning of the main amplifier in 2003 and a first experiment demonstrating a collisionaly excited X-ray laser in zirconium at a wavelength of 22 nm. First results on laser plasmas produced with intense laser beams as sources of particle radiation (electrons, protons, even heavy ions) were discussed in 2004 and 2005 as well as the possibility to inject such beams in conventional accelerator structures by pulsed power devices. The high-light of the 2008 report were the first combined laser-ion experiments, where a C-foil was simultaneously heated from one side with the nhelix laser beam and from the other side with the PHELIX-laser beam (both with 50 J in 6 ns) while an interacting 3.6 MeV/u Si-ion beam diagnosed the expanding C-plasma. This successful experiment at the Z6 experimental area was also chosen as the title picture of the 2008 issue of the report. It was the starting point for several experiments in the following years with international participation using combined interaction of UNILAC ion- and PHELIX laser beams. - Until the X-FEL facility was completed, GSI was the only research facility where experiments combining ion beams and intense laser beams to produce and diagnose plasmas in the WDM/HEDM regime was possible.

Meanwhile the HED/WDM physics research at HHT also made progress, the new final focusing system was installed. In 2002 first tests with U-beams from the SIS-18 for studying stopping ranges, EOS in lead and other solid targets and for investigating isochoric heating were carried out. Pyrometry as diagnostic was developed and tested in an experimental campaign 2003. Other diagnostic methods like contactless resistivity, interferometric velocity measurements or BIF (beam induced fluorescence) were further developed. In 2005 the intensities at the SIS-18 reached already $5*10^9$ particles for U^{73+} in a 110 ns pulse (300 μm beam spot). With these good intensities of the 200 – 400 MeV/u Uranium beams at HHT now WDM/HED matter experiments reaching 2 eV and several kJ/g with pressures in the multi-kilobar range in different metallic targets could be realized in 2007.

Besides the laser experiments and these at HHT also at Z6 new research topics were carried out and reported in the HEDP-report in the first decade of the new millennium:

- Plasma spectroscopy was a special topic in the 2005 issue of the report with an own section in chapter 1.
- Also new detector techniques were pursued for ion beam interaction with matter, diamond detectors or detectors for X-ray spectroscopy.
- Ion-beam interaction experiments at Z6 with new target types continued using foam and aerogel targets as well as shock-compressed gas targets driven by HE (high explosives) to create non-ideal plasmas
- Stopping power experienced a renaissance in this time in laser produced plasmas with the nhelix laser and foil- or hohlraum targets at Z6 in 2007 and 2008.

At the end of the first decade of the new millennium in 2009 the new accelerator project FAIR started with the partner states signing at GSI the FAIR convention. This was also the year of the 30th anniversary after HED/WDM physics research at GSI and the start of this report series with the feasibility study for ion beams as ICF drivers.

2009 -2019

After this official start of the FAIR project now the main emphasis of the contributions to the HEDP report concentrated on topics relevant for the HED/WDM physics research program at FAIR, which would be carried out with the collaborating institutes in the HEDgeHOB collaboration. All collaborating institutes were invited to participate with contributions at the annual report, but also groups feeling related to the HEDP topics and plasma physics as well.

For the year 2010 highlights could be presented in the report. The PHELIX laser operated routinely very well with a large number of experiments (heating of foams and hohlraum targets, laser acceleration of particle beams). And also in 2010 the PRIOR Project (Proton Microscopy to probe dense dynamic objects with monoenergetic protons in the GeV regime) was launched as diagnostic at HHT, while the SIS-18 U^{28+} -beams at HHT were improved up to 10^{10} ions/pulse.

Even if the HEDP-reports in the last years had demonstrated a broad spectrum of research at GSI and in the collaborating institutes related to the HED/WDM research field, the 2011 issue suddenly appeared to be the last. The concentration of GSI on building FAIR brought changes for the GSI departments, research departments were merged for a certain time-span with the accelerator department and basic research fell back behind organizational issues.

Between 2012 and 2014 no new issue of the HEDP-report was published. In 2015 the insight came, that after three years the annual report was missing as an overview on the many topics of research of the HEDgeHOB collaboration and associated research groups in the HEDP community, especially with many new collaborators. So in summer 2015 with a 2-years-report summarizing the years 2013/14 of HEDP-research the report was restarted under the new title ‘News and Reports from **H**igh **E**nergy **D**ensity **ge**nerated by **H**eavy I**o**n and Laser **B**eams’ as the report of the HEDgeHOB collaboration, and the first cover picture showed a view of the construction site of the new FAIR facility to indicate where the research path shall lead.

The report we restructured, with the first chapter now dedicated to reports on HEDP facilities of the collaborators built worldwide like NIF, NICA, HIAF, NDCX-II, Kumgang and Petal laser facilities and research directed to FAIR applications like plasma window (pulsed power option) or the design of Phase-0 and Day-One HEDP-experiments at FAIR (HIHEX, proton microscopy). The report concentrated now on results, activities and conference reports and presenting the statistic appendices like published papers, conference contributions and thesis was skipped.

Highlights of this two years report and the following reports were development of X-ray backlighting techniques, ion acceleration at PHELIX with new cryogenic targets and the LIGHT project for creating laser-driven sub-nanosecond bunches of proton and ion beams. Another highlight was the commissioning of the PRIOR proton microscope (PRIOR-I with permanent magnetic quadrupoles) at HHT and extending at Z6 the measurement of the energy loss of ions to dense but weakly-coupled plasma targets. Even if GSI researchers had to put their efforts on the realization of FAIR the research spectrum was still broad, while also between 2016 and 2018 due to the modification of the UNILAC and the SIS-18 upgrade ion beam-time was not available. The experimental program at PHELIX could go on unaffected.

In 2017 the HEDP collaboration reorganized under the new name HED@FAIR which led to the new subtitle of the report 'The HED@FAIR collaboration – Report 20xx'and it was decided to dedicate the first chapter now to a special topic. 'New Diagnostic Methods and Tools' was chosen as the special topic for chapter 1, because development of diagnostics for HED matter is crucial for all Phase-0 and Day-One experiments. And as a second change from the 2018 issue on was merging the theory chapter with the others and presenting experimental contributions and theoretical contributions of the same topic together in the respective chapter, for both complement each other.

High-lights of the last published issue 2018 (as well as the current one) were contributions on determining ion temperature in HED plasmas with the Stark effect, neutron generation with high-intensity lasers and of course the construction of the new PHELIX beam-line to HHT for HIHEX experiments as well as the design of the PRIOR-II set-up with electro-magnetic quadrupoles at HHT including the UEWE target (underwater exploding wire experiment), defining HHT as experimental area for FAIR Phase-0 experiments.

And recently - somehow like closing a circle - a new chapter in the annual report on **Fusion Related Issues** of plasma physics was introduced (taking into account current interest in research on p-^{11}B-fusion) after the report series was once initiated 1980 by the former BMFT program 'Feasibility of Heavy Ions for Inertial Confinement Fusion'.

The various changes in its title during the years and the newly introduced topics over the decades show how broad and complex this research field has evolved in the last 40 years, reflecting the various aspects of HEDP. It should not be concealed, that the here presented scientific topics concentrate on the development of the research fields at GSI. In the many institutes and research groups contributing from outside GSI to the report series over the years a much broader spectrum of HEDP research was represented and the editors are grateful for

this international input. – Find in the pictures below examples of the report covers with the changing titles over the years.

Karin Weyrich

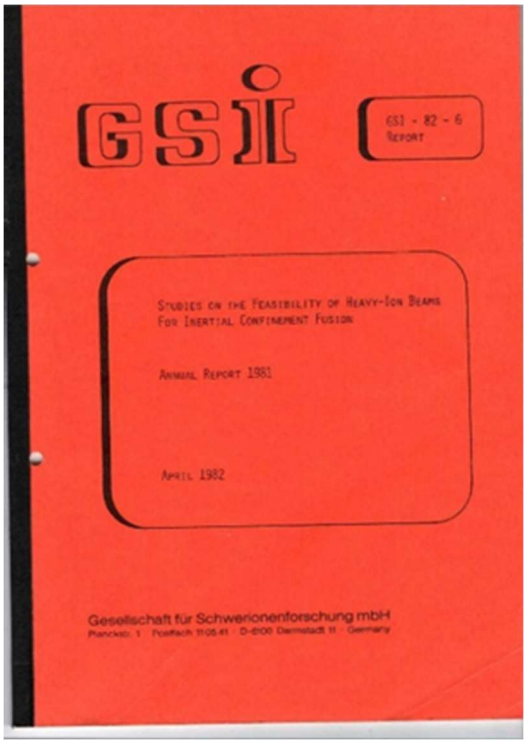

Cover 1981

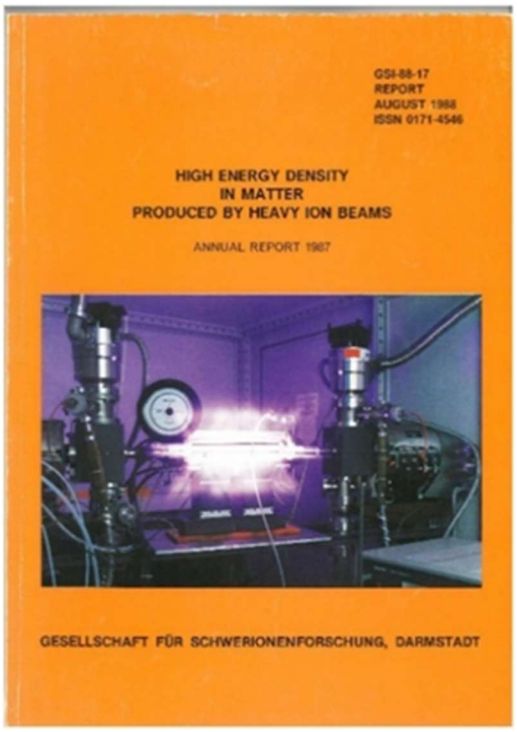

Cover 1987

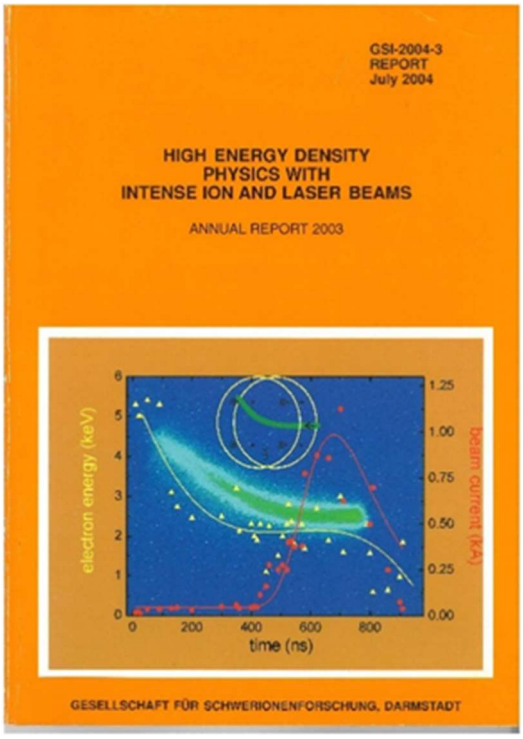

Cover 2003

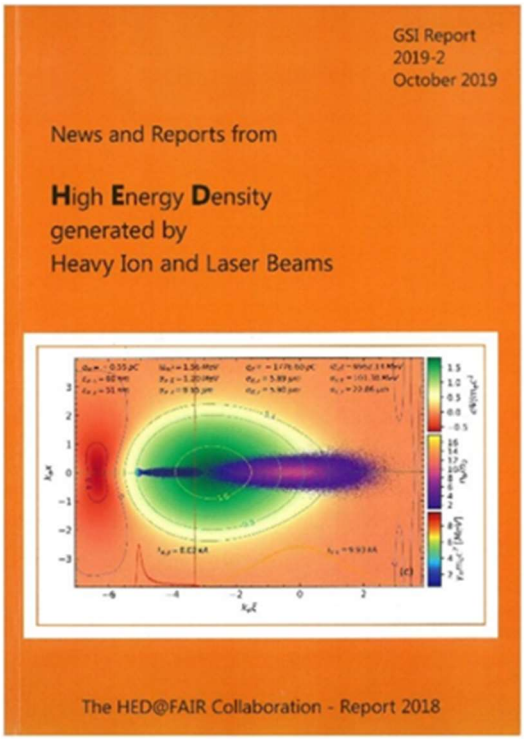

Cover 2018

1 New Diagnostic Methods and Diagnostic Tools

Laser-driven x-ray diagnostics for heavy-ion heated dense plasmas

Zs. Major[1,2], L. Geiger[3], C. Hyland[4], H. Karadas[3], M. Metternich[5], H. Nazary[5], D. Schumacher[1], D. Riley[4] and P. Neumayer[1]

[1]GSI, Darmstadt, Germany; [2]HI Jena, Germany; [2]Goethe Univ. Frankfurt, Germany; [3]Queen's Univ. Belfast, UK; [4]TU Darmstadt, Germany

The internal upgrade project to construct a high-energy laser beamline from the PHELIX facility to the HHT cave behind the SIS18 is well underway [1], with first laser pulses on target expected towards the end of 2020. Upon completion, laser pulses with energies up to 200 J at the second harmonic (wavelength 527 nm) with nanosecond duration will become available at this experimental station. These will allow to drive intense x-ray sources based on laser-produced plasmas, which will enable state-of-the-art x-ray probing techniques commonly used at high-energy density facilities worldwide, and which are consequently foreseen as diagnostics for dense plasmas produced with intense heavy-ion pulses at FAIR.

In order to verify the performance of such laser-driven x-ray sources with the laser parameters projected for the HHT-cave, and to demonstrate their suitability for the foreseen diagnostic applications we have performed an experiment at the Z6 experimental area. Laser pulses from both the nhelix and the PHELIX laser systems were used, with pulse energies up to 40 J (in 8 ns) and 160 J (in 1 ns), respectively. Focused down to spot sizes of approx. 50 µm these yield intensities from 10^{14} to $6\text{x}10^{15}$ W/cm^2. A variety of mid- to high-Z targets were irradiated, producing hot (few keV) highly-charged plasmas. X-ray emission spectra were recorded by two crystal spectrometers, while the x-ray source size was measured by means of a pinhole camera.

A dual-channel focusing spectrometer based on two conically curved KAP-crystals (developed in collaboration with the university Jena) measured the x-ray emission in the spectral range around 1.6 keV. In this range, targets made from rare earth elements (Sm, Dy, Yb) exhibit strong M-band emission. The high density of emission lines results in a near continuous emission spectrum, suitable for x-ray absorption spectroscopy. As an example, fig. 1 a) shows a single-shot high-resolution absorption spectrum through a 5 µm thick aluminum foil in the vicinity of the Al K-edge. This XANES (X-ray Absorption Near Edge Spectroscopy) technique has a high diagnostic potential and can be used to infer electron temperatures in samples at warm-dense matter conditions, detect edge shifts and shell rebinding, and is sensitive to the local ionic structure [2].

The second spectrometer employing a highly-oriented pyrolytic graphite crystal covered the spectral range 4…9 keV, measuring the strong line emission from Helium-like ions from mid-Z metal targets (Ti, Fe, Ni, Cu). The x-ray yield into this line radiation increases strongly with laser intensity, with a more than 1000-fold increase from the lowest (nhelix) to the highest (PHELIX) energy laser pulses, underlining the need for high-energy laser pulses to efficiently drive these x-ray sources. At the highest intensities the conversion efficiency (laser to x-ray energy) reaches values of nearly 10^{-3}, yielding up to 10^{14} photons at 4.5 keV. A prominent diagnostic application of such intense narrow-band x-ray sources is x-ray diffraction, fig. 1b showing as an example the Debye-Scherrer rings from a 5 µm thick iron foil. For heavy-ion heated targets diffraction will allow to measure changes of the lattice constant due to thermal expansion, observe solid-solid phase transitions [3] and indicate melting. Furthermore, the diffracted intensity can be related to the lattice temperature via the Debye-Waller-factor.

The pinhole camera employed a 25 µm diameter high-Z pinhole, filtering was chosen to image x-ray energies > 4 keV. X-ray source sizes between 50 and 150 µm were

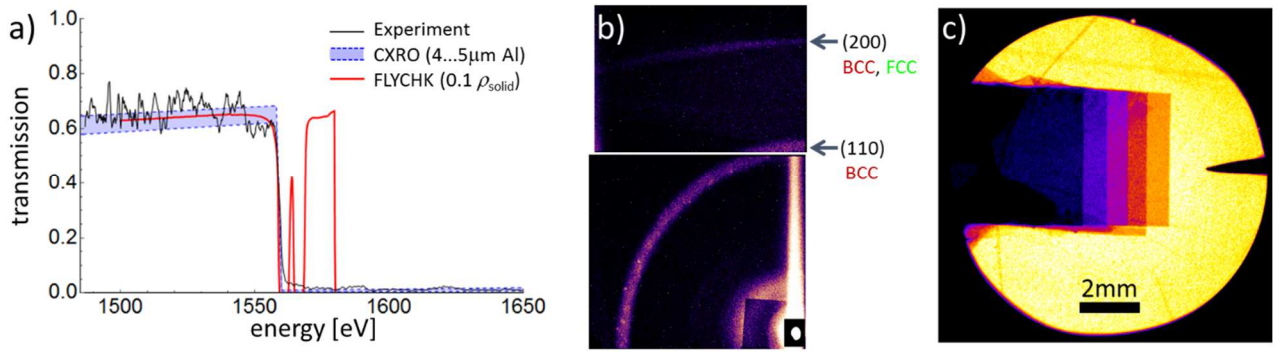

Figure 1: (a) Transmission spectrum around the Al K-edge. Measurements on an Al-sample at ambient conditions (black) sample (red, FLYCHK [5]). (b) X-ray diffraction rings obtained from a Fe-foil. (c) X-ray image of plastic foil stack and steel needle.

measured, with a tendency to larger sizes at higher laser energies. A small source allows for point-projection x-ray imaging as was also experimentally demonstrated with using a test target (cf. fig. 1c). Radiographic imaging of heavy-ion driven samples would allow to observe evaporation and isentropic expansion, interface movement as a heavy material pushes into a lighter tamper, or fracture and spallation events.

In summary, our proof-of-principle experiments demonstrate the feasibility of using the long-pulse mode of PHELIX to drive an x-rays source suitable for x-ray diffraction, absorption and imaging techniques. Our results on cold test samples show the potential of this laser-driven x-ray source for the investigation of heavy-ion heated states of matter.

References

[1] Zs. Major et al., HED-Report, GSI Report 2019-2, 21 (2019).

[2] F. Dorchies & V. Recoules, Phys. Rep. **657**, 1 (2016)

[3] D. H. Kalantar et al., PRL **95**, 075502 (2005)

[4] B. L. Henke et al., At. Data Nucl. Data Tables **54**, 181 (1993).

[5] H.-K. Chung et al., High En. Dens. Phys. **1**, 3 (2005).

Hard X-ray and Proton Radiography of Underwater Electrical Wire Explosion

A. Müller-Münster*[1], C. Hock[1], M. Iberler[1], J. Jacoby[1], P. Neumayer[2], D. Varentsov[2]
[1]Goethe University Frankfurt, Germany
[2]GSI, Darmstadt, Germany

By the use of Underwater Electrical Wire Explosion (UEWE) one can create and study warm dense matter (WDM) in laboratory. With a moderate pulsed power generator (see Fig. 1), with a total Capacity of 10µF, charging voltages up to 40kV, cylindrical strip line and a thyratron as switch, it is possible to create dense plasmas with 10-100 kJ/g specific energy, near-solid density and several eV temperature. Due to the high electric breakdown threshold of purified water (>300 kV/cm) and relatively small wire expansion velocity (~ 1km/s) there's no parasitic plasma formation along the wire surface. This makes UEWE an efficient method to study the fundamental properties of metals in extreme states [1-8].

One of the main challenges is the determination of plasma parameters and especially the temporally and spatially resolved measurements of the target density. Few keV x-rays, which are often used for radiography of thin tungsten wires exploding in vacuum [9], are not suitable for UEWE experiments. For the radiography of an opaque exploding wire in water one needs unique techniques like high energy x-rays (created@PHELIX) or charged particles (PRIOR), which are able to penetrate the surrounding water and the windows of the target chamber too. During the commissioning of PRIOR-II, which will employ radiation-resistant normal-conducting electromagnets, UEWE will be the first dynamic target. An accepted proposal foresees to use PHELIX to drive a short-pulsed hard x-ray source. Synthetic radiographs obtained from raytracing simulations, based on measurements of the hard x-ray yield and spectra, show that accurate density measurements of the expanding wire should be possible. The planned measurements will shed new light on the properties of matter under extreme conditions and will finally allow to access the EOS data of warm dense matter. So far UEWE experiments have not succeeded in measuring the density distribution of the exploding wire with sufficient accuracy. Thus the majority of all the EOS and conductivity data obtained in the numerous UEWE experiments during the past four decades rely on the assumption of the radial uniformity of the density distribution during the whole course of wire explosion. On the other hand, there're clear theoretical and numerical indications showing that the assumption of radial uniformity does not hold [4,7,9].

Therefore the question of uniformity of liquid metal in near critical state, formed by rapid ohmic heating in water bath still remains open.

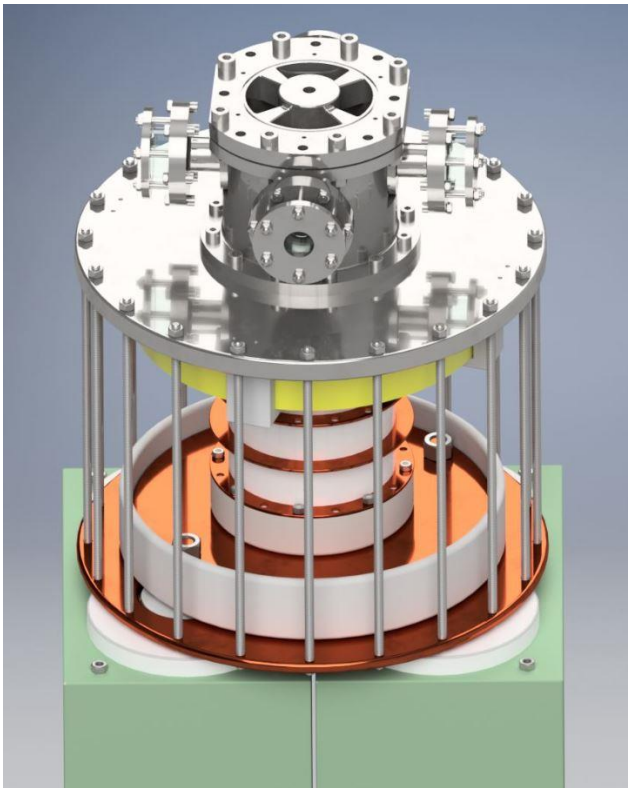

Figure 1: Setup for UEWE. Cylindrical strip line with thyratron in the centre and target chamber, which contains "exploding" wire, on top.

References

[1] M.M. Martynyuk Sov. Phys.-Tech. Phys. 17 (1972) 148.
[2] U. Seydel et al., Z. Nuturf. 30a (1975) 1166.
[3] A.W. DeSilva and J.D. Katsouros, Phys. Rev. E 57 (1998) 5945.
[4] A. Grinenko et al., Phys. Rev. E 72 (2005) 066401.
[5] T. Sasaki et al., Laser and Par. Beams 24 (2006) 371.
[6] A.W. DeSilva at al., Phys. Rev. E 83 (2011) 037402.
[7] D. Sheftman et al., Phys. Plasmas 18 (2011) 092704.
[8] Y.E. Krasik et al., IEEE Trans. Plasma Sci. 44 (2016) 412.
[9] T.A. Shelkovenko et al., Plasma Phys. Rep. 42 (2016) 226.

*Mueller-Muenster@iap.uni-frankfurt.de

Time-resolved interferometric diagnostics on a theta-pinch plasma*

P. Christ[1], *K. Cistakov*[1], *M. Fröhlich*[1], *R. Gavrilin*[3], *F. Heppner*[1], *M. Iberler*[1], *A. Khurchiev*[3], *L. Laghchioua*[1], *D. Mann*[1], *O. Rosmej*[2], *S. Savin*[3], *and J. Jacoby*[1]

[1]Goethe University, Frankfurt, Germany; [2]GSI, Darmstadt, Germany; [3]ITEP, Moscow, Russia

The theta-pinch in this experiment is a resonant circuit having a frequency of 10.5 kHz and consisting of a coil of 7.6 µH inductance, a capacitor bank of 30 µF capacitance and a thyratron switch as main components. When the theta-pinch is fired, up to 6 kJ stored energy from the capacitor bank is released producing a current of up to 40 kA. Inside the coil, a 4 l vessel filled with hydrogen gas of around 0.5 mbar pressure is exposed to the alternating magnetic field. Consequently, energy is inductively coupled into the gas by accelerating free electrons and a plasma is formed by collisional ionisation. Due to the induced azimuthal plasma current and the external magnetic field, the plasma is pinched to the coil axis by Lorentz-force and a high electron density is achieved.

Because of the time-dependent nature of the plasma parameters in an oscillating theta-pinch, spectroscopic diagnostics are often challenging or less accurate. To overcome this issue, an interferometric approach is in development. In a plasma, the interferometer is able to detect the integrated change of the refractive index along the line of sight in the form of a phase shift being directly connected to the integrated free and bound electrons densities present [1]. Figure 1 shows the current single wavelength set-up. The key part of this set-up is an acousto-optic modulator, which introduces a frequency shift to the reference beam. Interference of coherent beams with different frequencies leads to a beat signal on the detector. Moreover, the beat signal is carrying the plasma phase shift, which is extracted by an I/Q-demodulator by using a stationary reference signal.

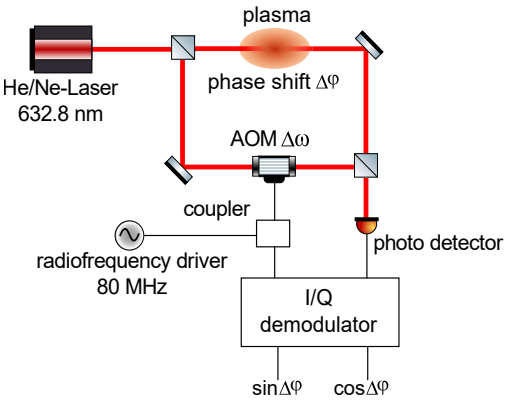

Figure 1: Interferometric set-up

Concerning the whole set-up, first diagnostic results have been obtained. These show, that up to 40 % of the stored energy can be coupled into the plasma, which is an increase of 20 pp compared to a previous set-up. Furthermore, the H_β-line has been recorded for an averaged electron density measurement along the coil axis. The results for a 0.4 mbar, 18 kV discharge using the Stark-broadening of the line width and a peak separation method according to [2] are shown in figure 2. Additionally, a very preliminary single wavelength interferometric measurement of the line integrated density for these conditions is also displayed. The error of the Stark-broadening

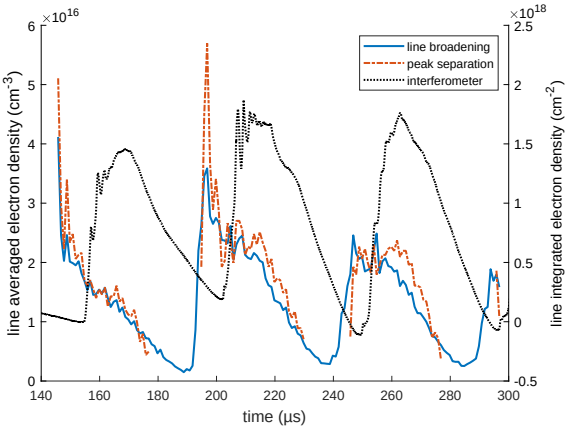

Figure 2: Diagnostic results

method should be around 10 %, but the error of the peak separation method is still under evaluation. It involves not only the error given in [2], but also variations coming from the smoothing of the noisy signal for extracting the peaks.

Future upgrades of this set-up will mainly consist of the introduction of a second wavelength making it possible to remove the error from neglecting bound electrons, e.g. negative integrated values in figure 2, and to determine the neutral gas density directly, which leads to an ionisation degree measurement.

References

[1] R. A. Alpher and D. R. White. In: Plasma Diagnostic Techniques. Academic Press, 1965

[2] D. Surmick and C. Parigger. International Review of Atomic and Molecular Physics, 5 (2), 2014.

* Work supported by GSI, HIC4FAIR, HGSHIRe

Spectroscopic Analysis of Cu □-ray Emission from □igh Intensity Laser Interaction

S. Sander[1,#], T. Abel[1], T. Ebert[1], D. Hartnagel[1], M. Hesse[1], G. Schaumann[1], M. Šmíd[2], A. Tebartz[1], K. Falk[2] and M. Roth[1]

[1]Technische Universität Darmstadt, Fachbereich Physik, Darmstadt, Germany; [2]HZDR, Dresden, Germany

Motivation

X-rays have widely been used to diagnose plasma experiments, either by some form of indirect observation (i. e. absorption spectroscopy or scattering experiments) or by direct characterization of the emission through spectroscopic methods [1,2]. The latter can help in understanding the plasma states achieved during the laser matter interaction and thus guide the development of targets towards higher yield backlighters.

Experimental Setup

The here presented spectrum was observed at the PHELIX laser system during an experimental campaign in February 2019. The PHELIX short pulse laser with a pulse length of 500 fs and an energy of 180 J was focused with an incident angle of 15° to best focus with a 45° off axis parabola to achieve intensities of around 5×10^{20} W/cm□. The target consisted of a flat copper foil with a thickness of 10 µm.

The X-ray emission was diagnosed on the target backside with a crystal spectrometer. A flat HOPG crystal was used as the dispersive element and the setup was chosen such that a large spectral range between 8 keV and 9 keV was covered. The spectra were recorded on imaging plates.

Spectroscopic Procedure

To determine the density and temperature of the plasma the collisional-radiative code FlyChk was used [3].

The first step is to calculate the distribution of ionization states, which mainly depends on density and temperature. Then, this distribution can be used to estimate the emission spectrum from tabulated electronic transitions. Additional parameters such as the opacity thickness or a secondary hot electron component can be included. As the parameter space increases, the limitations of this method become apparent and comparison between multiple codes and further simulations have to be done.

In addition, the experimental spectrum is time and spatially integrated. This results in combinations of multiple temperatures and densities that contribute to the spectrum.

Results

The experimental and synthetic spectra are displayed in figure 1. The experimental spectrum shows three main emission channels. Most peaks correspond to the 2p-1s transition for various ionization states: at approximately 8 keV the K_α-, around 8.4 keV the He_α- and at 8.7 keV the Ly_α-transition. Additionally, the 3p-1s transition is observed around 8.9 keV.

The Kα peak originates from a cold region of the plasma and is best described with an electron temperature

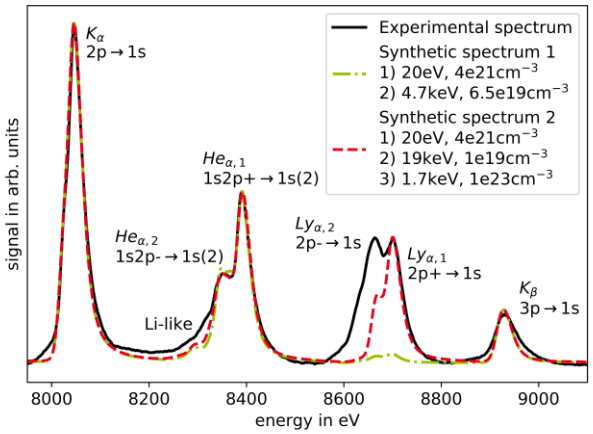

Figure 1: Experimental (continuous) and synthetic (dashed) spectra of X-ray emission from a pure copper flat foil. The synthetic spectra are derived from a sum of multiple temperatures and densities.

of 20 eV and an electron density of 4×10^{21} cm^{-3}. This also describes the K_β-peak reasonably well. The He_α and Ly_α peaks correspond to higher ionization states and thus a higher temperature. Two different plasma states are presented here to replicate the He_α peak. The first uses a single temperature of 4.7 keV and density of 6.5×10^{19} cm^{-3} to model the H e_α peak. The Ly_α peak is how-ever not represented. The second plasma state uses a high temperature of 19 keV and low density of 10^{19} cm^{-3}, which constitutes most of the $He_{\alpha,1}$- and $Ly_{\alpha,1}$-peak emission. However, the Li-like peak and the emission corresponding to negative spin-orbitals are not well replicated. An additional spectrum corresponding to a temperature of 1.7 keV and density of 10^{23} cm^{-3} is used to replicate the emission around 8.3 keV. This shows the limits, as multiple plasma states can be found to describe experimentally observed emission spectra and further studies must be done to derive temperatures and densities with reasonable certainty. In addition, the $Ly_{\alpha,2}$ peak could not be reproduced as part of the synthetic spectrum. The emission is exceptionally high in the experimentally observed spectrum and further analysis must be done to explain this behaviour.

References

[1] F. Dorchies et al., Phys. Rev. B □**2**, 085117 (2015).
[2] S. Glenzer and R. Redmer, Rev. Mod. Phys. **81**, 1625 (2009).
[3] H.-K. Chung et al., High Energ. Dens. Phys. **1**, 3 (2005).

#ssander@ikp.tu-darmstadt.de

Investigation of shoc□ed □ater by combination of □ISAR and P□□ methods

K. Gubskiy[1,3], T. Kazieva[1,3], A. Mikhaylyuk[1,3], A. Kuznetsov[1], V. Pirog[1,3] and S. Ananiev[2]

[1]National Research Nuclear University MEPhI (Moscow Engineering Physics Institute), Moscow, Russia
[2]Joint Institute for High Temperatures of the Russian Academy of Sciences, Moscow, Russia
[3]Limited Liability Company "Laser Eye", Moscow, Russia

The paper proposes a method for combining Photon Doppler Velocimetry and Velocity Interferometer System for Any Reflector, which allows to study transpar-ent materials in shock-wave experiments without using of additional reflective surfaces. The paper presents experiment results on a shock wave propagation in water. In this experiment, water was an absorber, however, the proposed method would also be useful provided that the test material is transparent, but provides reflection.

Some of the most popular methods for studying a material in an extreme state are unequal arm interferometry (ve-locity interferometer system for any reflector (VISAR)) [1] and photon doppler velocimetry (PDV) [2].

Despite the fact that these methods are both enable velocity measurements in a similar range, there are certain experiments where their combination allows obtaining additional information about the state of the shock-loaded substance.

For example, the interferometric studies of the strength of liquids under pulsed tension and compression require a thin layer of reflective material (for example, aluminium foil) is placed on the surface of transparent test substances when assembling the targets [3]. This may lead to ambiguous results or different interpretations of experimental data.

In this paper we propose a method that allows investigating materials with low reflectance in visible or near-IR range. To demonstrate the capabilities of this method, the experiment was carried out to study the shock wave propagation through water. In this experiment, PDV and VISAR methods were used together. The experimental setup is shown in figure 1.

In this work measuring systems KDNI-532-7 [4] (imple-mented using the VISAR method) and KIVI [5] (imple-mented using the PDV method) were used. KDNI-532-7 is a Vernier system consists of two doppler interferometers with 1280 m/s/fringe and 280 m/s/fringe interferometer constants. KIVI is a PDV system with a frequency band-width of 10 GHz. For target illumination KDNI-532-7 uses 532 nm laser light, while KIVI uses 1550 nm. Both devices have fiber-optic routes to deliver light to a target and back to signal processing units (figure 1).

The absorption coefficient of the light used in PDV (1550 nm) in water is 6.8 cm^{-1}, therefore, the reflection recorded by the PDV system corresponds to the reflection only by the water surface (reflection coefficient is 4%). VISAR laser light (532 nm) passes through water and is reflected by the metal surface. The plot (figure 2) shows time stamps when the metal surface begins to move (apx. 21 μs) and when the shock wave reaches the water surface after about 2 μs (PDV measurement starts).

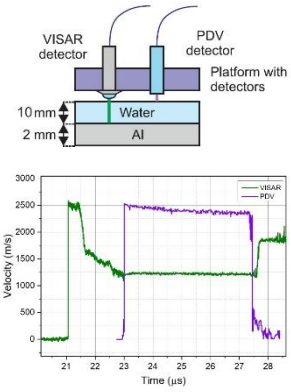

Figure 1. The scheme of the shock-wave experiment with KDNI

Figure 2. Mass velocity profiles obtained using KDNI and KIVI

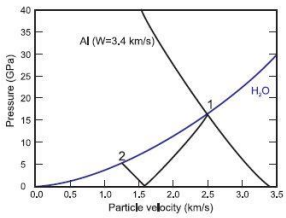

Figure 3. Shock adia-bats of aluminium and water.

When the shock wave leaves the aluminum plate to the water, state 1 is realized (figure 3). After about 0.5 μs, an unloading wave arrives at the boundary from the impactor free surface. In this case, velocity falls more than 1 km/s (state 2).

Proposed method expands possibilities of doppler interferometry in investigating of liquid and solid transparent samples and can be adapted for experiments with laser and heavy ion drivers.

References

[1] L. Barker and R. Hollenbach J. Appl. Phys. 1972, 43(11). P. 4669.
[2] G. Kanel, V. Fortov and S. Razorenov Phys.–Usp. 2007. 177. №8. P. 209.
[3] A. Bogach and A. Utkin J. Appl. Mech. Tech. Phys. 2000. 41. 752-8
[4] D.Koshkin, K. Gubskiy, A. Mikhailuk, A. Kuznetsov, Proc. SPIE 2015, 9442
[5] M. Gorbashova et al J. Phys.: Conf. Ser. 2017. 941.209

Study of Shock Compressibility of Anisotropic Materials Based on Aramid Fibers for Experiments at PRIOR*

V. Mochalova#, A. Utkin
Institute of Problems of Chemical Physics RAS, Chernogolovka, Russia

In this work, the experiments on developing of targets, study of the structure of compression pulse and shock wave velocity and the determination of Hugoniot parameters were performed for two anisotropic materials (textolite and kevlar) based on aramid fibers. The goal of this study is development of targets for experiments at a novel diagnostic system proton microscope (PRIOR) at the TU Darmstadt. Textolite and kevlar were made using the same epoxy resin and aramid fibers, but had a different structure - unidirectional fibers and plies of woven fibers, respectively. The density of these materials is approximately 1.27 g/cm^3. For both materials, the character diameter of the fibers is about 10 μm, and their volume fraction in the composites is approximately 60 - 62%.

To study the shock wave compressibility of materials under high pressure, the explosive propellant charges were used. Shock waves in investigated composites were initiated by aluminum impactors, accelerated by explosion products to velocities W from 1.1 to 3.3 km/s. The samples were loaded through base plates made from aluminum or copper. To reflect a laser beam, aluminum foil of 7 μm thickness was used, which was glued to the sample surface. In each experiment, the particle velocity of the sample-water boundary was recorded by a VISAR interferometer and value of the shock wave velocity D was determined using interferometric data. To find the absolute value of the particle velocity, two interferometers with velocity fringe constants of 280 m/s and 1280 m/s were used simultaneously.

On the velocity profiles, for both investigated composites with transverse orientation of the fibers, after the initial shock jump the particle velocity is almost constant until the arrival of a rarefaction wave from the impactor. The oscillations are observed relative to a certain average value, due to the heterogeneous structure of composites. This value correlates with the size of the heterogeneities in the materials, determined by the thickness of the fibers. For both materials, at the same speed of impactor, the profiles have approximately the same amplitude of particle velocity. The differences are observed in the size and period of oscillations, the arrival of the release wave, which is related to the structure of the sample, the size of the fibers, the thickness of the samples. When a shock wave propagates along the fibers, a two-wave configuration is recorded (precursor and shock wave), which is due to high sound speed of anisotropic materials along the fibers. The velocity of propagation of disturbances along the fibers is higher than the shock wave velocity, that results in the formation of precursor. Particle velocity profiles for kevlar and textolite differ in the duration of the release wave and precursor, its amplitude, as well as in the oscillations size, which is related to the size of heterogeneities, the structure, the thickness of the samples, and the speed of sound along the fibers in composites. The two-wave configuration is observed until the propagation velocity of the shock wave exceeds the velocity of the first wave, which is almost the same as the speed of sound at zero pressure for each material.

From the obtained experimental data, Hugoniot states of textolite and kevlar in the coordinates of shock wave D – particle velocity u were plotted at the wave propagation along and across the fibers (fig.1). The particle velocity was calculated using the known velocity of aluminum impactor and measured in experiment value of D.

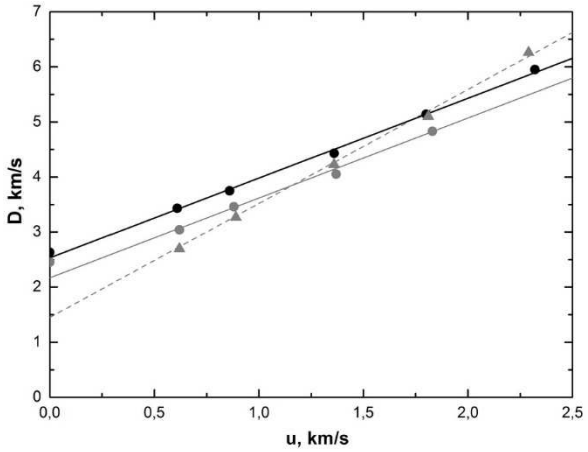

Figure 1: Hugoniot parameters of kevlar and textolite.

The experimental data for kevlar with transverse orientation of the fibers (filled circles) can be approximated by the linear dependence of $D = 2.53 + 1.45*u$, km/s (solid line). Hugoniot of kevlar with parallel orientation of the fibers is close to that for transverse direction. The experimental data for textolite with transverse direction of the fibers (grey circles) are approximated by the linear dependence of $D = 2.17 + 1.45*u$, km/s (grey line). In textolite, Hugoniots for two directions of the shock wave propagation are different and Hugoniot parameters (grey triangles) can be approximated by the dependence of $D = 1.45 + 2.05*u$, km/s (grey dashed line). Experimental results show, that Hugoniots of two investigated composites with transverse orientation of the fibers are almost parallel to each other and differ only in the first coefficient determined by the sound speed of the composite. The angle of inclination of Hugoniot is determined by the thermal properties of the material, and most likely the properties of epoxy resin, which is a common binder in both composites, are the most significant in this direction of the fibers.

* Work supported by FAIR-Russia Research Center and government contract "Investigation of thermophysical properties of substances under compression to record high pressures and magnetic fields".
# roxete20000@hotmail.com

Spectroscopic observation of isolated dense plasma generated through laser driven gold hohlraum radiation

Bubo Ma[1], Jieru Ren[1] , Yongtao Zhao[1*], Zhigang Deng[2], Wei Qi[2], Rui Cheng[3], Xing Wang[1], Wei Liu[1], Shuai Yin[1], Benzheng Chen[1], Jianhua Feng[1], Shaoyi Wang[2], Quanping Fang[2], Bo Cui[2], Xingming Zhou[3], Weimin Zhou[2], Leifeng Cao[2]

[1] MOE Key Laboratory for Nonequilibrium Synthesis and Modulation of Condensed Matter, School of Science, Xi'an Jiaotong University, Xi'an 710049, China

[2]Laser Fusion Research Center, Chinese Academy of Engineering Physics, Mianyang, 621000, China

[3] Institute of Modern Physics, Chinese Academy of Sciences, Lanzhou,730070, China

Spectroscopy is the most common method for plasma state diagnosis, which plays an important role in inertial confinement fusion (ICF), astrophysics and other related researches [1]. In general, the plasma information obtained from laser produced plasma spectrum has a large error, because the plasma parameters will produce a large gradient with the change of time and distance and the hydrodynamic behavior of the target cannot be neglected. The preparation of a homogeneous dense plasma and the measurement of its spectrum are particularly important in the study of ion transport in plasma and plasma state diagnosis.

The measurement was carried out at the XGIII facility. Combined target consisting of a gold hohlraum converter and a 2mg/cm^{-3} TAC foam ($C_9H_{12}O_8$) layer was used. Within this scheme, the ns laser (2ω) with energy of 150J interacts with the inner gold wall of the cylindrical hohlraum, which will induce blackbody-like radiation. The emitted X rays then volumetrically heat the foam to plasma state [2]. The emission spectra of both Au-hohlraum and CHO plasma were measured. Pinhole cameras which is sensitive to X rays are used to image the plasma. XRDs were used for the time-resolved measurement of X-ray flux. Transmission Grating Spectrometer and Flat field Grating Spectrometer are used for the measurement of X ray emission with spectral resolution.

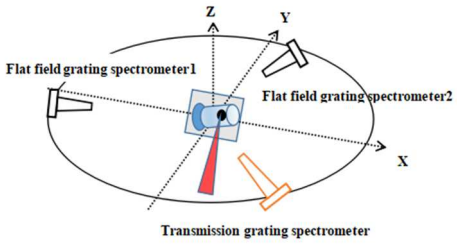

Fig.1. The layout of experimental setup and diagnostic equipment. With this indirect method, the hydrodynamic effects of target could be neglected in timescale of 10ns.

The emission spectrum of plasma between 1nm and 140nm band was obtained with single stage diffraction grating spectrometer，as shown as Fig.2, the main linear spectra were distinguished with theory of resonance and companion lines and branch ratios which also agree well with the NIST database [3].

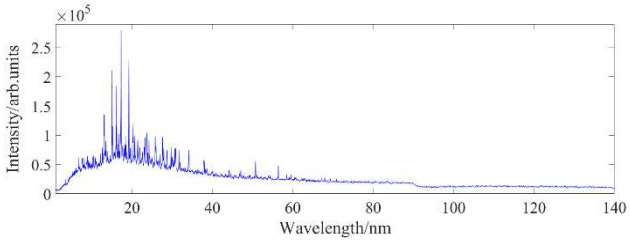

Fig.2. Emission spectra of plasma between 1nm and 140nm band in our experiment obtained by single stage diffraction grating spectrometer located at back of target.

In the experiment, we calibrated the response of the imaging plate, the energy spectrum resolution of the spectrometer, and the multistage diffraction of the grating.

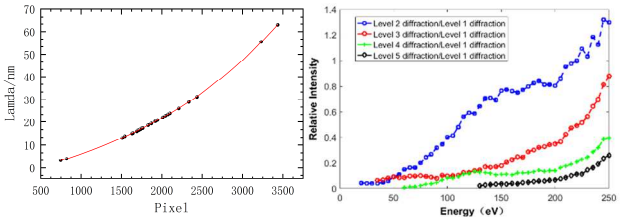

Fig.3. (Left) Emission spectral calibration and (Right) multistage diffraction calibration of grating spectrometer.

By selecting characteristic emission lines of Carbon and Oxygen atoms, C V (4.026nm. $1s^2\ ^1S_0$-$1s2p\ ^1P_1$), O V (22.75nm $1s^22p^2\ ^3P_2$-$1s^22p3s\ ^3P_2$), O IV (55.45nm $2s^22p\ ^2P_{3/2}$-$2s2p^2\ ^2P_{3/2}$) and others[3], and comparing the results of NIST database with the ratio of relative strength, we identified most of the emission lines of plasma generated in the experiment. In our experiment, the Carbon and Oxygen atoms were ionized highly, and the intensity of the linear spectrum distribution is relatively concentrated. Moreover, many characteristic spectra of Carbon and Oxygen ions were observed as well as their intensity and width, which laid a foundation for related research of atomic processes and plasma diagnosis.

[1] Dolan T J , Costley A E , Brotankova J . Plasma Diagnostics [M]// Magnetic Fusion Technology. 2013.

[2] Rosmej O et al. *Nuclear Instruments and Methods in Physics Research Section A* (2011) **653**:52-57

[3] NIST, *http://physics.nist.gov/*

* zhaoyongtao@xjtu.edu.cn

Calibration of Radiochromic □ilms for Laser-Ion Acceleration E□periments

P. Neumayer[1], A. Blazevic[1], C. Brabetz[1], A. Denker[2], G. Kourkafas[2]
[1]GSI, Darmstadt, Germany; [2]HZB, Berlin, Germany

The response of the film, i.e. the amount of darkening per absorbed dose, is non-linear and consequently quantitative dose measurements require a calibration of the response curve over the application dose range. With new generations of RCF being developed, these calibrations have to be redone. Differences in thickness, density and composition of the active layer, and even the crystallinity of the color molecules affect the response, and a simple scaling from one generation to the next is generally not possible. Even for the same film type, the manufacturer advises that "…the thickness of the active layer will vary slightly between different production lots…" [1], which would lead to different response curves for films from different production batches.

We have performed calibration irradiations to measure the dose response for two of the latest types of GAFChromic™ film, namely EBT3 and HD-V2, specified for a dynamic dose range of 0.1…20 Gy and 10…1000 Gy, respectively. These film types thus cover a wide dose range and combinations of them are often used to cover the entire spectrum of a proton pulses produced in laser-driven proton acceleration experiments [2]. Calibration measurements were done for several different production batches from each of these two RCF types, in order to assess the variability of the response curve, and also to provide individual calibrations for each film batch, used in our experiments.

The films were irradiated at the Helmholtz-Zentrum Berlin (HZB), using protons from the sector cyclotron at an energy of 68 MeV. Since the energetic protons loose only about 350 keV traversing each film a stack of several RCF were irradiated simultaneously, the small energy loss yielding a change in deposited dose by less than 0.5% from one film to the next. The proton therapy scattering system was employed to achieve a high spatial homogeneity (<2%) of the proton beam over an area of 22x12 mm, defined by a rectangular aperture located a few cm in front of the films to be irradiated. The total number of protons reaching the RCF during irradiation was measured by an ionization chamber, located directly behind the aperture. The uncertainty in this measurement is estimated to approx. ±3%, based on cross-calibration measurements against a second ionization chamber. The ionization chamber was initially calibrated against the absolute beam current measurement from a Faraday-cup.

RCF were exposed to fluences between 10^8 and $8.5x10^{11}$ protons/cm^2 by variation of the exposure time (from 30 sec to 25 min) and reducing the primary beam current (86 pA) by use of "pepper-pot" attenuators. This resulted in absorbed doses ranging of 0.17…22 Gy in EBT3 and 5…1340 Gy in HD-V2, respectively. Fig. 1 shows the result, the change in optical density (netOD) vs. the absorbed dose respective proton fluence. As can be seen, the relative dose error, i.e. the maximum error in dose determination using the calibration from a different batch, can be as high as 50-200%. Having the calibration data for the actual production batch though allows to measure the dose with an uncertainty on the level of a few percent.

References

[1] http://www.gafchromic.com/gafchromic-film/
[2] F. Wagner et al., Phys. Rev. Lett **1**□□, 205002 (2016)
[3] S. Reinhardt et al., Rad. Env. Biophys. □□, 71 (2015)
[4] D. S. Hey et al., Rev. Sci. Instrum. **7**□, 053501 (2008)

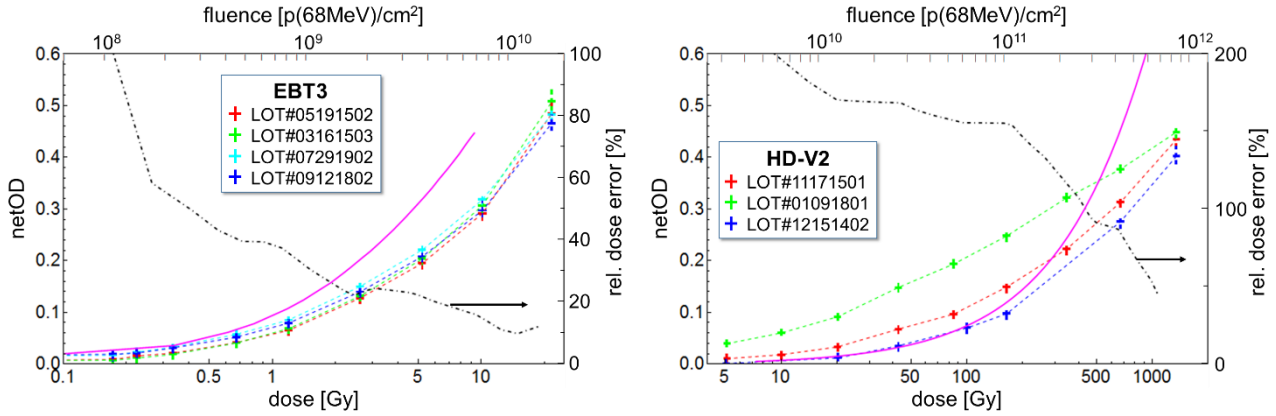

Fig. 1: Dose response of EBT3 (left) and HD-V2 (right) for films from different production batches. For comparison, the solid (magenta) curves show previous calibrations of EBT3 [3] and HD810 ([4], Kodak Wratten 94 filter), the predecessor to HD-V2. The dash-dotted (black) curve shows the relative dose error due to the variability of the response curve.

Measurement of magnetic field compression by imploding plasma *

M. Cvejic[1#], D. Mikitchuk[1], E. Kroupp[1], R. Doron[1], Y.Maron[1]
[1]Weizmann Institute of Science, Rehovot 7610001, Israel

Compression of magnetic flux and magnetized plasma is a fundamental problem manifested in a variety of conducting fluid phenomena in laboratory plasmas and astrophysics. Recently, this subject has gained particular interest due to the advances in producing plasmas of high temperature and density for fusion purposes, based on the approach of magnetized plasma compression [1]. This report refers to measurement of compressed axial magnetic field which is initially embedded in a plasma that undergoes an implosion. The plasma is produced in a Z-pinch configuration in which oxygen gas-puff load is ionized and implodes under the J×B forces resulting from a 1-μs long, 300 kA current pulse

Knowledge of axial magnetic field (B_z) evolution and distribution is essential for understanding basic processes involved: effect of electrodes on the compression, Ohmic heating, implosion dynamics and energy balance.

Here, we present an experimental determination of B_z distribution on plasma axis, throughout magnetized plasma implosion using non-intrusive spectroscopic techniques, based on the polarization properties of Zeeman effect [2]. Measured values are than compared to expected ones, which assumes that B_z flux is conserved during implosion and follows the curve: $B_z(t) = B_{z0}\,(R_0/r(t))^2$, where B_{z0} = 0.26 T, R_0 is the initial radius of gas-puff and $r(t)$ is imploding plasma radius.

Determination of B_z inside the plasma shell possesses two major difficulties: (*i*) to distinguish between the axial and the azimuthal magnetic fields along the line of sight, and (*ii*) the absence of light emission from the nearly hollow axial central region of the plasma column. To circumvent these difficulties a dopant plasma is introduced into the central region of the cylinder, along the imploding plasma axis in two ways: (*i*) either by the dopant plasma generated by laser ablation (λ = 512 nm, t_{pulse} = 7 ns, E_{pulse} = 300 mJ) of a Al-target mounted on the anode at $z = 0$, (*ii*) or by introducing a small amount of CH4 gas through the jet nozzle. The spectral lines from dopant-plasma, different than those originating from surrounding oxygen plasma, provide local information on B_z in the near axis region.

By recording σ-Zeeman polarization component of Al III 4*s* - 4*p* (λ =5696.6-Å and 5722.7-Å) or C IV 3s - 3p (l = 5801.3-Å and 5812-Å) spectral line transition with high-resolution (0.3-Å) imaging spectrometer, and by resolving respective Zeeman patterns, B_z is measured. Example of B_z determination from resolving the σ-Zeeman component of Al III transitions is shown in Fig. 1.

Using the Al III transitions from Al-dopant plasma was found to be possible in early stage of implosion, up to t~ -70 ns, when laser plasma can expand inside the imploding oxygen shell. At later stages of implosion C IV transitions from injected CH_4 gas are used. B_z is measured through implosion process up to ~ -20 ns before stagnation, which occurs ~700 ns after current initiation with pre-embedded axial magnetic field, B_{z0} = 0.26 T.

By recording Al III / CIV spectral lines form dopant plasma at different times during implosion, in separate shots, time evolution of B_z is obtained. Fig. 2 shows that measured values follow the curve of ideal magnetic flux compression, meaning that axial magnetic field is ideally conserved within imploding plasma shell.

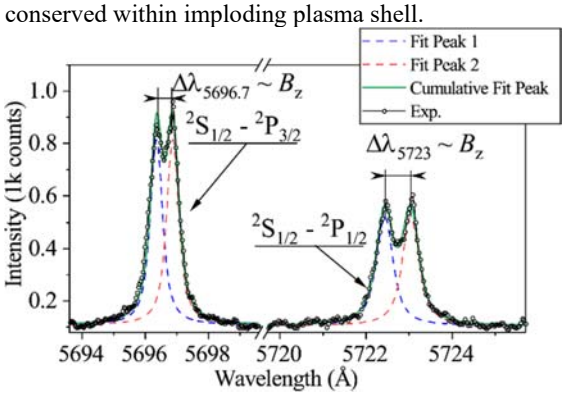

Figure 1: Spectral lines of Al III Al III 4*s* - 4*p* (λ =5696.6-Å and 5722.7-Å) from laser dopant plasma, recorded at t = -115 ns from stagnation (t = 0), z = 7 mm (z = 0 is anode-nozzle surface). Zeeman splitting pattern is clearly observed. From peak separation of individual Al III transitions, proportional to B_z, it is obtained B_z = (1.6±0.1) T.

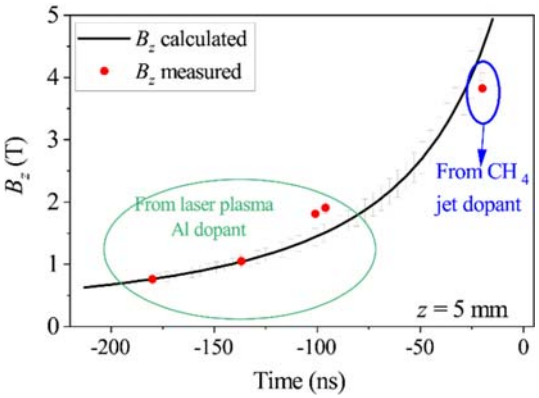

Figure 2: Evolution of B_z at z = 5 mm.

References

[1] M.R.Gomez et al., Phys. Rev. Lett., 113:155003, (2014).

[2] D. Mikitchuk, Investigation of the Compression of Magnetized Plasma and Magnetic Flux, Springer Theses (Springer International Publishing, 2019); D. Mikitchuk, et al., Phys. Rev. Lett., 122, 045001 (2019)

* Work supported by Israel Science Foundation
# marko.cvejic@weizmann.ac.il

In-situ imaging and control of intense hard X-ray FEL beams with submicron spatial resolution by means of LiF fluorescence detector

T.A. Pikuz[1,2], A,Ya. Faenov[1,2], S.S. Makarov[2,3], N. Ozaki[4], T. Matsuoka[1], K. Katagiri[4], K. Miyanishi[4], S.A. Pikuz[1,5], M. Nishikino[6], M. Ishino[6], T. Kawachi[6], T. Yabuuchi[7], Y. Inubushi[7], T. Togashi[7], Y. Tange[7], K. Tono[7], M. Yabashi[7], A. Grum-Grzhimailo[8], K.A.Tanaka[9,10], I. Skobelev[2,5], R. Kodama[10]

[1]Open and Transdisciplinary Research Initiatives Institute, Osaka University, Suita, Osaka, Japan, [2]JIHT RAS, Moscow, Russia, [3]Faculty of Physics of Moscow State University, Moscow, Russia, [4]Graduate School of Engineering, Osaka University, Suita, Osaka, Japan, [5]MEPhI, Moscow, Russia, [6]Kansai Photon Science Institute, Kizugawa, Kyoto, Japan, [7]JASRI and RIKEN Spring-8 Center, Hyogo, Japan, [8]Skobeltsyn Institute of Nuclear Physics, MSU, Moscow, Russia, [9]Horia Hulubei National Institute of Physics and Nuclear Engineering, Bucharest, Romania,[10]ILE, Suita, Osaka, Japan

Powerful X-ray sources can pump and probe exotic material states with high density and multiple inner-shell electronic excitations. Unique properties of X-ray free-electron lasers (XFELs) to probe matter on the atomic length and femtosecond time scale give new opportunity in such type of investigations. The ability to fully characterise the ultrashort, ultra-intense XFEL pulses is a crucial task both for correct evaluation of X-ray fluence and future improvement of the quality of the various x-ray optical systems.

Measurements of ultra-intense X-ray beam parameters with high resolution across and along focal caustic become possible with the application of photoluminescence LiF detector technique. High sensitivity and uniquely large dynamic range of the detector allows to record both the intensity profile of whole beam very far from focus (including boundary of the beam limited by mirrors aperture, where signal is very low), and the intensity profile in the best focus, where signal increases 5-7 orders of magnitude, The method is attractive for in-situ full 3D visualization of the beam profiles with a submicron resolution.

The principle of LiF detector operation is based on the ability of LiF crystal to generate stable color centers (CCs) under bombardment of ionizing radiation, like high energy photons and elementary particles, EUV, gamma and hard x-ray, neutrons, electrons, and ions. The features of LiF as an imaging detector include a high spatial resolution < 1 μm, dynamic range exceeding of 10^7, large field view, simple implementation, and ability to store recorded images for many years. Under optical excitation stored CCs emit light in the visible spectral range which can be readout by a conventional confocal fluorescence microscope.

The results obtained in experiments at SACLA BL3 facilities at Spring-8 at photon energy of 10.1 keV are presented. The caustic of the XFEL beam, intensity distribution along the beam propagation as well as displacement of the beam relatively to the axis of focusing KB system was measured by in-situ positioning of LiF detector in the beam (Fig.1). The 3D distribution of CCs deep inside of crystal exposed near to the beam focal plane allowed to determine the best focus position with 40 μm accuracy [1]. In the beam dimensionally limited by slit a high-resolution high contrast diffraction pattern was observed (Fig. 2). Measurement of diffraction patterns in the irradiation schemes

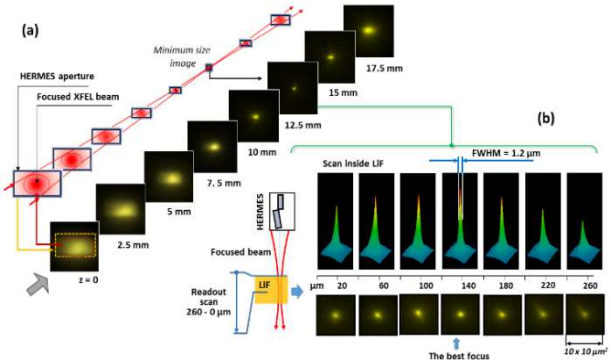

Fig.1. (a) Iintensity distribution of focused XFEL beam near the focal position and shape of beam caustic retrieval; (b) observation of PL caused by XFEL beam in the volume of LiF and prices determination of the best focus position [1].

with different Fresnel numbers and comparison experimental results with precise modelling allowed revealing of coherence and spectral distribution in a single exposure, with the resolution across the beam profile and the accuracy of 10 - 20 %. The developed technique was particularly applied at BL3 to control and optimize the beam profile in pump-probe experiments on investigation of a shock-compressed matter.

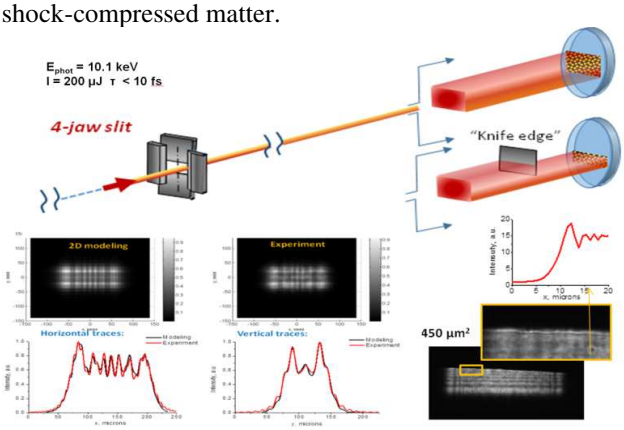

Fig. 2. Control of SACLA 10 keV beam profile using LiF detector. The fringes in diffraction patterns forming after beam passing through the slit can be seen in tiny details (~ 1 μm size) [2].

References

[1] T.Pikuz et al. Sci. Rep., 5, 17713 (2015)
[2] T. Pikuz et al. MRE, 3,197 (2018)

2 FAIR related Issues HED/WDM - Research for Phase-0 and Day-1

Preparations for high energy density experiments at FAIR

S. Neff[*1] *and A. Blazevic*[2]
[1]FAIR, Darmstadt, Germany; [2]GSI, Darmstadt, Germany

The Facility for Antiproton and Ion Research (FAIR), which is currently under construction at the site of the GSI accelerator facility, will offer unique high-intensity heavy-ion and proton beams. The experimental program at FAIR will cover a wide range of topics ranging from studying the properties of quark-gluon plasma to applied research in materials research and biophysics[1].

One focus of research is the study of high-energy density (HED) samples and warm-dense matter (WDM), which will be carried out by the High-Energy Density at FAIR (HED@FAIR) collaboration, which is part of the APPA research pillar. The intense heavy-ion beams allow to create macroscopic samples of warm dense matter, while the intense proton beams can be used for proton microscopy of HED samples created with secondary sources. The HED@FAIR research program will focus on four areas of interest[2]:

- The study of the properties of materials driven to extreme conditions of pressure and temperature.
- The study of shocked matter and equations-of-state.
- The study of the basic properties of strongly coupled plasma and warm dense matter.
- Nuclear photonics, including the excitation of nuclear processes in plasmas and laser-driven particle acceleration and neutron production.

Three key experimental schemes are currently planned for FAIR: HIHEX (Heavy-ion Heating and Expansion), LAPLAS (Laboratory Planetary Sciences) and PRIOR (Proton Microscope for FAIR).

Some key parts of FAIR needed for HED@FAIR experiments, namely the UNILAC linear accelerator and the upgraded SIS-18 synchrotron, are already in operation. They will be complemented with the heavy-ion synchrotron SIS-100 and a dedicated proton linear accelerator. The beamline for the HED@FAIR experiments will be located in the so-called APPA-cave, which also houses a second beamline that will be used for atomic physics, biophysics and materials research experiments.

Last year the FAIR Council reviewed the cost increases of FAIR. The FAIR Council has emphasized the need to realize the full Modularized Start Version and Germany has already made a financial commitment for its share of the cost increases. This additional funding already covers all accelerator components and most of the civil construction (the buildings for the collector ring, the high-energy storage ring and the proton LINAC are not covered), so that these parts can be contracted without delay. As soon as FAIR receives financial commitments from the other FAIR shareholders, the civil construction of the remaining buildings will be contracted. With respect to HED@FAIR, the only impact might be a possible delay of the proton LINAC. However, as earlier experiments at GSI have demonstrated, Day-1 experiments can already be carried out with lower-intensity proton beams from the UNILAC.

Many major components of the HED@FAIR setup are currently under construction. The superconducting magnets of the final focussing system are constructed at the IHEP in Protvino as a Russian in-kind contribution. The final design review of the magnets has been completed successfully and the construction of the magnets has started. Also, a test facility for the magnets has been built at IHEP.

The quadrupole magnets of the PRIOR-II proton microscope are being constructed as a German in-kind contribution. A factory acceptance test (FAT) of the magnets is currently in process. After a first inspection by GSI experts, the supplier is currently working on correcting some minor deviations from the specifications in order to complete the FAT.

The target chamber and the target positioning system for Day-1 experiments will be provided by TU Darmstadt, GU Frankfurt and the FSU Jena and will be funded via BMBF Verbundforschung. The design of the target chamber has been finished and the tender for the construction of the chamber is currently in progress. A nanosecond diagnostic laser system (100 J, 532 nm) is currently being constructed by the PHELIX laser group at GSI in collaboration with the TU Darmstadt and the FSU Jena.

In order to allow for the commissioning of FAIR equipment and for experiments before the start of FAIR, the so-called Phase-0 experimental campaign has been initiated using the existing GSI facilities. In the case of HED@FAIR, it is planned to carry out HIHEX and PRIOR experiments before the start of FAIR at the GSI HHT experimental area as part of the Phase-0 research program. These experiments will also be used to commission the PRIOR-II proton microscope and the target chamber. In order to carry out coupled experiments using heavy-ion beams from SIS-18 as well as nanosecond laser pulses from PHELIX, a laser beamline from PHELIX to the HHT experimental area is currently under construction. First experiments using this beamline are scheduled for 2021. These preparations for Phase-0 experiments are covered in separate contributions to this annual report.

[*] The work reported in this paper has been carried out by the research and accelerator departments of GSI and the HED@FAIR collaboration.

References

[1] M. Durante et. al., Phys. Scr. **94**, 2019, 033001

[2] K. Schoenberg et. al., Physics of Plasmas **27**, 2020, DOI: 10.1063/1.5134846

Test Facility for FFS Quadrupoles

A. Ageev, A. Kalchuk, A. Kharchenko, E. Kashtanov, S. Kozub,
A. Orlov, M. Stoliarov, L. Tkachenko, A. Vlasov
NRC "Kurchatov institute" – IHEP, Protvino, Moscow region, Russia, 142281

Superconducting (SC) wide-aperture high-gradient quadrupoles for the final beam focusing system for experiments of the HED@FAIR collaboration are being developed as part of a cooperation agreement between FAIR and the NRC "Kurchatov Institute"-IHEP. Before being sent to FAIR, all manufactured quadrupoles must pass the manufacturer's acceptance tests (FAT), including cold tests, to ensure that they meet the requirements of the contract specification. At the NRC "Kurchatov Institute"-IHEP, on the basis of the existing cryogenic and electrophysical equipment, a test facility was created for testing these quadrupoles. A description of the test facility of the quadrupoles, and information on its design and main characteristics are presented in this report. The main characteristics of the quadrupole are: the operation mode is a direct current; the internal diameter of the SC coil is 260 mm; the geometric length is 2 m; the central field gradient is 37.6 T/m; the operating current is 5.73 kA; the maximum field in the SC coil is 5.87 T; the stored energy is 1079 kJ; the current value is up to 6.3 kA [1]; the calculated heat leakage to helium at T = 4.5 K is 7.5 W; the calculated heat leakage to helium at T = 50-80 K is 53 W; the helium consumption at T = 50 K for cooling the copper part of a pair of HTSC current leads is less then1 g/s; the volume of helium in the cold-mass cryostat of the quadrupole is 70 liters; the cold mass of the quadrupole is about 6.5 tons; the total weight of the quadrupole is about 8.5 tons [2].

The basis of the cryogenic system of the test facility is a helium liquefaction plant with a capacity of 150 l/h, a satellite refrigerator with a cooling capacity from 0 to 400 W at a temperature of helium flow cooling magnet from 4.5 to 280 K and its flow rate up to 30 g/s. The working pressure of a helium in the liquefier and refrigerator is 20-23 bar. The scheme of the test facility cryogenic system is presented in Fig. 1. The satellite refrigerator with sub-cooler provides helium flow with preset parameters for cooling the quadrupole. The maximum consumption of a liquid helium (130 l/h) occurs at the temperature of 4.5K and the cooling capacity of 400 W, which is less than the capacity of the liquefier 150 l/h. The expected consumption of a liquid helium in the operating mode of cryostatting with a maximum current in the quadrupole will be approximately 40 l/h. Thus, the liquefier will not work continuously, but about 8 hours per day, pouring liquid helium into the liquefier vessel. A liquefier vessel with a distribution box through the CV 22 valve provides round-the-clock intake of a liquid helium into the satellite refrigerator – a subcooler system. At the test facility, the quadrupole heat shields will be cooled with liquid nitrogen. Flows cooling magnet and heat shield are sent to the cryostat through the distribution box.

There are measures to ensure the safe operation of the equipment in the following emergencies: a deterioration of the insulating vacuum, a transition of the quadrupole to a normal state (quench), an unauthorized power failure.

A liquefier with a liquid helium vessel are the serial production equipment and for them the manufacturer has developed and carried out his own set of measures for the deterioration of the insulating vacuum, which during operation at IHEP has not changed or been disturbed.

When the distribution box, the satellite refrigerator or the helium subcooler vacuum deteriorate, a helium through the safety valves SV11, SV21 and SV22 enters the gasholders of the compressor shop, the volume of these gasholders is enough to receive a helium from these devices without losses to the atmosphere.

The helium volume in the cold mass of the quadrupole is 70 liters, which is equivalent to 50 nm^3. The gasholders of the compressor shop will not be able to accept such a volume without loss of helium and therefore a quench receiver with a volume of 63 m^3 was included in the cryogenic system of the stand for the rapid reception of this helium. After an emergency case, a helium from the quench receiver is fed to the gas-holders through the valve CV51 with a rate, that eliminates the loss of helium.

Information about the current state of each of the facility subsystems, such as a pressure, a liquid nitrogen and helium levels, a helium flow rate, s current temperature and s degree of vacuum, should be available to the operators, and they should monitor the status of the subsystems in accordance with the operation algorithm. In order to obtain this information, various types of sensors are installed on the facility, the information from which is collected and transmitted by the operator control and the monitoring system to a computer for a visualization and a control of the processes by the operator. The number of measured signals is given in Table 1.

Table 1. Measurement points on test facility.

Type of signal	Amount
Temperature	12
Pressure	3
Vacuum	5
Valves position	16
Level meters	2
Flowmeter	1

The thermometers T21, T31, T32 and T33 are calibrated TVO type resistive temperature sensors. The thermometers T41, T42, T43, T44 of the CLTS-2B type are mounted on the quadrupole, the other thermometers are platinum temperature sensors. A pressure is measured by intelligent pressure sensors with a HART interface and a 4-20 mA output signal.

Vacuum measurements provide two types of sensors, the first one for the $5 \cdot 10^{-1}$ range - $1 \cdot 10^{-4}$ Torr, and the second one for higher vacuum levels. The first range is measured with thermocouple vacuum gauges. High vacuum is measured using WRG-S sensors with an inverse-magnetron converter.

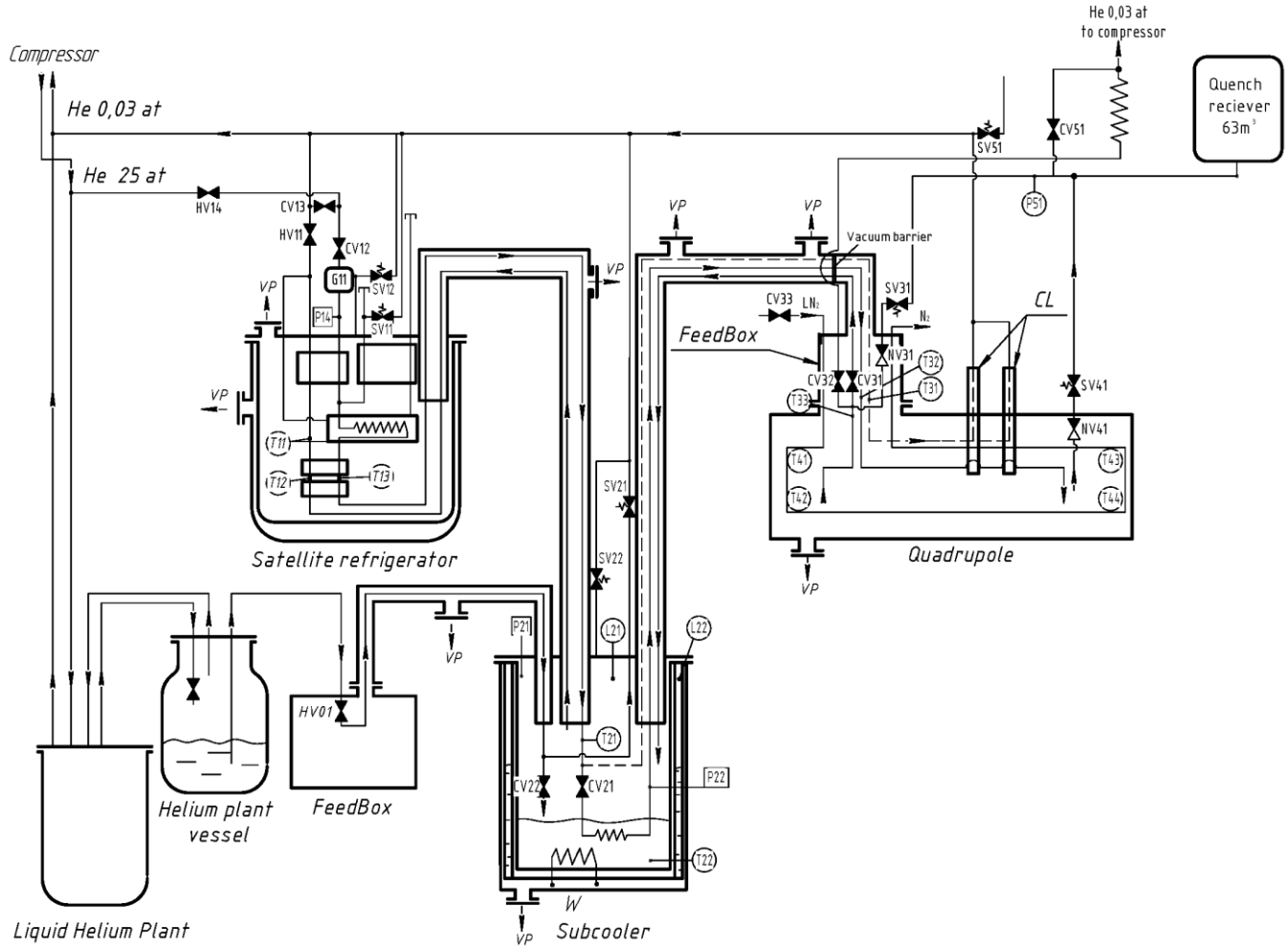

Fig. 1. Scheme of the cryogenic system of the test facility for the FFS quadrupole.

The valves with the name HV are manually operated, the valves with the name CV have pneumatic remotely controlled actuators with a 0-5 mA interface for the connection to the controller. L21 is a superconducting helium level sensor, and L22 is a capacitance liquid nitrogen level sensor. Both are connected to a 2-channel liquid cryoagent level monitor. Flowmeter G11 is vortex type with 4-20 mA interface.

A key part of the hardware is the CompactRIO system controller with a processor and a user-programmable FPGA logic array, which includes nine National Instruments I/O modules. These modules provide direct sensor connections and special functions. The system consists of four NI9219 modules and four NI9265 modules.

The NI9219 module can measure signals from sensors, such as resistance temperature sensors (RTD), thermocouples, strain gauges, and other sensors with an electrical signal, as well as perform quarter-bridge, half-bridge and full-bridge current measurements, with built-in voltage and current sources. The NI9265 is used to interface and control industrial drives, driven by a current signal at high speeds. This module allows one to control the position of the valves of the stand.

In addition to the CompactRIO system, the test stand hardware consists of independent analog I/O modules of the MB110 type. These modules are installed in a separate rack, collect data from pressure and vacuum sensors and send them to the operator's PC via RS-485 bus to USB AC-4 converters. The level gauges are equipped with a fluid level monitor with RS-485 interface and are connected to the operator's PC directly.

The software part of the test facility was made in Labview 2014 with NI-DAQmx and CompactRIO drivers. This development environment helps to organize a unified management system using hardware from different manufacturers. The CompactRIO chassis with the included modules connects to the system through the standard Ethernet port and the National Instruments remote system explorer. The auxiliary equipment is connected to the diagnostic system via USB and COM ports, using Data Socket technology and OPC servers. The graphic panel represents all the necessary parameters of the object in order to control the cooling down and the testing processes in real time. The experimental data received from the sensors will be saved in a TDMS file format for further analysis. After a trial run, the software generates a report in the .doc format, which depends on the type of test performed and may include measurements, shown in various formats (charts, tables, etc.).

References

[1] L. Tkachenko, A. Ageyev at al., Development of HED@FAIR Quadrupole", Proceedings of RuPAC2018, p.78, IHEP, Protvino.

[2] M. Stolyarov, A. Ageyev at al., Development of Test Facility for HED@FAIR Quadrupoles. Proceedings of RuPAC2018, p.366, IHEP, Protvino.

Hydrodynamic Simulation of the Future HED Matter Properties Research Experiments at FAIR

V. Kim, D. Nikolaev, I. Lomonosov, V. Mintsev
IPCP RAS, Chernogolovka, Russia

New ion beam experiments cycle for HED matter properties and EOS research is scheduled at FAIR facility. Based on previous HIHEX (Heavy Ion Heating and EXpansion) experiment results held at GSI [1] it was proposed to use the focused heavy ion beam for rapid and uniform heating of thin metallic (Lead) foil, that melts, evaporates and expands to the sides in quasy-1-D regime. In order to reach closer to the main area of interest on the metal phase diagram - critical point (CP) and evaporation curve - it was supposed to use enclosing high-pressure assembly, filled with heavy transparent gas (**Ar,** initial pressure 100 bar).

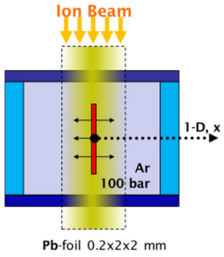

Figure 1: 1-D scheme of the experiment

The shock wave generated in **Ar** by hot expanding Lead creates counterpressure up to few kilobars, while remaining transparent. It allows to use different registration and diagnostic techniques: pyrometry, interferometry, reflectivity measurement, shadowgraphy and schlieren shadowgraphy.

From the announced list of feasible projectile beam configurations on the 2020-2021 FAIR operation we chose **U**, **Ni**, **Ar** and **N** ion beams as the most promising for our goals. Realistic intensities estimated for these beams were selected (see Table 1). Bunch duration is 100 ns with parabolic temporal distribution. Considering the geometry of the lead specimen 2-D Gaussian distribution for spatial beam focal spot was used, with fixed $Sigma_x$=0.25 mm and varying $Sigma_y$=0.5-1.5 mm. Staying in that range preserves high enough energy deposition value as well as quasy-1-D hydrodynamic flow regime even at the later stages of experiment.

Multidimensional hydrodynamic implementation of finite size particle-in-cell method was used for 1- and 2-D modelling [2]. SRIM-based ray tracing ion stopping procedure was used for heavy ion beam energy deposition effect in the **Pb**-target and ambient **Ar** gas. Tabular wide-range multiphase equation of state for Lead was used [3].

The result peak specific internal energies in the center of Lead foil at t=100 ns for the different beam configurations are shown in Table 1. It was found that in order to get to near-critical point region states in Lead during expansion phase of experiment the peak projected specific internal energy values in the target should be higher than 1 kJ/g. Thus only the usage of **Ni** ion beam looks appropriate and **N**, **Ar** and **U** beams are not sufficient.

Table 1: ion beams energy deposition in Lead (F1: $Sigma_y$=1.1 mm, F2: $Sigma_y$=0.5 mm.)

Proj.	Intensity, part./bunch	e_0, GeV/amu	E_{Max}@F1, (kJ/g)	E_{Max}@F2, (kJ/g)
Ni	1.0E+11	0.50	**1.032**	**2.306**
N	7.0E+10	0.50	0.046	0.100
Ar	3.0E+10	0.50	0.135	0.298
U	2.0E+09	0.35	0.269	0.602
Increased intensity				
U	3.0E+09	0.35	0.410	**0.903**
U	4.0E+09	0.35	0.547	**1.204**

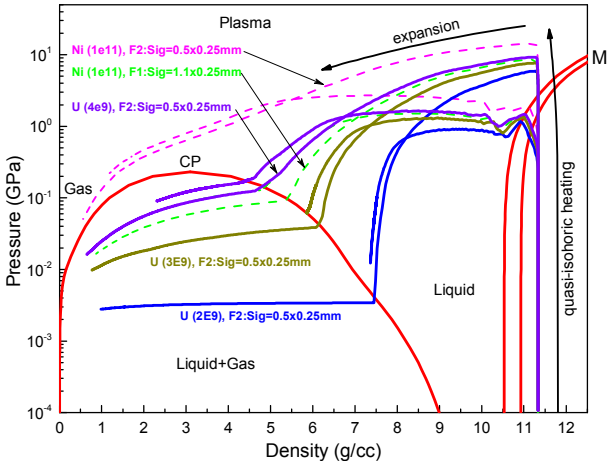

Figure 2: pressure-density phase diagram of Lead

In order to estimate the level of intensity needed for the **U** ion beam, we simulate the impact of increased values of I=3.0E+09 and I=4.0E+09 particles/bunch. Figure 2 shows the trajectories of states in central "in-depth" point and "near-surface" point of **Pb**-target for the selected **Ni** and **U** beam configurations on Pressure-Density phase diagram. One can see that for highly focused **U** beam with I=3.0E+09 the parameters in lead in expansion phase of the experiment are at a lower end of the main area of interest, and higher beam energetic parameters are desirable.

References

[1] D. Varentsov et al., Nucl. Instr. & Meth. in Phys. Res. A. 577(1-2) (2007) 262-266
[2] V.E. Fortov et al., Int. J. Impact Eng. 33 (2006) 244
[3] V.E. Fortov et al., Nucl. Instr. & Meth. in Phys. Res. A. 415, 3 (1998) 604-608

Construction□characteri□ation and optimi□ation of a plasma □indo□ for □AIR□ status update□

A. Michel[1]□, B. F. Bohlender[1], M. Iberler[1], J. Jacoby[1]

[1]IAP, Goethe University, Frankfurt, Germany;

Introduction

A Plasma window provides a membrane free particle and x-ray beam transmission between two regions of different pressures, e.g. target chambers or gas stripper cells and the vacuum of an accelerator. For details on the working principle, the reader is referred to [1], [3], [4].

Experimental setup

In comparison to the experimental setup described in the report of last year [2], the current setup features two cathodes, pointed towards each other and touching in the centre of the discharge axis. Figure 1 shows a schematic view of this setup including a cross-section of the plasma window with an aperture of Ø = 5 mm. The high-pressure side with the gas supply is to the left, as are the cathodes. A scroll pump was used during operation, keeping the pressure on the anode side between p_L = 1 mbar to 10 mbar.

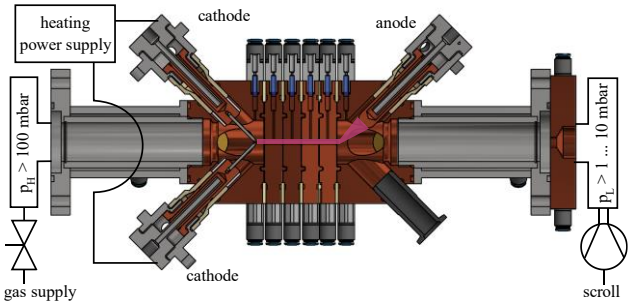

Figure 1: Schematic and cross section of the experimental setup with heating power supply

An external power supply was used for conducting a current of I = 140 A at U = 1.5 V through the touching cathode needles made from $WLaO_3$. This preheating technique was used to generate free electrons at the cathode tips to support the arc ignition which is carried out by applying a HV pulse (U_P = -1 kV, t_P = 5 µs) to the cathodes.

Experimental results

In comparison to the former setup, featuring no thermionic emission and only one cathode, the new setup offers an improved arc ignition and stable burning in different working gases.

The two-cathode setup did not affect the plasma parameters that were estimated for argon as working gas in former experiments [1], [2]. The maximum arc current did not exceed 60 A with a burning voltage between 60 to 85 V.

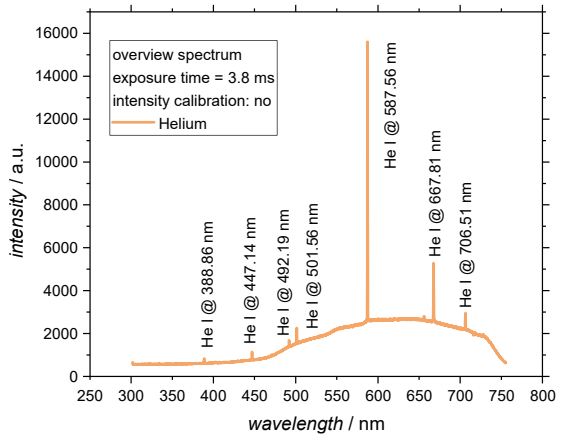

Figure 2: Helium overview spectrum taken from the cathodes interface

Successful arc ignition could be carried out with helium as a working gas. Figure 2 shows the overview spectrum taken from the cathodes interface. As can be seen, no other elements were identified to alter the spectrum that were assumed to diffuse from the $WLaO_3$ cathode tips due to the additional heating. Compared to the discharge in argon, the burning voltage was 25 to 75% higher allowing for an increasing thermal power input in the discharge column and therefore an increase in the plasma viscosity [3].

Conclusion and Outlook

The current setup offers a stable pressure separation with a ratio of (p_H/p_L) between 40 and 60 for the 5mm aperture.

The lifetime of the cathodes is slightly below 5h due to the discharge anchor drifting towards the cathode body which is assumed to stem from LaO_3 diffusion processes.

Future experiments will utilize the complete differential pumping system, including a turbo-stage. In addition, the impact on the overall sealing properties of different working gases, higher arc currents as well as magnetic fields in the discharge column will be investigated.

Higher apertures with Ø = 7.5 mm will be tested and a new gas cooled cathode body with pure tungsten tips will be set up for an improved cathode lifetime and for clearance of the beam transmission channel.

References

[1] B. F. Bohlender et al Phys. Rev. Accel. Beams 2020
[2] B. F. Bohlender et al GSI HED report 2018
[3] A. Hershcovitch, J. Appl. Phys, 1995
[4] B. F. Bohlender et al GSI HED report 2017

* Work supported by BMBF, Ref.no: 05P15 RFRBA
#michel@iap.uni-frankfurt.de

X-Ray Fluorescence Imaging of the Heavy-Ion Beam Distribution on Target at Experiments in Phase-0 and at FAIR*

S. Zähter[1], *M. Gyrdymov*[2], *J. Jacoby*[2], *and O. Rosmej*[1,2]
[1]GSI, Darmstadt, Germany; [2]Goethe University, Frankfurt, Germany

Motivation

In the HIHEX experiment, planned by the HED@FAIR collaboration for Phase-0 at HHT and the APPA-cave at FAIR, precise knowledge of the energy density distribution deposited by the heavy-ion beam into the target is of great importance. Simulations on the hydrodynamic response of the target to the energy deposited by the heavy-ion beam rely heavily on this information. Intensity distribution of the heavy ion beam on target during the shot can be measured using X-ray target and/or ion beam fluorescence that occurs in the ion-target interaction process and can be imaged using a pinhole camera or a crystal spectrometer. Due to high radiation levels around the interaction area, transport of the signal far away from the target chamber and remote controlled detection are required. This is achieved by the conversion of the X-ray signal into an optical one. The X-ray Conversion to Optical Radiation and Transport (XCOT)-system was developed at the Goethe University, Frankfurt in the frame of a BMBF-project for the high demands in its application at the HHT-cave in Phase-0 and in the APPA-cave at FAIR.

Experimental Results

Pilot experiments were performed at the Z6 experimental cave to commission the XCOT-system in the frame of FAIR Phase-0. The XCOT-system consists of a 100 microm thick CsI(Tl)-scintillator which converts the X-rays into visible light. That light is imaged by a lens system onto a micro channel plate based image intensifier unit in front of a sCMOS-camera. The scheme of the XCOT-system and the setup used is shown in fig. 1. The UNILAC provided an 11.4 MeV/u Au26+-beam that irradiated foil- and mesh-targets of different materials and mesh widths. Multi pinholes were used to improve the signal-to-noise ratio. Cu-mesh's with mesh distances of 250 microm (mesh width 60 microm, see fig. 2) and smaller were used to determine the spatial resolution of the XCOT-system. By overlaying several of the images taken by the multi pinholes and then taking a lineout (see Cu100-mesh image and diagram on the right), the heavy-ion beam distribution on target can be measured on shot.

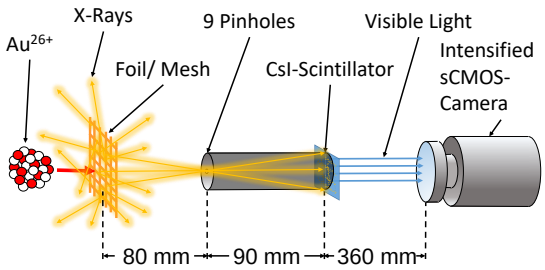

Figure 1: Schematic view of the XCOT-system with multi pinholes for X-ray imaging.

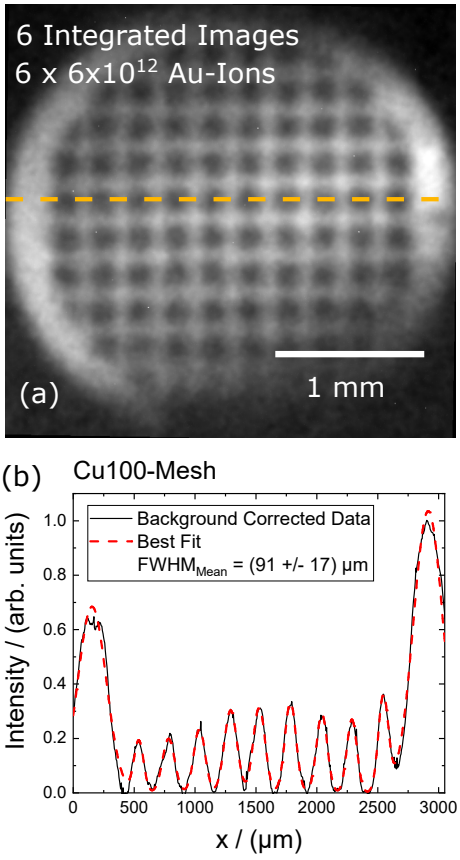

Figure 2: (a) Cu100-mesh imaged with the XCOT-system. (b) Corresponding lineout.

* Work supported by BMBF, FKz. 05P19RFFA1

The SIS100 laser cooling facility

S. Klammes[1,2], M. Bussmann[3], V. Hannen[4], D. Kiefer[2], Th. Kühl[1,5], X. Ma[6], P. Spiller[1], U. Schramm[3,7], M. Siebold[3], Th. Stöhlker[1,5,8], Th. Walther[2], W. Wen[6], and D. Winters[1]

[1]GSI Helmholtzzentrum, Darmstadt, Germany; [2]Technical University Darmstadt, Germany; [3]Helmholtz-Zentrum Dresden-Rossendorf, Germany; [4]Münster University, Germany; [5]Helmholtz Institute Jena, Germany; [6]Institute of Modern Physics-CAS, Lanzhou, China; [7]Technical University Dresden, Germany; [8]Jena University, Germany

The FAIR synchrotron SIS100 will be the worldwide first and only user synchrotron equipped with a facility to cool accelerated heavy-ion beams at final energy by means of lasers [1]. The goal of the work package 'SIS100 laser cooling', which is part of the FAIR subproject SIS100, is to build this facility and to start *cooling* right after the commissioning of the SIS100 (in 2026). We gratefully acknowledge support from POF III ARD (accelerator research and development) subtopic 2 in the Helmholtz program "Matter & Technologies".

Laser cooling is well established for atom and ion traps, where the velocities are very low, but can also be applied to relativistic velocities, where the huge Doppler-shifts are being exploited to cool extreme ions using 'normal' lasers. Calculations have shown that relative ion beam momentum spreads of $\Delta p/p < 10^{-7}$ (depending on the ion beam intensity) and cooling times of only a few seconds are possible [2]. Correspondingly, also intense ultra-short ion bunches can be created, even shorter than those obtained using the bunch compression method (50 ns). This will offer unique possibilities for extracted beams from the SIS100, especially for the generation of high energy-density in matter (*e.g.* dense plasmas).

The laser systems for this work are being developed and built by the TU Darmstadt (cw laser & pulsed ps-ns laser) and the TU Dresden/HZDR (ps pulsed laser), supported by the BMBF. The pulsed laser systems have variable repetition rates (up to 1-10 MHz). This offers the unique possibility to synchronize the laser pulses with the ion bunches in the SIS100, and could further increase the laser cooling efficiency. All laser systems use frequency doubling stages to convert the initially IR laser (1028 nm) light, via visible light (514 nm), to the final UV light (257 nm). These laser systems have up to a few 10 W of average power. The laser systems will finally be transported to and installed in the SIS100 maintenance tunnel (where the laser lab will be).

The detector system, which will detect the fluorescence from the laser excited ions during laser cooling, will be built by the University of Münster (BMBF support). A similar system has already been successfully tested at the ESR in 2016 using stored $^{12}C^{3+}$ ions. At the SIS100, the Doppler shifts are much larger, uniquely enabling laser cooling studies with more intense and much heavier ion beams. However, the XUV fluorescence will shift to much smaller wavelengths, requiring partially different technology, which is currently being developed in Münster [3].

The SIS100 vacuum chamber (built by *Kurt. J. Lesker*) was shipped to (Fig. 1) and tested at GSI (Fig. 2) [4]. The chamber is made out of the highest quality stainless steel (electro-polished), and comes with a frame, alignment bridges, bellows (*Witzenmann*), and heater jackets (*Isoheat*). The chamber has now passed the vacuum Site-Acceptance Test (SAT) for installation at the SIS100.

List of components purchased in 2019:
- *DFB laser (Dynamic Feedback) + controller (Toptica)*
- *chiller for laser system, ,max. 1200 W (FRYKA)*
- *Laser Spectrum Analyzer (Toptica /HighFinesse)*
- *2 optical shutter systems (MRC and Thorlabs)*
- *2" optical mounts (Thorlabs & Newport)*
- *UV mirror set 2" and 3" (CVI/Melles Griot)*
- *DN160CF pressurized vacuum valve (VAT)*
- *DN200CF ion pump (Agilent VacIon Plus 500)*

Figure 1: SIS100 laser vacuum chamber (*Kurt J. Lesker*)

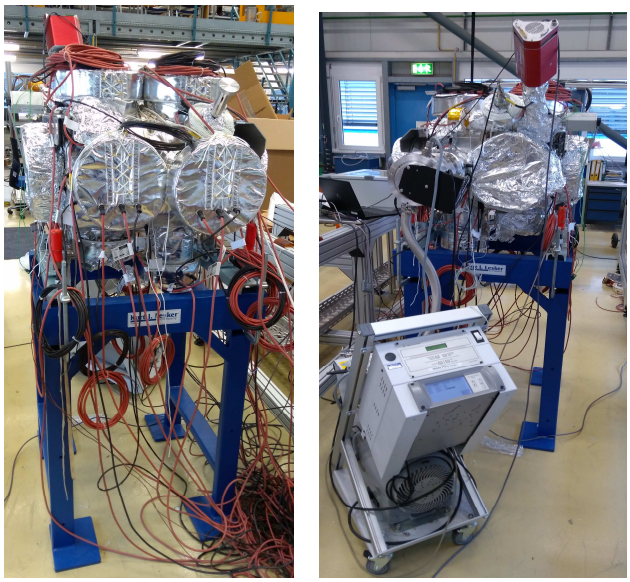

Figure 2: SIS100 laser vacuum chamber with heater jackets (*Isoheat*) and support frame (*Lesker*) during the vacuum Site Acceptance Test (SAT) @ GSI (Leichtbauhalle).

References

[1] D. Winters et al., Phys. Scr. T166 014048 (2015).
[2] L. Eidam et al., Nucl. Instr. Meth. Phys. Res. A 887 102 (2018).
[3] J. Ullmann et al., GSI scientific report (2017).
[4] D. Winters et al., GSI scientific report (2017).

Temporal coupling of nanometric inhomogeneities in an excited target at the initial stage of a FAIR bunch*

S. A. Gorbunov[1,#], A. E. Volkov[1,2,3]

[1]LPI of the RAS, Moscow, Russia; [2]JINR, Dubna, Russia; [3]NRC'Kurchatov Institute', Moscow, Russia;

Facility for Antiproton and Heavy Ion Researches (FAIR) will provide unique experimental conditions for investigation of unusual extreme matter states under intense heavy ion beams [1].

We applied a hybrid model to study the joint kinetics of electronic and ionic systems with account of appearing nanometric and temporal inhomogeneities of target excitation at the initial stage of a FAIR bunch. Monte-Carlo code TREKIS [2] provides this model with radial distributions of electron concentrations and energy densities up to 10fs, when the most of the ionization cascades finishes, and propagation of electrons changes from the ballistic to diffusion one.

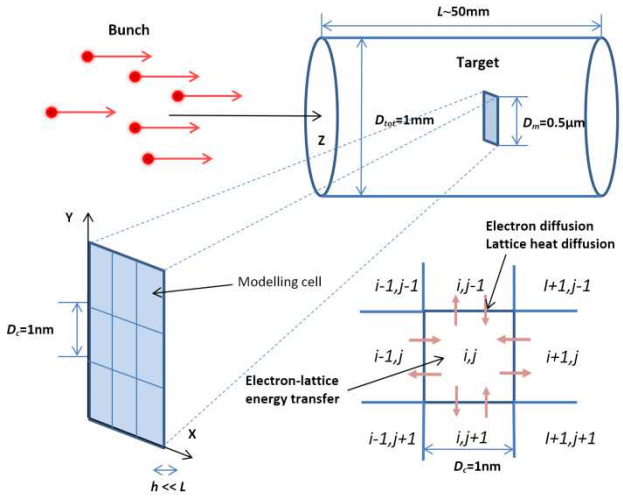

Figure 1: Geometry of the modelled volume.

Periodic boundary conditions were applied in all directions for the modelling cell (Fig. 1).

We use microscopic kinetic approach [3] to describe subsequent electron diffusion. The dynamical structure formalism is applied to evaluate cross sections governing electron-lattice coupling [4]. Thermal diffusion approach describes spatial spreading of lattice excitation in this initial "first generation" model. We take Al_2O_3 for modelling, since most of our model blocks have already been built and well tested for this system [4]. The beam intensity $4 \cdot 10^{10}$ ions mm^{-2} ns^{-1} [5] of Xe 167 MeV ions was used to illustrate detected effects.

Radial asymmetry of relaxation of electron cloud (right part of Fig. 2) caused by overlapping of excited (left part of Fig. 2) areas is illustrated in Fig. 2.

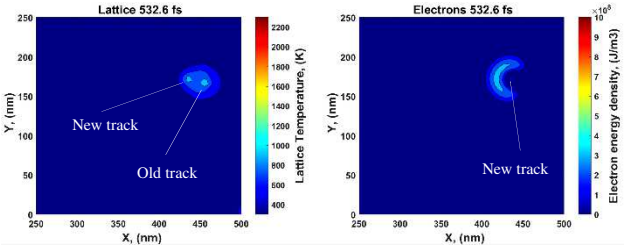

Figure 2: Temperature of the ionic subsystem (left) and energy density in the electronic subsystem (right) after 30fs the new ion pass close to the previously excited area.

Fig. 3 demonstrates a subsequent increase of the fluence resulting in overlapping of excited areas, and finally in appearece of a percolation threshold of molten zones in the beam spot.

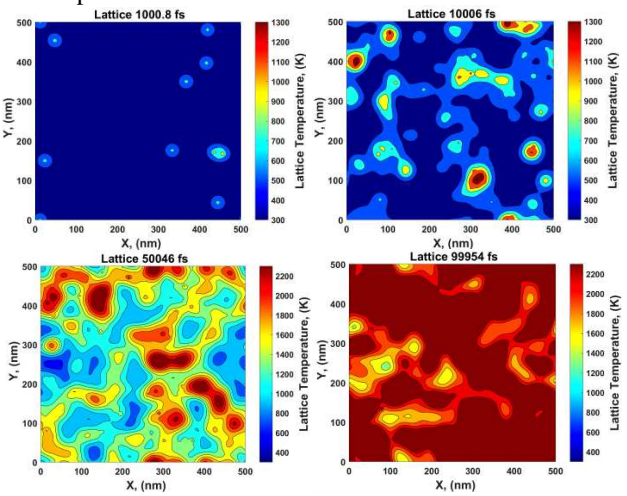

Figure 3: Temperature of ionic subsystem of a target after 1ps-10ions (top-left), after 10ps-100ions (top-right), after 50ps-500ions (bottom-left) and after 100ps-1000ions (bottom-right).

References

[1] T. Stöhlker, V. Bagnoud, K. Blaum, A. Blazevic, A. Bräuning-Demian, M. Durante, et al., 365 (2015).

[2] N.A. Medvedev, R.A. Rymzhanov, A.E. Volkov, J. Phys. D. Appl. Phys. 48 (2015) 355303 (24pp).

[3] S.A. Gorbunov, N.A. Medvedev, P.N. Terekhin, A.E. Volkov, Phys. Status Solidi. 10 (2013) 697–700.

[4] S.A. Gorbunov, N. Medvedev, R.A. Rymzhanov, A.E. Volkov, Nucl. Instruments Methods Phys. Res. Sect. B Beam Interact. with Mater. Atoms. 435 (2018) 83–86.

[5] Hed. Collaboration, Technical proposal for design, construction, commissioning and operation of the: HEDgeHOB High Energy Density Matter Generated by Heavy Ion Beams, 2005.

* Work supported by FAIR-Russia Research Center.

#gorbunovsa@lebedev.ru

Prototype Quadrupole Chamber with Cryogenic Components

S. Aumüller[1,2], *L. Bozyk*[1], *K. Blaum*[2], *and P. Spiller*[1]
[1]GSI, Darmstadt, Germany; [2]Universität Heidelberg, Germany

Introduction

One goal of the FAIR project is to generate heavy ion beams of ultimate intensities. SIS100 aims to reach intensities of 5×10^{11} heavy ions per pulse. Therefore medium charge states have to be used, to avoid stripping losses and to shift the space charge limit to higher intensities. However, under these conditions the probability for charge exchange at collisions with residual gas molecules is much higher. Since such ions do not match the ion optical lattice any more. These processes lead to increase losses of ions. At the position of impact on the vacuum chamber, the lost ions induce a desorption process, which significantly increases the residual gas density. This self-amplification process can lead to a complete loss of the beam. To limit this effect, the residual gas particle density has to be reduced. In SIS18 several upgrade measures have been realized [1]. For example 55% of the circumference of SIS18 are already coated with NEG. This coating provides high and distributed pumping speed for Hydrogen and light residual gas particles. However Nobel and Nobel-like residual gas components are not pumped [2]. Ions (like Argon) have a very high ionization cross section [3]. Simulations show, that the FAIR intensity goal of 1.25×10^{11} particles per pulse in 3 Hz operation can not be reached [4]. The transmission strongly depends on the partial pressure of Argon in the residual gas composition. A cryogenic environment at moderate temperatures, i.e. at 50-80 K, provides a high pumping speed for all heavy residual gas particles. Hydrogen remains as the only typical residual gas particle which can not be pumped at these temperatures. With an additional NEG coating of the chamber, the pumping will be optimized for all residual gas particles. Therefore a new type of quadrupole chamber with cryogenic components has been designed and constructed, bases on a study by ILK Dresden.

Prototype Quadrupole Chamber

The prototype chamber is segmented with a similar structure as the SIS18 magnet chamber, see Fig. 1, and has a length of 3 m. The main part are three thin walled sections, which mimic the existing quadrupole chambers in SIS18. These segments will be used to investigate the effect of cryogenic components on construction of the room temperature chamber. The thick walled measuring chambers in Fig. 1 are used for the installation of measurement instruments. On the right and left side of the setup are two pumping chambers. Similar to the SIS18 setup one of these is equipped with a turbo pump and the other with an Ion getter pump. The pumping chambers further serve as mounting points for the feedthroughs of the coolant (Fig. 2). The two feed pipes can be used independently of each other.

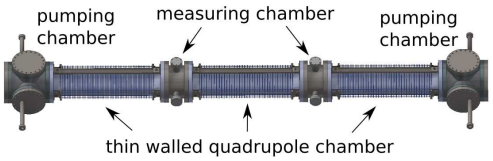

Figure 1: Prototype quadrupole chamber setup

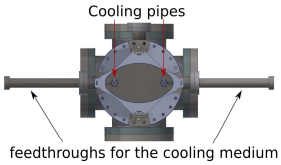

Figure 2: Profile of the chamber setup

Planned Measurements

- Static pressure profile with cooled pipes at different temperatures, with and without NEG coating
- Different cooling setups:
  One or two pipes, cooled serial or parallel
- Simulation of dynamic vacuum:
  The impact of an heavy ion beam will be simulated by a dedicated gas inlet system with a fast dosing valve
- Capacity and saturation effects of the cryogenic surfaces
- Long term evolution of the residual gas composition

References

[1] P. J. Spiller, L. H. J. Bozyk, and P. Puppel. “SIS18 – Intensity Record with Intermediate Charge State Heavy Ions”. *Proc. 2nd Int. Particle Accelerator Conf. (IPAC’11)* (2011).

[2] C. Benvenuti. “Extreme High Vacuum Technology for Particle Accelerators (Invited)”. *Proc. 19th Particle Accelerator Conf. (PAC’01)* (2001).

[3] L. Bozyk et al. “Multiple-electron losses in uranium ion beamsin heavy ion synchrotrons”. *NIM-B, vol. 372* (2016).

[4] L. H. J. Bozyk and P. J. Spiller. “Ionization Loss and Dynamic Vacuum in Heavy Ion Synchrotrons”. *Proc.8th Int. Particle Accelerator Conf. (IPAC’17)* (2017).

3 Interaction of Ion- and Laser Beams with Matter

Contribution of recombination processes to ion beam induced light emission

[1]R. Hampf, [2]J. Wieser and [1]A. Ulrich
[1]Technical University Munich, Garching, Germany; [2]Excitech GmbH, Schortens, Germany

Collision of energetic projectiles with target atoms or molecules leads to ionization and population of excited states. Subsequent transitions can lead to light emission in a wide spectral range. The observation of this light can be used for optical beam diagnostics by sending the beam through an appropriate gas target.

We have performed a systematic study of the fundamental processes on this subject. It has in part already been described in references [1-2]. Here, a 85 MeV ^{32}S beam from the Munich Tandem van de Graaff accelerator, with neon and argon gas targets, was used in most of the experiments. The results are interpreted on the basis of an earlier study on ion beam induced light emission [3].

One of the results was that the effective emission cross-sections of atomic lines are much larger than those of ionic lines at higher target gas densities. This is demonstrated by the pressure dependence of selected emission lines shown in Fig. 1.

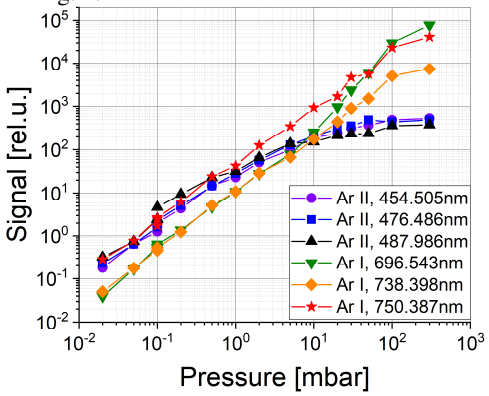

Figure 1: Pressure dependence of the intensity of selected atomic and ionic argon lines excited by a 85 MeV ^{32}S beam.

The following interpretation is used to describe this behaviour: It is known that heavy ions can effectively populate excited states in target ions in single collisions, whereas electrons have a much smaller dross-section for such processes. Thus, it can be expected that recombination processes and subsequent optical transitions in the target atoms of lower ionization stage play an important role in the light emission process. Since the excitation and ionization cross-sections are in general decreasing with increasing stages of ionization it is expected that emission following recombination is particularly intense for neutral target atoms (e.g. the ArI lines in Fig.1) recombining from singly ionized target species (ArII in Fig. 1).

Light emission following recombination in partly ionized low temperature plasmas can be studied by observing the time dependence of light emission following short-pulsed excitation. We have performed such measurements for a selected atomic line (ArI, 696.5nm) for various gas densities (Fig. 2).

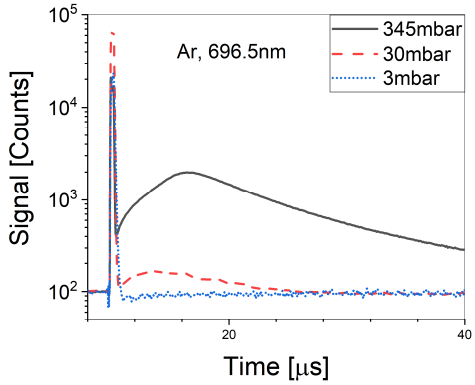

Figure 2: Time dependence of light emission on the 696.6nm ArI line for target gas pressures ranging from 0.4 to 345mbar, after excitation with a 100ns 85MeV ^{32}S beam.

The prompt peak in Fig. 2 is due to direct population of the upper excited level and subsequent optical transitions on the nanosecond scale. The following increase of light intensity is a clear signature for a recombination process (see ref. [4]). The increase is due to cooling of the electron component of the plasma, accompanied by an increased recombination rate. The final decay of the light intensity is just due to the lowering of the electron- and ion density due to the recombination process.

In summary we have studied processes which are relevant for optical beam diagnostics. The experiments were mainly limited to a medium heavy ion projectile and neon and argon as the target species. However, extrapolating the atomic physics processes which have been addressed, it should be possible to predict parameters relevant for optical beam diagnostics for other beam and target combinations.

References

[1] R. Hampf et al. GSI Report High Energy Density 2018
[2] R. Hampf et al., "Evaluation of CCD cameras for beam profile monitoring with high intensity particle beams traversing gases", submitted to EPJT
[3] A. Ulrich, „Lichtemission und Lasereffekt…", Habilitationsschrift, Fak. f. Physik, TU München, Dez. 1998
[4] G. Ribitzki et al., Phys. Rev. E **50** (1994) 3973

Acknowledgement

Work has been funded by BMBF FKZ. 0P2015WOFA1, GSI F&E TUMULRI1719, and MLL Lab. Munich

Research activities at 400 kV High-voltage Ion Beam Platform of Xi'an Jiaotong University

Shuai Yin[1], Wei Liu[1], Jieru Ren[1], Bubo Ma[1], Xing Wang[1], Benzheng Chen[1], Jianhua Feng[1], Yongtao Zhao[1*], Dieter H.H. Hoffamnn[1]

[1] MOE Key Laboratory for Nonequilibrium Synthesis and Modulation of Condensed Matter, School of Science, Xi'an Jiaotong University, Xi'an 710049, China

A 400 kV high-voltage ion beam platform for multidiscipline researches is constructed at Xi'an Jiaotong University (see Fig.1). Currently, a radio-frequency (rf) driven plasma is used as ion source. This enables to provide H^+, H_2^+ and H_3^+ beam with energies up to 400*q keV, where q is the charge state of the ion species. ECR ion source which can provide much wider range of ion species are ready to be coupled to the acceleration lines in the near future. In the current rf ion source, a 13.56 MHz rf power source assembled with a matching system has been used to feed power into the plasma chamber through a copper coil. The current of the ion beam achieves 3 mA at the rf power of 300W. The beam spot size is monitored to be about 1cm after the acceleration tube (see Fig. 2).

Fig.1. The 400 kV high-voltage ion beam platform at Xi'an Jiaotong University.

At this stage, two experimental terminals have been built. On terminal one, the ions are moving along with at the ion-extraction direction. On this terminal, plasma target can be easily mounted on the beam-line for ion-plasma interaction studies, such as energy loss measurements and beam-plasma instability investigations [1]. Another research project in progress on terminal one is to extract a micrometer-scale ion beam into the atmosphere by using a capillary tube [2]. This will provide great opportunities for study of ion induced damages in bio-molecules and cells.

On terminal two, the ions are deflected by 90 degrees with a electromagnet. After passing through another quadrupole electromagnet system, the ion beam is focused into a meter-scale cylindrical chamber. This terminal provides great opportunities for 1) ion-atoms/molecules collision dynamics including the charge transfer process, collisional spectroscopy et al. [3]; 2) ion-surface interactions including secondary electron emissions and capillary guiding effect et al. [4]; 3) ion irradiation effects including damage to materials and widget et al.; 4) nuclear reactions at low energies such as hydrogen-boron reactions that are in progress. Our platform is open to the researcher all over the world.

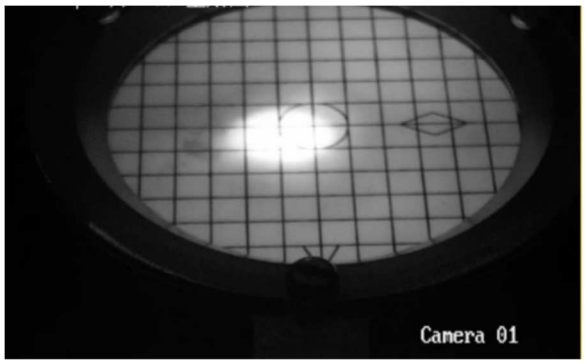

Fig.2. The beam spot after the acceleration tube.

Reference

[1] Rui Cheng et al., Matter and Radiation at Extremes 3, 85-93 (2018).
[2] Shidong Liu et al., Phys. Rev. A 91, 012714 (2015).
[3] Jieru Ren et al., Phys. Rev. A 92, 062710 (2015).
[4] Yuyu Wang et al., Sci. Rep. 4, 5742 (2014).

* zhaoyongtao@xjtu.edu.cn

Z-Pinch Study with Discharge Initiation by an Electron Beam

A. Drozdovsky[1], P. Sasorov[2], A. Bogdanov[1], S. Drozdovsky[1], R. Gavrilin[1], A. Kantsyrev[1], V. Panyushkin[1], I. Roudskoy[1], S.Savin[1]

[1]NRC "Kurchatov Institute" - ITEP, Moscow, Russia, [2]Keldysh Institute of Applied Mathematics, Moscow, Russia

We study the discharge process when an injected electron beam creates a plasma channel after the application of high voltage pulse to the discharge tube. That causes the breakdown throughout the tube cross section. The results of the first experiments in argon at a pressure of 0.2 mbar are given in previous paper [1]. The experimental setup was described in [2]. At present we were able to expand the capabilities of our installation to perform some experiments at a higher gas pressure, up to 10 mbar.

A special carousel-type system was created for vacuum separation of the Z-pinch discharge chamber and the electron beam transport channel (Fig. 1). The system consists of a disk with Mylar windows rotating in a chamber. The electrons pass through the upper window located on the beam axis. Each window is a plastic shell ring, in which a 0.5 μm Mylar film is fixed (Fig. 2). This device allows a pressure drop between the electronic gun and the discharge chamber from ~ 0.02 to ~ 10 mbar.

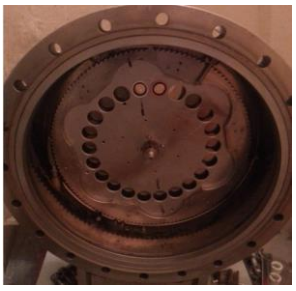

Figure 1: The chamber

Figure 2: The window

Plasma escaping from the discharge tube burns the film. After shot the rotary device sets a new window. During the session, one can make 21 shots. Replacement of the windows is made through a special vacuum opening. This procedure, can be performed in 2 hours.

After the setup upgrading, the initial series of z-pinching studies was carried out using a quartz tube 20 cm long and 4 cm in diameter. The electron beam parameters were as follows: the inlet current ~10 A, the pulse duration ~50 ns, the beam diameter ~1.5 cm. The discharge current amplitude was ~40 kA. The Figures 4÷6 show the time scan of the discharge plasma luminosity at different gas (oxygen) pressures. In each of the pairs of images, the lower one is obtained without the electron beam. The beginning of the scan corresponds to the moment when the discharge current occurs (Fig. 3). At the same time, the voltage on the discharge tube fall sharply due to the breakdown initiated by the electron beam. The surge and dip on the voltage and current curves display the features of the pinching process visible in the luminosity pictures.

One can see from the luminosity images that the effect of pinch narrowing during initiation by beam decreases at a pressure of more than ~0.5 mbar. The main reason for this seems to be the broadening of the electron beam due to scattering at a higher gas density.

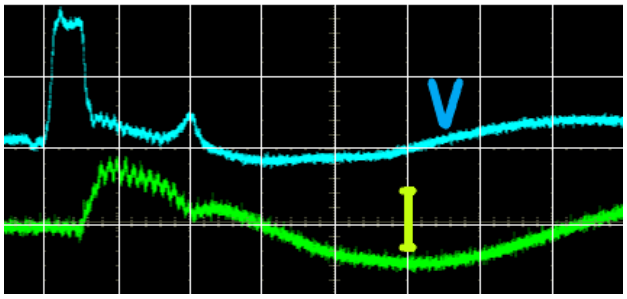

Figure 3: Discharge voltage and current waveforms, Δt = μs

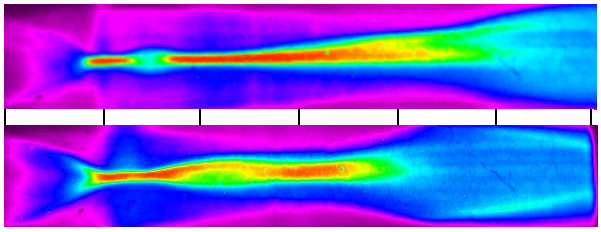

Figure 4: Discharge luminosity for 0.1 mbar, Δt = 1μs

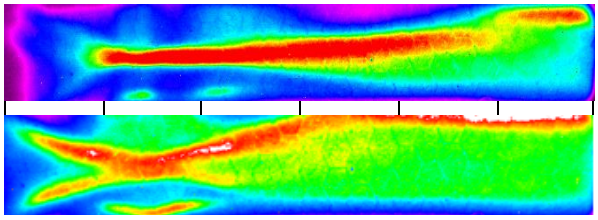

Figure 5: Discharge luminosity for 0.2 mbar, Δt = 1μs

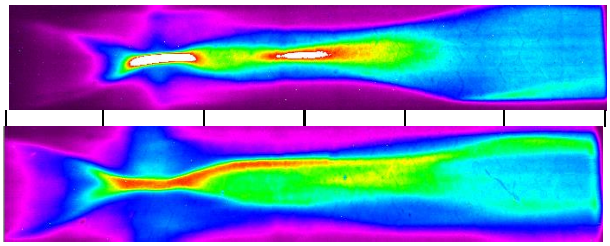

Figure 6: Discharge luminosity for 0.4 mbar, Δt = 1μs

References

[1] A.A.Drozdovsky et al., Research on Plasma Lens with Discharge Initiation an Electron Beam, GSI Report 2019-2, October, 2019, 41.

[2] A.A.Drozdovsky et al., The Research of the Plasma of Z-Pinch Initiated by the Electron Beam. Physics of Particles and Nuclei Letters, Vol. 15, No. 7, 2

* Work supported by the Russian Foundation for Basic Research (grant 18-02-01187/18)

Ablation mode of polymers by nanosecond intense pulsed ion beam□

X. Yu[1], S. Zhang[2], S. Yan[3], G.E. Remnev[2], X. Le[2,#]
[1]GSI, Darmstadt, Germany; [2]Beihang University, Beijing, China, [3]Peking University, Beijing, China.

Intense pulsed ion beam (IPIB) in nanosecond pulse length was first proposed for inertial confined fusion (ICF) and is also widely used for material surface treatment and material performance verification for fusion reactors. Nowadays, IPIBs used for the above research are characterized by generation from plasma ion source with ion energy typically within 1 MeV, pulsed length hundreds of ns and current density up to several hundred A/cm^2. These IPIBs can introduce pulsed power in the order of GW/cm^2 on the target surface and may induce surface ablation.

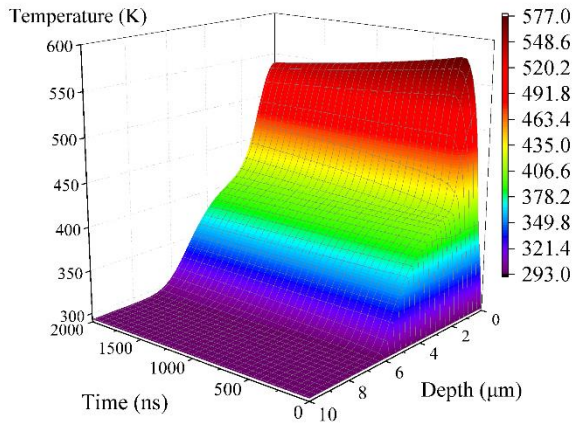

Figure 1: Temperature distribution in PMMA under 0.13 J/cm^2 after IPIB irradiation.

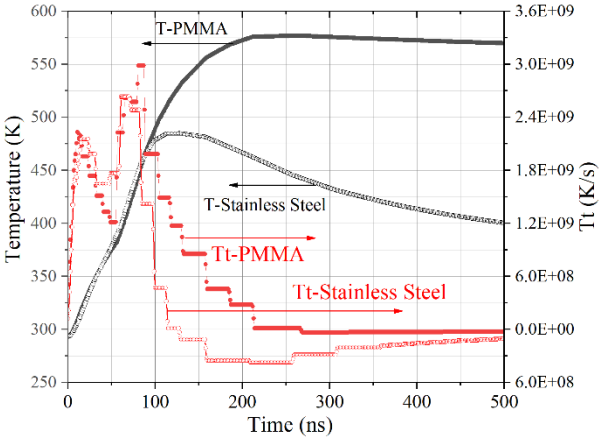

Figure 2: Calculated temperate and its change rate in 304 stainless steel and PMMA with a cross-sectional energy density of 0.13 J/cm^2.

As revealed experimentally when IPIB acts on material with high thermal resistance and low evaporation threshold, the ablation plasma may form a shield layer and a high portion of over 80 % of the beam energy may be shielded from depositing in the target [1]. Recently this phenomenon was further explored. The temperature field induced by IPIB irradiation on polymer was calculated by finite element method [2], and mass loss measurement was carried out on PMMA under IPIB irradiation with a Mettler XP205 balance with a precision of 10 μg.

For the temperature field distribution, it is demonstrated that under an energy density of 0.13 J/cm^2, the maximum surface temperature of PMMA already approaches the decomposition temperature (Fig. 1). In PMMA, the thermal conductivity is typically smaller by two or three orders of magnitude than in metals and the temperature evolution exhibits a different trend compared with that in stainless steel during IPIB irradiation (Fig. 2). For its low thermal conductivity, although the power density is lower in PMMA due to the larger range of ions, the rate of temperature increase is higher. Also, the temperature decreasing rate in the near-surface region of PMMA is much smaller than in stainless steel and generally the heating and cooling of PMMA exhibit a quasi-adiabatic trend.

The mass loss experiment of PMMA was carried out with PMMA samples with dimensions of 10×10×1 mm^3 under IPIB energy densities of 3.78 and 1.96 J/cm^2. The average mass loss by one pulse is 0.38 mg at an energy density of 1.96 J/cm^2 and further increased to 0.49 mg at 3.78 J/cm^2. Regarding a density of 1.2 g/cm^3, a thickness of 3.16 to 4.08 μm was ablated away and this is already more than the maximum range of carbon ions which forms the later portion in a pulse that arrives at the sample [3]. Also, it is observed that under given beam energy, the mass loss increases proportionally to the pulse number. This is dissimilar to the ablation of metals in which the first pulse may lead to much larger mass loss [4]. This can be explained by different ablation modes under varied degrees of ablation. On metals, the ablation is relatively weak and a large portion of the beam energy can deposit in the target and the surface properties may gradually evolute and reach a relatively stable state under the irradiation of initial pulses. While on materials such as polymers where ablation is more easily induced, the heating and ablation of the target are achieved more by ablation plasma heated by IPIB rather than directly by IPIB. The thermal effect is strong enough to make the target conditioning done during the first pulse, making the ablation of the target more uniform for pulses in a series, leading to a proportional increase in the mass loss with the increase of pulse number from the first pulse.

References

[1] X. □u, et al., GSI Report 2019-2, p. 40
[2] X. □u, et al., Vacuum, 113 (2015), pp. 36-42
[3] X. □u, et al., Vacuum, 122 (2015), pp. 12-16
[4] J. Zhang, et al, Nucl. Instrum. Meth. B, 365 (2015) pp. 210–213

* Work supported by China, NSFC contract No. 11875084.
# xyle@buaa.edu.cn

Development of Ion Stopping Models for HED Plasmas Using Unified Self-Consistent Field Models and Self-Consistent Electron Distributions

T.A. Mehlhorn[1,#] and I.E. Golovkin[2]

[1]U. Michigan, Beaverton, OR, U.S.A.; [2]Prism Computational Sciences, Inc, Madison, WI, U.S.A.

Ion stopping power is a fundamental transport property in plasma physics and plays a central role in a wide variety of high energy density laboratory plasmas (HEDLP) experiments, including charged particle energy deposition in fusion burn waves. Ion stopping power was extensively studied as a primary source of energy deposition in light ion beam fusion [1] and remains of interest in heavy ion beam experiments to generate warm dense matter (WDM) [2]. The topic is especially relevant given the exponential growth in the use of ultrashort pulse laser (USPL) systems to accelerate beams of light and heavy ions to increasingly higher energies and at ever greater intensities. Ion stopping power is central to the generation of many diagnostic signals as a result of inflight atomic and/or nuclear reactions. The favorable transport, focusing, and deposition properties of USPL-generated light ions have led to proposals for their use in fast ignition inertial confinement fusion (ICF) targets, as well as a non-equilibrium approach to efficiently accessing the $(\mathrm{p,B^{11}},3\alpha) + 8.9\ MeV$ fusion reaction. The irradiation of clusters by USPLs has been used to both produce fusion reactions (cluster fusion) as well as the production of high energy x-rays from inner shell atomic processes, through inflight reactions. There is emerging evidence from China and Germany that the intensity of USPL-generated ions is reaching conditions where correlated ion stopping power is relevant. Work in Europe and Japan using cluster ion beams rely on the enhanced stopping power of correlated ions to achieve higher specific energy densities at lower beam currents. Ion stopping power is essentially the first moment of the Fokker-Planck collision operator and plays an important role in determining the "ion drag term" in multi-fluid plasma simulations, which are becoming of greater importance. It is important to verify the accuracy of ion stopping power models for non-hydrogenic plasmas, especially high-Z plasmas. Development and inclusion of improved models for ion stopping power for simulation of pulsed power transmission lines and convolutes is important to next generation pulsed power designs.

We are developing improved ion stopping models for the electronic component of HED plasmas using unified self-consistent field models and self-consistent electron distributions, based on based on the random phase approximation (RPA) formalism of Wang, Mehlhorn, and MacFarlane [3]. This approach uses the dielectric formulation of stopping power combined with the local density approximation as applied to electron distribution functions computed using relevant atomic physic models. We are exploring the inclusion of the latest results in dielectric response functions and dynamical ion structure factors. We will also undertake a careful evaluation of the electron distribution function in HED regimes, especially in WDM (strong coupling) or plasmas where quantum effects (Fermi degeneracy) are important, as well as compute ion stopping powers for materials under extreme conditions (MEC), where high pressure electrides have been observed to form. We will also explore inclusion of the effect of the intense USPL fields on effective potentials [4]. We are using our experience with both detailed atomic physics simulations (muffin tin models), as well as computations using electron distributions calculated with the PQEOS model. We are also developing a framework for efficiently computing in-flight beam reactions for diagnostic and fusion applications. The goal of this work is to provide an efficient and robust framework for computing energetic ion energy deposition in HED plasmas spanning a wide range of temperatures and densities relevant and to incorporate these models into the HELIOS-CR hydro code (Prism) as well as the Chicago hybrid code (Voss). We plan to study the impact of electric and magnetic fields on ion stopping power through Chicago simulations. We will validate the models and the codes using available data from stopping power experiments and by comparing with other published results. Finally, we plan to use these codes to study the impact of these improved models on two important HED applications: 1) pulsed power transmission lines and convolutes, 2) various USPL ion beam acceleration and interaction experiments.

References

[1] T. A. Mehlhorn, "A finite material temperature model for ion energy deposition in ion-driven inertial confinement fusion targets," *JAP* **52**,11, p6522 1981.

[2] Schoenberg, K., V. Bagnoud, A. Blazevic, V. E. Fortov, D. O. Gericke, A. Golubev, D. H. H. Hoffmann, D. Kraus, I. V. Lomonosov, V. Mintsev, S. Neff, P. Neumayer, A. R. Piriz, R. Redmer, O. Rosmej, M. Roth, T. Schenkel, B. Sharkov, N. A. Tahir, D. Varentsov and Y. Zhao (2020). "High-energy-density-science capabilities at the Facility for Antiproton and Ion Research." Physics of Plasmas **27**(4): 043103 .

[3] P. Wang, T. A. Mehlhorn and J. J. MacFarlane (1998). "A unified self-consistent model for calculating ion stopping power in ICF plasma." Physics of Plasmas **5**(8): 2977-2987.

[4] H. B. Nersisyan and C. Deutsch, "Stopping of ions in a plasma irradiated by an intense laser field," *Laser and Particle Beams,* vol. 29, no. 4, pp. 389-397, 2011.

[#]tamehlhorn97@gmail.com

New unified model for fast charged particle cross sections, mean free paths, and stopping powers in solids

N. Medvedev[1,#], A.E. Volkov[2,3,4]

[1] Institute of Physics and Institute of Plasma Physics, CAS, Prague, Czechia; [2] NRC 'Kurchatov Institute', Moscow, Russia; [3] P.N. Lebedev Physical Institute, RAS, Moscow, Russia; [4] Joint Institute of Nuclear Research, Dubna, Russia

We have developed an analytically integrable model of the differential inelastic cross sections of scattering of charged projectiles in solids [1]. It provides closed solutions for inelastic cross sections, mean free paths, and energy losses (stopping power, S_e) for an arbitrary charged particle (electrons, positrons, protons, ions, etc.) within a unified framework. It is applicable within a broad range of incident energies (e.g., from 30-50 eV up to GeV in a case of an electron). Only the optical data are used as an input, without any *ad-hoc* correction terms, splitting into close and distant collisions, or fitting and adjustable parameters.

Our derived total inelastic cross section of scattering is defined by the simple expression:

$$\sigma = \frac{Z_{eff}^2(E)}{n_{at}\pi a_0 m_e c^2 \beta^2} \sum_i^{N_{osc}} \frac{\alpha_i(0) m_t c^2}{E_{0_i} m_e c^2} \left[\ln\left(\frac{\widetilde{W}_+ - E_{0_i}}{\widetilde{W}_- - E_{0_i}}\right) - \ln\left(\frac{\widetilde{W}_+}{\widetilde{W}_-}\right)\right] \quad (1)$$

where E is the incident particle kinetic energy, n_{at} is the atomic density of the target, M is the incident particle rest mass, m_t is the rest mass of the scattering centre (free electron mass m_e), $Z_{eff}(E)$ is the effective charge of the incident particle, a_0 is the Bohr radius, $\beta = v/c = \sqrt{1-(1+E/Mc^2)^{-2}}$ is the incident particle velocity normalized to the speed of light in vacuum c, constant $\alpha_i(0)$ is defined by the optical coefficients, and the integration limits $\widetilde{W}_\pm$ are defined in [1] (related to positions of optical oscillators, E_{0_i}).

The inelastic energy loss is defined as [1]:

$$S_e = \frac{Z_{eff}^2(E)}{\pi a_0 m_e c^2 \beta^2} \sum_i^{N_{osc}} \frac{\alpha_i(0)}{m_e c^2} \left[(2Mc^2 - m_t c^2)\ln\left(\frac{2Mc^2 + \widetilde{W}_+ - E_{0_i}}{2Mc^2 + \widetilde{W}_- - E_{0_i}}\right) + m_t c^2 \ln\left(\frac{\widetilde{W}_+ - E_{0_i}}{\widetilde{W}_- - E_{0_i}}\right)\right] \quad (2)$$

Usage of the derived formulae greatly saves computational time of evaluation of cross sections with respect to the numerical integration required by other models [2].

* Partial financial support from the Czech Ministry of Education, Youth and Sports, Czech Republic [grants numbers LTT17015, LM2015083] is acknowledged by N. Medvedev. The work was supported by the Ministry of Science and High Education of the Russian Federation *in the frameworks of* Project No. 16 APPA (GSI).

nikita.medvedev@fzu.cz

Fig.1 shows examples of calculated electron inelastic scattering cross sections and energy losses of gold ion in solid aluminum [1]. The results compare very well with those of the standard models.

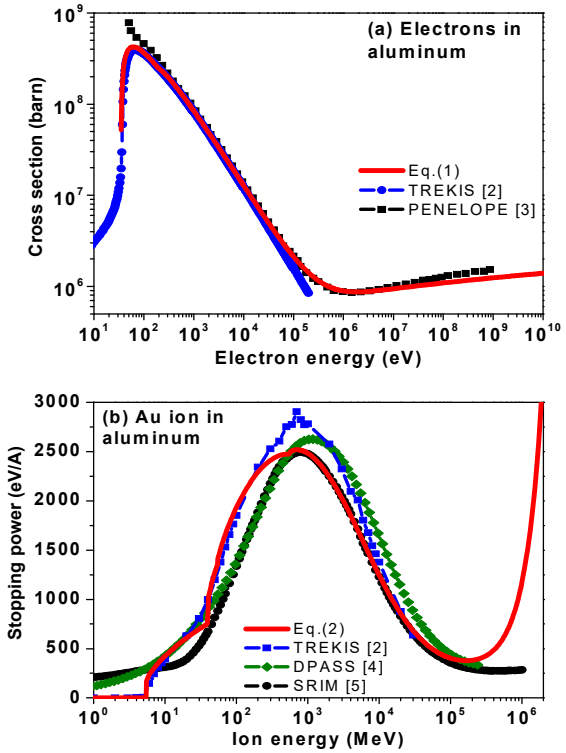

Fig. 1: (a) Electron inelastic mean free path in aluminum calculated with our cross section [1], results from TREKIS [2], and PENELOPE [3]. (b) Inelastic energy loss of gold ion in Al calculated with our model [1], compared to TREKIS [2], SRIM [4] and DPASS [5].

References

[1] N. Medvedev, A.E. Volkov, J. Phys. D. Appl. Phys. (2020): https://doi.org/10.1088/1361-6463/ab7c09

[2] N.A. Medvedev, R.A. Rymzhanov, A.E. Volkov, J. Phys. D. Appl. Phys. **48**, 355303 (24pp) (2015).

[3] F. Salvat and M. Fern, *PENELOPE-2014 – A Code System for Monte Carlo Simulation of Electron and Photon Transport*, 2015th ed. (NUCLEAR ENERGY AGENCY, Organisation for Economic Co-operation and Development, Barcelona, Spain, 2015).

[4] J. P. Ziegler, U. Biersack, and J. F. Littmark, *The Stopping and Range of Ions in Solids* (Pergamon Press, New York, 1985).

[5] A. Schinner, P. Sigmund, NIMB **460**, 19 (2019).

Monte Carlo simulation of the energy distribution in laser-irradiated solids under the influence of a magnetic field

X. del Arco[1], *J. Amann*[1], *M. Schäfer*[2], *F. G. Keabou*[2], *G. Torosyan*[2], *J. A. L'huillier*[2], *P. N. Terekhin*[1], *and B. Rethfeld*[1]

[1]Department of Physics and Research Center OPTIMAS, Technische Universität Kaiserslautern, Erwin-Schrödinger-Strasse 46, 67663 Kaiserslautern, Germany

[2]Photonik-Zentrum Kaiserslautern e.V. and Research Center OPTIMAS, 67663 Kaiserslautern, Germany

We study the distribution of electrons in lateral space of a surface irradiated with an ultrashort laser pulse, using a Monte Carlo method. We aim to study the energy transfer to the lattice in order to optimize the conditions for material ablation. In such a system the excited electron can share its energy with another electron, that gets then excited as well (secondary electrons) or with the lattice itself, which results in an increase of the temperature of the solid. Motivated by Farrokhi et al. [1, 2], we investigate whether the application of an homogeneous external magnetic field can optimize this ablation process. As a first approach we allow the electrons to have two kinds of interactions: *inelastic scattering* and *impact ionization*. In the first, the electron loses energy to the lattice and changes its direction randomly. In the second, the electron excites a new electron. The initial one doesn't change its direction, while the second one is initialized with a random direction.

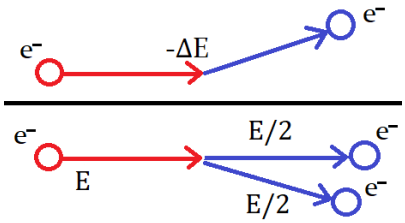

Figure 1. The process depicted in the top figure corresponds to *inelastic scattering* and the process in the bottom figure to *impact ionization*. The color change from red to blue represents the interaction taking place. In inelastic scattering the energy is transferred to the lattice, while in the impact ionization process the energy gets equally divided between the two electrons.

We use the program without the magnetic field to check whether the energy is conserved and to be sure that the two processes discussed in Fig. 1 work as expected. The interesting part comes when we plug the magnetic field on. We analyze the electrons movement in a x-y plane whereas the magnetic field is directed in z direction. In such configuration charged particles start a circular movement in the x-y components of their velocity, as we can observe in Fig. 2. This circular movement has a radius called gyroradius or Larmor radius, with $R_L = \frac{m_e v_\perp}{eB}$, where m_e is the electron mass, e is the electron charge, B the magnetic field induction and $v_\perp$ the module of the velocity in the plane perpendicular to the magnetic field.

In Fig. 2 we can also observe the behaviour of a single particle, only allowed to have *inelastic scattering* inter-actions, with a magnetic field applied. Without magnetic field the particles are free to keep moving to any direction once they don't have more energy for more interactions, however, with magnetic field the particles will be traped in a circular movement after the stabilization time. In this way, after time passes and secondary electrons are gener-ated, electrons stay in a Gaussian profile, as can be seen in Fig. 3.

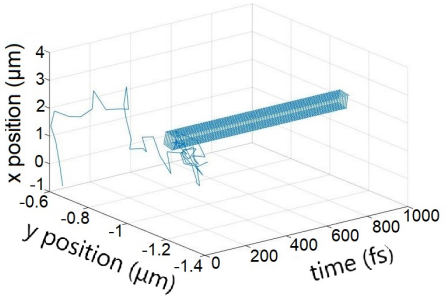

Figure 2. The electron changes its direction randomly due to *inelastic scattering* processes. This behaviour keeps going until the electron has no more energy to perform more interactions (stabilization time). Normally at this point the electron would follow a linear movement, but the magnetic field generates the circular movement.

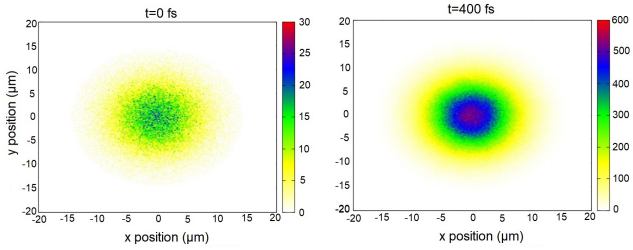

Figure 3. Evolution of the number of particles organized in colour code for 10^5 initial electrons with both interactions allowed and a magnetic field of 1 T. After 400 fs the Gaussian shape is preserved, so there is no diffusion.

This results in the total energy to stay more concentrated in a focused area within the material, what is very promissing for an improved ablation process.

References

[1] H. Farrokhi et al., Appl. Phys. Lett., **108**: 254103 (2016).

[2] H. Farrokhi et al., J. Opt. Soc. Am. B, **36**: 1091 (2019).

Transport of intense particle beams in large scale plasmas

B. Z. Chen[1,2], D. Wu[2,*], J. R. Ren[1], D. H. H. Hoffmann[1], and Y. T. Zhao[1,#]

[1]MOE Key Laboratory for Nonequilibrium Synthesis and Modulation of Condensed Matter, School of Science, Xi'an Jiaotong University, Xi'an 710049, China

[2]Institute for Fusion Theory and Simulation, Department of Physics, Zhejiang University, Hangzhou 310058, China

Transport of particle beams in plasmas is widely employed in fundamental research, industry and medicine. Due to the high inertia of ion beams, their transport in plasmas is usually assumed to be stable. Here we report the focusing and flapping of intense slab proton beams transporting through large scale plasmas (Fig.1) by using a newly developed particle-in-cell simulation code [1-3].

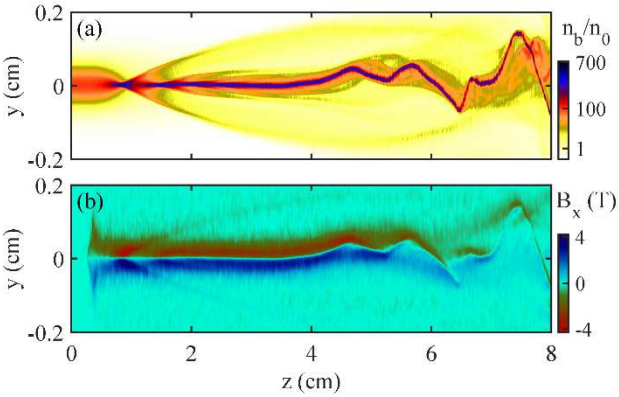

Figure 1: Distributions of (a) beam density (in units of $n_0 = 10^{14}$ cm^{-3}) and (b) magnetic field for a proton beam with initial density of 1×10^{16} cm^{-3} and energy of 0.4 MeV at 12 ns

The beam self-focusing effect in the simulation is prominent and agrees well with previous experiments and theories. Moreover, the beam can curve and flap like turbulence as the beam density increases in Fig.1(a). Simulation and analysis indicate the self-generated magnetic fields, produced by movement of collisional plasmas, are the dominant driver of such behaviours. By analysing the growth rate of magnetic energy (Fig.2) and energy deposition of injected proton beams, it is found that the focusing and flapping are significantly determined by the injected beam densities and energies. And a remarkable nonlinear beam energy loss is observed [4]. Our research might find great applications in inertial confinement fusion and also might be of interests to the laboratory astrophysical community.

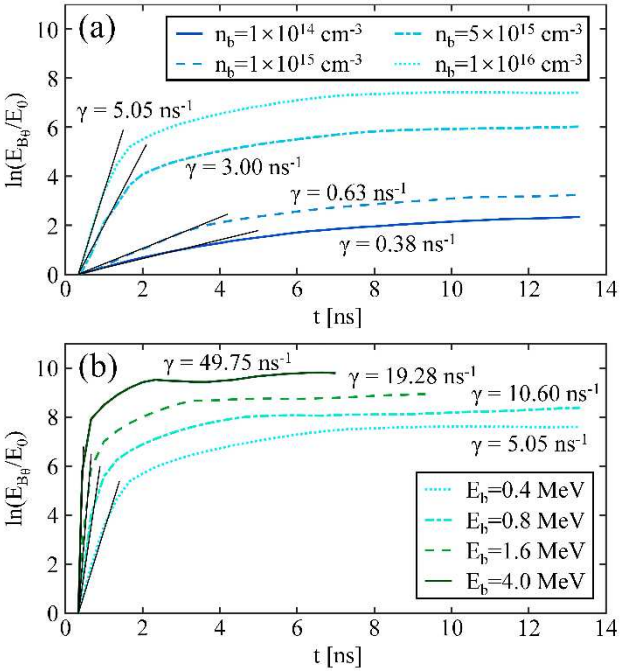

Figure 2: Magnetic field energies for (a) proton beams with fixed 0.4 MeV but with different densities and (b) proton beam with fixed density 10^{16} cm^{-3} but with different energies as functions of time.

References

[1] D. Wu, W. Yu, Y. T. Zhao, D. H. H. Hoffmann, S. Fritzsche, and X. T. He, Phys. Rev. E 100, 013208 (2019).

[2] D. Wu, X. T. He, W. Yu, and S. Fritzsche, High Power Laser Sci. Eng. 6, e50 (2018).

[3] D. Wu, W. Yu, S. Fritzsche, and X. T. He, Phys. Rev. E 100, 013207 (2019).

[4] B. Z. Chen, D. Wu, J. R. Ren, D. H. H. Hoffmann, and Y. T. Zhao, Phys. Rev. E 101, 051203 (2020).

* dwu.phys@zju.edu.cn

zhaoyongtao@xjtu.edu.cn

Effects of an additional current on laser heating of silicon

S. Hirtle[1], *Y. Kang*[2], *G. Torosyan*[2], *M. Schäfer*[2], *J. A. L'huillier*[2], *P. N. Terekhin*[1], *and B. Rethfeld*[1]

[1]Department of Physics and Research Center OPTIMAS, Technische Universität Kaiserslautern, Erwin-Schrödinger-Straße 46, 67663 Kaiserslautern, Germany

[2]Photonik-Zentrum Kaiserslautern e.V. and Research Center OPTIMAS, 67663 Kaiserslautern, Germany

In this report, we extend a density-dependent two-temperature model (nTTM) [1], which describes laser heating of silicon, by introducing an additional current. This can be understood as a first approach to investigate the effects of an external electric field.

The nTTM is governed by rate equations for the three independent parameters, namely the free carrier density n_e, the electron-hole temperature T_e and the phonon temperature T_{ph}:

$$\frac{dn_e}{dt} = G - R - \vec{\nabla} \cdot j \,, \tag{1a}$$

$$\frac{du_e}{dt} = L - \vec{\nabla} \cdot \left(\Pi j - \kappa_e \vec{\nabla} T_e \right) - g \left(T_e - T_{ph} \right) \,, \tag{1b}$$

$$\frac{du_{ph}}{dt} = \vec{\nabla} \cdot \left(\kappa_{ph} \vec{\nabla} T_{ph} \right) + g \left(T_e - T_{ph} \right) \,. \tag{1c}$$

Eq. (1a) describes the time evolution of the free carrier density. Carrier Generation (G) by one- and two-photon absorption and impact ionization, as well as Auger recombination (R) are taken into account. The last term considers transport by the carrier current j. Eqs. (1b) and (1c) describe the evolution of the energies of the electron-hole system and the phonon system u_e and u_{ph}, respectively, from which the corresponding temperatures are obtained. The electron-hole system is heated by a $800\,\mathrm{nm}$ laser pulse with a pulse duration of $100\,\mathrm{fs}$. L stands for one- and two-photon absorption by electrons in the valence band, as well as one-photon absorpion by free carriers in the conduction band [1]. Heat transport in the phonon-subsystem is described by Fourier's law, whereas a treatment of the Peltier effect is additionally included for the carrier-subsystem. The energy exchange between electrons and phonons is governed by the coupling coefficient g.

The nTTM assumes ambipolar diffusion, which means that electrons and holes move together as pairs and carrier and current densities are prohibited from differing from each other. Consequently, the carrier densities and current densities used here correspond to electron-hole pairs. The carrier current j is caused by gradients in the free carrier density, the energy gap, as well as the electron-hole temperature. In a first approach to investigate the effects of an external electric field, an additional carrier current j_{add} proportional to the carrier density

$$j_{\mathrm{add}} = v \cdot n_e \tag{2}$$

is added to j. The proportionality constant v can be understood as the drift velocity of the free carrier pairs. For negative v, the additional current is headed from the inside of the material towards the laser-irradiated surface and vice versa.

Fig. 1 depicts the spatial profile of the phonon temperature obtained by solving Eqs. (1a)-(1c) for a sample thickness of 800 nm, 40 ps after the start of the laser irradiation, approximately the time when the maximum phonon temperature at the laser-irradiated surface is reached. Compared to the profile without an additional current (solid line), the phonon temperature is raised near the laser irradiated surface and lowered near the back side for an additional current, that is headed from the inside of the material towards the laser irradiated surface (dashed line). The opposite effect can be observed for an additional current headed in the other direction (dash-dotted line).

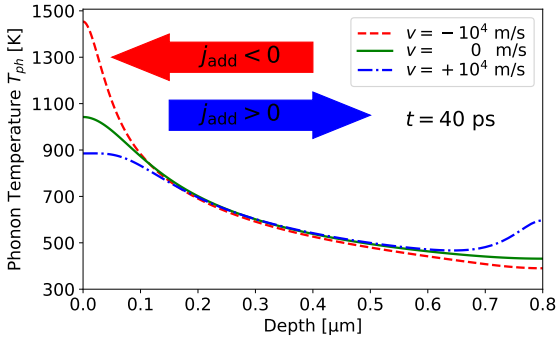

Figure 1. Spatial profile of the phonon temperature T_{ph} at 40 ps after the laser irradiation for different drift velocities v of the additional current.

Two mechanisms play a role in influencing the electron temperature and consequently also the phonon temperature profile. Primarily, the additional current causes a carrier heat current that changes the electron temperature profile.The additional current also changes the spatial carrier density profile during the laser irradiation, which has an effect on the local free carrier absorption coefficient and consequently on the energy absorbed by the free carriers locally.

It has been shown that an additional carrier pair current has an effect on the spatial phonon temperature profile of a laser-heated silicon sample. Further research is needed to extend these results to the case, in which electrons and holes are treated separately in an external electric field and the electric potential that builds up due to the corresponding charge separation is taken into account.

References

[1] A. Rämer, O. Osmani and B. Rethfeld, *J. Appl. Phys.*, **116**, 053508 (2014).

Monte-Carlo Simulation of Bremsstrahlung Photon Spectra from 10 µm Au Target Induced by Laser-driven Electron Beams

N. Zahn[1], O. Rosmej[1,2], A. Sokolov[2], M. Gordimov[1], F. Horst[2,4], E. Kozlova[2], T. Radon[2], N. Borisenko[3], J. Jacoby[1]

[1]Institute for Applied Physics (IAP), Goethe University, Fankfurt, Germany; [2]GSI Helmholtzzentrum für Schwerionenforschung, Darmstadt, Germany; [3]Lebedev Physical Institute (LPI), Russian Academy of Sciences (RAS), Moscow, Russia; [4]Justus-Liebig-University, Giessen, Germany;

The detailed description of the distribution of the photon emission induced by an interaction of relativistic electron beams with different target materials and definition of the characteristics of the produced bremsstrahlung photons such as energy, intensity and angular distribution is important for optimization of the photon source for nuclear applications. The intensity of bremsstrahlung depends on the energy of the incoming electrons, the atomic number (Z) and the thickness of the target material.

The interaction of relativistic sub-picosecond laser pulses produced by the PHELIX-system with extended, sub-mm long near-critical electron density plasmas provides essential acceleration of electrons and consequent effective transfer of the laser energy to fast MeV energetic electrons. The laser had parameters of 80-100J energy measured after compressor, 750 fs pulse duration and 1-2×10^{19} W/cm^2 intensity. Low density polymer foam layers (2mg/cc Triacetate-Cellulose $C_{12}H_{16}O_8$) with a thickness of 325 µm were used as targets to create such type of hydrodynamic stable, large scale, quasi-homogeneous plasmas [1].

For measurements of the gamma bremsstrahlung spectra 8 channels TLD-spectrometer based on thermoluminescence dosimetry method was used. This spectrometer is created for an energy range from 30 keV to 100 MeV and is designed as a compact version of the TLD spectrometer described in [2]. Eight TLD-cards are placed between absorbers of different material and thickness (Cu-6mm, 9mm, 10mm; Fe-14.5mm, 19mm, 20mm; Pb-15mm) inside a Pb shielding with four collimator windows in the front. The absorbers cause a different response of every TLD, which can be used as information about the spectrum of the incident x-rays. The electron energy distribution spectra were directly analysed with an electron spectrometer by applying a static magnetic field.

Employing the Monte Carlo code FLUKA [3] the generated by electrons beam bremsstrahlung spectra and exiting electron spectra from Au target were simulated.

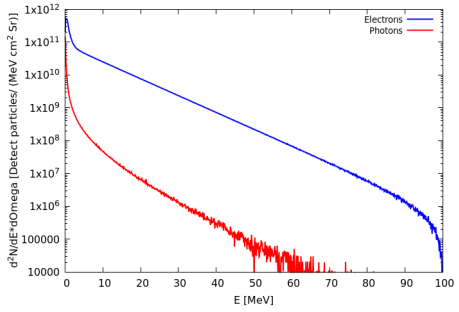

Figure 1: Double differential fluence of photons and electrons from 10 µm Au target.

Figure 1 shows electrons and the bremsstrahlung photon fluences obtained as the result of interactions of laser-driven electrons with a spectral energy distribution within the energy range of 100 keV - 100 MeV with 10µm thick Au foil-target along the beam direction. The angle between the electron beam and the position of TLD spectrometer was 16°. Since the laser interacts with a plasma created on a very thin Au foil the produced electron spectrum is only dependent on the laser characteristics and not on the target material [1]. The distribution of the photons in the simulated area which included target and TLD spectrometer is shown in Figure 2.

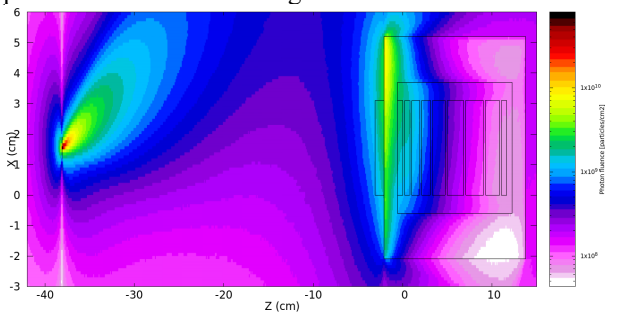

Figure 2: Top view of photon fluence distribution in space of target and 8-channels TLD spectrometer [photons/cm^2].

Figure 3 presents the simulated and the experimental results of the dose on crystals of TLD-spectrometer. They have a very good agreement that indicates the reliability of the established model and supports the results of measurements of electron and photon spectra.

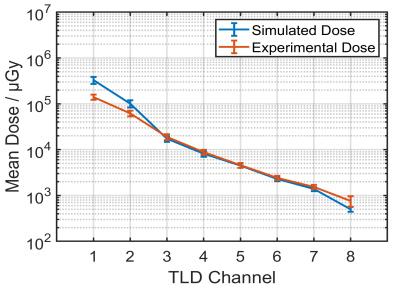

Figure 3: Comparison of the dose distribution in the spectrometer obtained by measurements and by Monte Carlo simulations.

References

[1] F. Horst *et al.*, NIM A **782** (2015) p. 69-76.
[2] O. Rosmej *et al.*, 2019 *New J. Phys.* https://doi.org/10.1088/1367-2630/ab1047
[3] A. Ferrari *et al.*, CERN–2005–10 (2005), INFN/TC 05/11, SLAC–R–773

PIC Simulation of the Directionality of Proton Acceleration in Laser irradiated Micro-Plasma*

V. Pauw[†1,2], *P. Hilz*[1], *and H. Ruhl*[2]
[1]LMU, Munich, Germany; [2]LRZ, Garching, Germany

We used PIC-simulations (PSC [1]) to investigate the fast ions produced by irradiating hydrogen-clusters and polystyrene spheres with short ultra-strong laser pulses (30-90 fs FWHM, 68 J).

Optimizing Target Properties for Higher Directionality and Maximum Energy of the Proton Beam

Target size and density are varied while the laser focal spot is matched to the sphere size for optimal energy transfer. The target is irradiated with a 30fs FWHM (E-field intensity) Gaussian pulse for three target sizes ($1.3\,\mu m$, $2\,\mu m$, $3\,\mu m$) . Varying a_0 for the different pulse lengths and foci keeps the total pulse energy constant. Scanning densities from $2\,n_c$ (n_c non-relativistic critical electron density) to solid densities ($336\,n_c$), we observe that in addition to the proton acceleration driven by Brunel heating and ponderomotive electron removal (TNSA, Coulomb explosion), an RPA driven shock can significantly contribute to the acceleration, when the target density is in the relativistically transparent range. If this is the case, the initial position of the fastest protons shifts from the target rear to the target front (Fig. 1) and the directionality of the expelled fast protons rises significantly (Fig. 2).

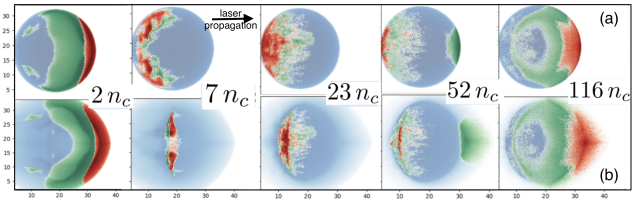

Figure 1: Fast particle back-tracking in a $2\,\mu m$ sphere showing the starting positions of fast protons (red: $> 0.85\,\epsilon_{max}$ of, green: $> 0.3\,\epsilon_{max}$) 100 fs (a) before and 15 fs (b) after pulse maximum

The maximal kinetic energy ϵ_{max} and the ϵ_{tot} of the forward directed fast protons also follow this pattern, showing that at a density in the optimal range, a much better proportion of the laser energy can be delivered into the forward directed proton beam.

The ratio of forward directed protons can e further when using circularly polarized (CP) instead of linearly polarized (LP) pulses. For a $1.3\,\mu m$ radius, $7.5 n_c$ hydrogen target, the kinetic energy delivered in the forward cone relative to the sideward cone increases from 7.4 to 16.4.

* Computing resources provided by GCS project pr74si
† viktoria.pauw@physik.uni-muenchen.de

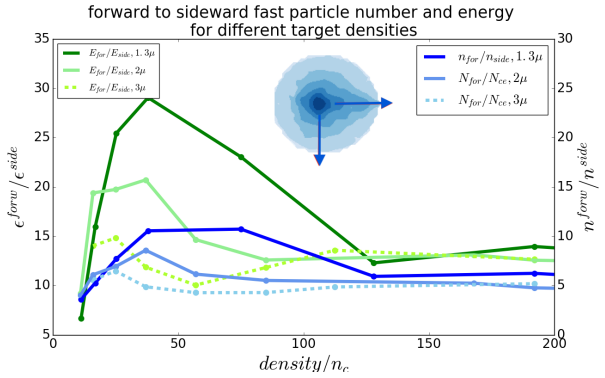

Figure 2: Relative number/Relative cumulative energy of the fast protons inside a forward directed cone to a sideward directed cone within 10 degree angle

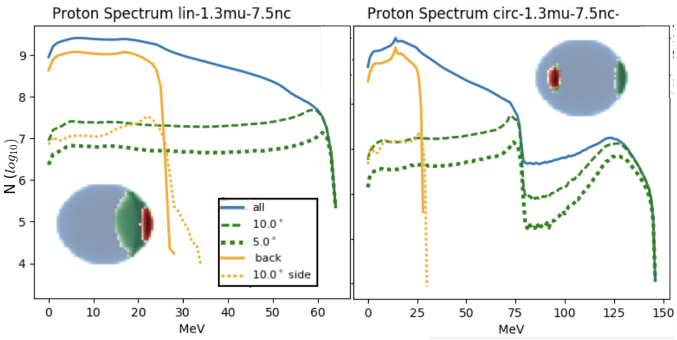

Figure 3: Proton spectrum in different directions for LP ($a_0 = 112$) and the corresponding CP pulse. Inlay: initial position of fast (green and red) protons, shifts from back to front.

For higher densities ($23\,n_c$) there is no significant gain in energy or directionality by employing a CP pulse. In conclusion we see that if the size and density of the target can be sufficiently well defined in experiment [3], the angular distribution of accelerated protons can be expected to be either more isotropic or more directed.

References

[1] K. Germaschewski, H. Ruhl, A.Bhattacharjee, , et al "The Plasma Simulation Code: A modern particle-in-cell code with patch-based load-balancing", Journal of Computational Physics 318 (2016)

[2] T.M. Ostermayr , et al, 'Proton acceleration by irradiation of isolated spheres with an intense laser pulse", Phys. Rev. E 94, 033208 (2016).

[3] P. Hilz, et al "Isolated proton bunch acceleration by a petawatt laser pulse", Nat. Comm. (2018)9:423.

Studies on Spin Polarization in High Density Degenerate Plasma

Punit Kumar, Shiv Singh and Nafees Ahmad
Department of Physics, University of Lucknow, Lucknow, Lucknow-226007, India

The growing interest in investigating new aspects of high density (quantum) plasmas is motivated by its potential applications in modern technology e.g., quantum well and quantum dots, quantum plasma echoes, metallic nanostructures, microelectronics devices, thin metal films, metal clusters, nano-plasmonic devices, quantum x-ray free electron lasers, in high intensity laser produced plasmas, in nonlinear quantum optics, in metallic nanostructures, in super dense astrophysical environment (e.g. in the interior of Jupiter, white dwarfs, and neutron stars), in dusty plasmas and in next generation of laser based plasma compression experiment (LBPC), etc. The studies involving interaction of intense laser beams with quantum plasma were carried out by the quantum plasma group.

The interaction mechanisms were developed on the recently developed quantum hydrodynamic (QHD) model which consists of a set of equations dealing with transport of charge, momentum and energy in a plasma. The effects of quantum Bohm potential, the Fermi statistical pressure and the electron spin were incorporated. All the prevalent models consider electrons as a single fluid of macroscopically averaged spin-1/2 plasma. The earlier papers did not show a full picture and didn't took spin-up and spin-down interaction force into account. Very recently, a modified separate spin evolution (SSE) treatment of electrons in accordance with Pauli equation has been developed. We have incorporated this treatment in our studies to study the role of spin polarization.

Filamentation of short laser pulses

Filamentation of short laser pulse in magnetized quantum plasma has been studied. The direction of external magnetic field was taken to be along the direction of electron beam propagation in the first case and oblique in the second case. The dispersion for both cases were obtained and growth rate were evaluated. The numerical analysis for growth rate was carried out. The result of both the cases were compared and analysed. Comparison was also done with earlier studies and the difference was critically analysed and interpreted. The filamentation instability of short laser pulse in magnetized quantum plasma is significantly enhanced by the ambient magnetic field. The growth rate increases with spin polarization in case of longitudinal wave, but in case of oblique the growth rate reduces with increase angle.

Two stream instability in magnetized quantum plasma

The two stream instability for a circularly polarized electromagnetic wave propagating through a high density magnetized plasma using modified SSE-QHD model has been studied. The dielectric permeability of the high-density plasma medium has been evaluated and the dispersion relation for the beam-plasma instability has been setup and critical wave number for beam-plasma instability has been obtained. The results show that the spin-polarization and streaming speed of electron beam significantly effect dispersion and growth rate of instability. It is found that the frequency increases with spin polarization due to increase in the Fermi pressure which decreases with streaming speed of electron i.e. v_b, the growth rate of instability also increases with spin-polarization and shifts the threshold of instability towards higher values. Increasing the beam velocity also enhances the growth rate as well as wave number at which instability terminates. It is also noticed that the magnitude of growth rate for classical plasma is greater than spin-polarized quantum plasma and for spin polarized plasma is larger than the quantum plasma (QHD model). It is evident from the analysis that in classical case, the growth rate increases up to a point, then saturates and in quantum case the growth rate increases and then falls. This is due to the role of Fermi pressure that the instability terminates at a certain wave number depending upon choice of parameters. The spin polarization increases the Fermi pressure which terminates the instability well before and also reduces the role of Bohm potential. It is also noticed that increasing value of streaming beam velocity increases the magnitude of growth rate and range of wave number k. The critical wave number increases with increase in the beam density as well as spin polarization. The current study may be useful towards better understanding of the existence of new waves and in streaming instability in astrophysical as well as high density laboratory plasmas.

Laser induced electron acceleration

The effect of spin polarization of electrons on the electron acceleration produced by the ponderomotive force of an intense circularly polarized traversing in axially magnetized quantum plasma has been analyzed using recently

developed QHD model to incorporate the effects of quantum statistical pressure, quantum Bohm force and electron spin. The spin-up and spin-down electrons have been taken to be two different species of particles and spin polarization produced due to difference in electron concentration induced under the influence of applied field have been studied. Equation for energy exchange between the incident electron and ponderomotive wave has been setup. The electron acceleration by intense laser pulse is significantly affected by the presence of magnetic field, density perturbation and spin polarization. It is noticed that the electron energy rises with increase in the magnetic field strength as well as the normalized frequency. The energy gain also increases with spin polarization. The energy gain is about 13% more in spin polarized plasma than unpolarized quantum plasma. The electron energy have intense fluctuations initially which finally get damped along the propagation distance. The electron gain energy during the rising part of laser pulse and loses during trailing part. The quantum diffraction effects tend to reduce the energy gain which can be compensated by further increasing the strength of the applied magnetic field. The present study will be useful in explaining the observed particle acceleration in dense plasma existing in astrophysical objects, next generation of intense laser-high-density plasma interaction experiments, in inertial confinement fusion, x-ray free electron laser and quantum free electron laser experiments.

Third harmonic generation in magnetized quantum plasma

The study of third harmonic generation resulting from propagation of circularly polarized laser pulse through homogenous high density quantum magnetoplasma has been analyzed. The static magnetic field applied for magnetization is in the longitudinal direction. The interaction mechanism has been built using the recently developed quantum hydrodynamic (QHD) model. We have proceeded with the self-consistent field approximation of the QHD equations. The effects of Fermi statistical pressure, the quantum Bohm potential and the spin of electron have been taken into account. The quiver and third order velocities along with electron densities and the spin angular momenta have been obtained through the perturbative expansion of QHD equations. The electron has two main quantum corrections, a quantum force produced by density fluctuations and a force considered through magnetization energy. The quantum effects and the electron spin modify the plasma current density and introduce correction terms in the harmonic field amplitude. The quantum diffraction effects contribute and enhance the nonlinear third harmonic radiation generation. It has been found that the third harmonic generation grows with the plasma density and the magnetic field up to the respective saturation values. The harmonic generation stops beyond saturation. The saturation of plasma density occurs earlier for increasing magnetic field. This is due to the polarization field effect in strongly magnetized dense plasma. It is also noticed that the efficiency of third harmonic radiation is more by about 12.5% in quantum plasma due to presence of diffraction (Bohm potential, spin effect) effects compared to classical plasma i.e. absence of quantum diffraction effects and electron spin effects also contribute to the harmonic generation by about 10% in quantum plasma. The increase in the third harmonic efficiency can serve as a diagnostic tool for presence of clusters and measurement of their size during laser plasma interaction with gas jet in clustered plasma.

Effect of dust grains on electron acceleration

A detailed analysis of particle acceleration by ponderomotive force of an intense circularly polarized electromagnetic wave in high density magnetized quantum dusty plasma has been presented using the recently developed quantum hydrodynamic (QHD) model. The effects of the Fermi pressure, Quantum Bohm potential and electron spin have been taken into account. We have used the continuity and momentum equations to obtain the perturbed density and quiver momentum for plasma species. Equation for energy gain during ponderomotive electron acceleration is setup. Electron acceleration by circularly polarized e. m. pulse is significantly affected by presence of the electric and magnetic fields and the charged dust grains. Optimum acceleration is achieved near the normalized Doppler upshifted cyclotron resonance. It is found that an electron gains energy during rising part and looses energy during trailing part of laser pulse. The presence of positive dust grains increases the growth of ponderomotive acceleration in quantum dusty plasma about 2.78% as compare to quantum plasma without dust. The presence of positive dust grains enhances the energy exchange as the localization of positive charges on dust grains improves ambipolar potential which sharpens the density profile, whereas the negative dust grains reduce the nonlinearity of the medium and as a consequence the growth rate is also reduced. The growth rate of electron acceleration becomes nonlinear as a result of ponderomotive force due to magnetic component of radiation field and externally applied field. The quantum diffraction effects play a greater role as compared to dust and the electron energy gets damped by about 6% due to quantum effects. The present study will be helpful in analyzing the dust behavior in the cores of giant planets, crusts of old stars, superdense astrophysical objects like interiors of white dwarfs, magnetospheres of neutron stars, magnetostars, quantum x-ray free electron lasers, future generation inertial confinement fusion and future generation intense laser-high density plasma experiments.

Conversion efficiency of even harmonics of Whistler pulse in magnetized quantum plasma

A study of second harmonic generation (SHG) resulting from propagation of whistler wave in homogenous high density magnetized quantum plasma is presented. The static magnetic field applied for magnetization is in the longitudinal direction. The interaction mechanism has been built using the recently developed quantum hydrodynamic (QHD) model. The effects of Fermi statistical pressure, the quantum Bohm potential and the spin of electron have been taken into account. The quiver and second order velocities along with electron densities and the spin angular momenta have been obtained through the perturbative expansion of QHD equations. The nonlinear current density is the sum of conventional current and the current due to spin magnetic moment. The linear current results from the self-consistent field. The efficiency of SHG has been obtained for the phase mismatched case. It has been found that the SHG grows with the plasma density and the magnetic field up to the respective saturation values. The harmonic generation stops beyond saturation. The saturation of plasma density occurs earlier for increasing magnetic field and similar saturation is observed for the magnetic field. This is due to the polarization field effect in strongly magnetized dense plasma. The efficiency of SHG also increases with intensity of whistler pulse. The noteworthy observation is occurrence of enhanced second harmonic generation for high density degenerate plasma at lower values of external magnetic field strength. The present study of second harmonic of whistler will be useful in acceleration of whistler pulse in astrophysical environments, fabrication of microelectronic devices, for high quality plasma processing and to derive dc current in toroidal fusion devices.

Oblique propagation of Whistler wave in axially magnetized quantum plasma

The dispersion relation for the oblique propagation of electromagnetic wave in high density homogenous quantum plasma is stabilised. The growth rate has been evaluated. The difference in the concentration of spin-up and spin-down electrons have been taken into account and effects of spin polarization is analysed. Projection of spin density on the direction of external magnetic is not an independent variable. It appears as a difference of concentration of two different spin states electrons. It is found that The spin polarization increases the dispersion of electromagnetic wave.

Stimulated SPW excitation in magnetized quantum plasma

Due to the great degree of miniaturization of semiconductors in electronic devices (in which the electron density is high and temperature is low) the thermal de- Broglie wavelength of charge particles is comparable to the spatial variation of the doping profiles. The typical quantum effects such as the exchange correlation, quantum fluctuation due to density correlation and the degenerate pressure will play a significant role in electronic components to be constructed in future. We studied the basic features of surface wave excited due to collective oscillations of free electrons at the interface of plasma of different densities or plasma vacuum interface in semi-bounded semiconductor plasma under the influence of quantum tunnelling, the spin of fermions, the collisional effects, the nonlocality effects, the exchange effects, coulomb exchange (CE) as well as the external magnetic field. The dispersion properties of electromagnetic surface waves on the quantum plasma half space with the effects of exchange correlation were analysed. We also studied the excitation of surface plasma waves via stimulated electron hole recombination in the proximity of the guiding surface considering a three-layer system: a thin layer of n-type semiconductor sandwiched between the metal and p-type semiconductor. Since, electron spin is important especially in the presence of external magnetic field as it is not only effects wave instabilities but also give rise to a new wave phenomenon in degenerate plasma. We took into account spin-up and spin-down interaction and spin polarization while describing the surface phenomenon. It was found that the dispersion and pointing flux properties differs slightly in spin polarized and unpolarized plasma. This result may be important for ultra small electronic devices like travelling wave amplifier and solid density plasma.

The instability of electron-hole in quantum semiconductor plasma

The instability of electron-hole in quantum semiconductor plasma was examined. The growth rate of the wave depends on varying the parameters normalized by cyclotron-plasma frequency, like the angle between propagation vector and external magnetic field parallel to and speed of the externally injected electron beam parallel to the propagation vector. We derived a dispersion relation from which it was shown that inclusion of streaming effects in finite geometry opens up the possibility of a number of wave modes. Some of these modes were found to be linearly unstable. It has been shown that the finite boundary, stream velocity of plasma particles, quantum diffraction parameter, electron-hole mass ratio and the charge imbalance parameter all have significant effects on the instability growth rate.

Amplification of a surface electromagnetic wave by running over plasma surface ultrarelativistic electron bunch as a new scheme for generation of Teraherz radiation*

S. P. Sadykova† [1] *and A. A. Rukhadze*[2]

[1]Forschungszentrum Jülich (Jülum.), Jülich, Germany; [2]Prokhorov General Physics Institute of RAS, Moscow, Russia

The amplification of a surface electromagnetic wave (SEW) by means of ultrarelativistic monoenergetic electron bunch of $n_b = 10^{11}$ cm^{-3} running over the flat plasma surface of $n_p = 3\cdot 10^{19}$ cm^{-3} and temperature $T_e > 2\cdot 10^5$ K in absence of a magnetic field is studied theoretically. Here we consider the plane spatially unbounded plasma-(long)bunch systems which can also be referred to as the spatially unbounded plasma-bunch systems. It is shown that when the ratio of electron bunch number density to electron number density multiplied by a powered to 5 relativity factor is much higher than 1, i.e $\gamma^5 n_b/n_p \gg 1$, the saturation field of the surface electromagnetic wave induced by trapping of bunch electrons approaches the surface electromagnetic wave front breakdown threshold in plasma: $eE_x = eB_y = 0.16\omega_p \frac{mc}{e}(2\gamma^5 n_b/n_p)^{1/7}$. The SEW saturation energy density in plasma can exceed the electron bunch energy density. Here, we discuss the possibility of generation of superpower Teraherz radiation and on a basis of such scheme [1] (See Fig.1).

The SEW on plasma surface and plasma-like media (gaseous plasma, dielectric and conducting media, etc.) attract special attention of researchers due to their unique properties. First of all, due to its high phase and group velocities close to light speed in vacuum at high media conductivity what makes them the most valuable in radiophysics [2]. The SEW are widely applied in physical electronics due to its high phase velocity leading to its uncomplicated generation by relativistic electron bunches and output from plasma. We consider the case of ultrarelativistic monoenergetic electron bunch which remains relativistic in the frame of reference of SEW generated by this bunch compared to the works [3]-[5], where the bunches were nonrelativistic. Such a problem of generation of three-dimensional electromagnetic wave (wakefields) in plasma with the help of ultrarelativistic electron and ion bunches through Cherenkov resonance radiation was solved in [6]. The estimated SEW transverse electric field is $E_x = B_y =$ 10^9V /cm=10^{11} V/m, hence, the energy density flux (Poynting vector) $P = (c/4\pi){E_x}^2 \simeq 6\cdot 10^{15}$ W /cm^2. We are working on the scheme of a real cylindrical SEW bunch-plasma amplifier.

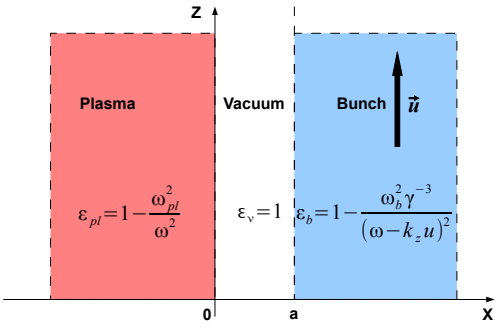

Figure 1: Schematic illustration of interaction of the ultrarelativistic ($\gamma = 100$) monoenergetic electron bunch with plasma; ε- dielectric permitivities.

References

[1] S. P. Sadykova, A. A. Rukhadze, T. G. Samkharadze, Engineering Physics (Transl. from Russ. "Inzhenernaya Phizika"), Nr. 12, P. 33-37 (2013)

[2] A. V. Kukushkin, A. A. Rukhadze and K. Z. Rukhadze, Physics-Uspekhi 2012, Vol. 55. No. 11. P. 1124.

[3] R.I. Kovtun, A.A. Rukhadze, ZETF, 58, Nr. 5, 1709 (1970).

[4] M.V. Kuzelev, A.A, Rukhadze, Plasma Free Electron Lasers (Edition Frontier, Paris, 1995).

[5] A.F. Alexandrov, L.S. Bogdankevich, A.A. Rukhadze, Principles of Plasma Electrodynamics (Springer, Heidelberg, 1984).

[6] A. A. Rukhadze and S. P. Sadykova, Phys. Rev. ST Accel. Beams 15, 041302 (2012).

*To the Great memory of Prof. Anri A. Rukhadze

† saltanat.sadykova@gmail.com

4 Particle-, Radiation- and Plasma Sources

Improved laser-to-proton conversion efficiency utilizing p-polarization at PHELIX*

J. Hornung[1,2,3], Y. Zobus[1,4], P. Boller[1,4], C. Brabetz[1], T. Kühl[1,5], Zs. Major[1,3], M. Zepf[2,3] and V. Bagnoud[1]

[1]GSI, Darmstadt, Germany; [2]FSU Jena, Jena Germany; [3]HI-Jena, Jena, Germany; [4]TU-Darmstadt, Darmstadt, Germany, [5]Johannes Gutenberg University, Mainz, Germany

PHELIX, the Petawatt High-Energy Laser for Heavy-Ion Experiments in Darmstadt, Germany, has by now been in operation for more than a decade, with one of the main research directions being that of laser-driven acceleration of light ions, such as protons. As this field is developing from the study of the acceleration processes themselves to more application-oriented experiments, a precise know-ledge of the optimal experimental conditions, yielding the highest ion energies and particle numbers, is necessary. Therefore, an experimental campaign at PHELIX has been conducted to optimize these properties, whilst using a large interaction angle of 45° between laser and target. This configuration is of particular interest from an operational point of view, due to the mitigation of back-reflected light and target debris, which can be detrimental to the last optical component in the laser-beam delivery system that is crucial for reaching the highest possible intensities on target. In this scheme, the performance of the acceleration was studied while varying parameters such as target thickness, temporal contrast values and the polarization of the laser with respect to the target. To evaluate the effects a comparison is made to the regularly used setup with a high nanosecond contrast of 10^{-12}, 1 µm-thick targets and s-polarization.
In order to increase the absorption of the laser, the temporal contrast was increased to 10^{-6} and a 10 µm-thick target was used to prevent a burn-through due to the increased preplasma formation.

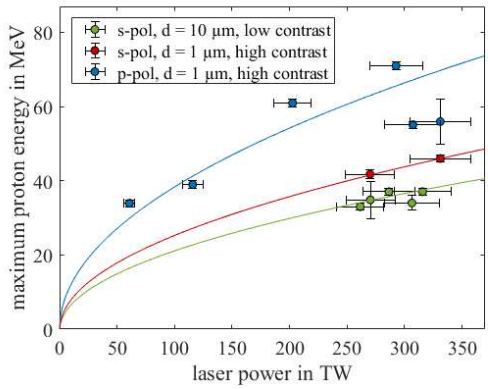

Figure 1: Scaling of the maximum proton energy with laser peak power on target. The different colors represent different laser and target conditions.

Additionally, a third setup was tested using p-polariza-tion, which is achieved by rotation of the target around the laser axis, whilst utilizing the high temporal contrast and the thin targets. The peak-power on target was varied for each configuration and the resulting maximum proton energy recorded using radiochromic films (RCF). The result of each setup can be seen in figure 1, including a laser-power scaling law by Zeil. et. al. [1], corresponding to the colored lines. When using the thick target and low temporal contrast, the maximum achievable proton energy is slightly reduced compared to the standard setup (red). However, when changing to a p-polarized laser pulse with respect to the target, the maximum proton energy increased by 60% up to 71 MeV.
This improvement is also shown by the proton spectra (figure 2) showing an increased amount of particles (blue) above 10 MeV up to $3.2\text{x}10^{12}$, which is an improvement of 57% in comparison to the standard setup (red). This leads to an improvement of the conversion efficiency, from laser energy to protons, from 3.9 % to 5.2 % [2].

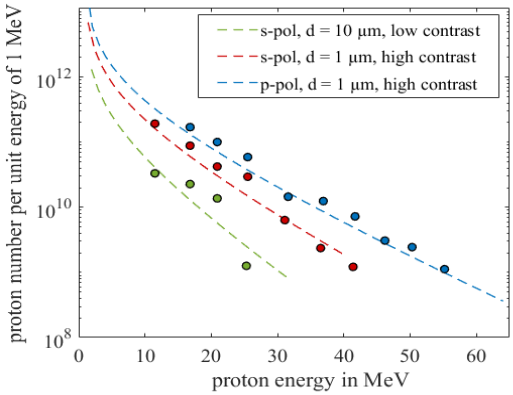

Figure 2: Proton spectra of each configuration with similar laser-peak-power on target.

The findings of this study will improve further application oriented experiments with light ions at PHELIX and the knowledge can be useful to optimize the proton sources at other facilities.

References

[1] K. Zeil, et. al., "The scaling of proton energies in ultrashort pulse laser plasma acceleration" New Journal of Physics, 12(4):045015, 2010.

[2] J. Hornung, et. al., "Optimization of the laser-driven proton source at PHELIX", submitted to High Power Laser Science and Engineering, 2020

* This work has been carried out within the framework of the EUROfusion Consortium and has received funding from the Euratom research and training programme 2014-2018 and 2019-2020 under grant agreement No 633053. The views and opinions expressed herein do not necessarily reflect those of the European Commission.

Recovery of Nanodiamonds Produced by Laser-Induced Shock-Compression of Polystyrene *

A. K. Schuster[1,2], N. J. Hartley[1], J. Lütgert[1,2], K. Voigt[1,2], J. Vorberger[1], M. Zhang[1], A. Benad[2], A. Eychmüller[2], B. Klemmed[2], D. O. Gericke[3], A. Rack[4], V. Bagnoud[5], A. Blazevic[5], C. Brabetz[5], U. Eisenbarth[5], S. Götte[5], D. Reemts[5], D. Schumacher[5], M. E. Toimil Molares[5], M. Tomut[5], and D. Kraus[1,2]

[1]HZDR, Dresden, Germany; [2]TU Dresden, Dresden, Germany; [3]University of Warwick, Coventry, U.K.; [4]ESRF, Grenoble, France; [5]GSI, Darmstadt, Germany

Introduction

Hydrocarbons are highly abundant in icy giant planets like Uranus and Neptune and their interior conditions can be created in the laboratory on a nanosecond timescale by applying the technique of laser-induced shock compression using high energy lasers [1]. Based on this method, nanodiamond formation in a simplified hydrocarbon representative, polystyrene (C_8H_8), was observed via in situ X-ray diffraction (XRD) [2,3]. The goal is to physically recover the nanodiamonds that are ejected at hypervelocities upon shock-break out to understand the underlying hydrocarbon separation mechanism by analysing their shape, size, surface modifications and defects. This work is important for planetary interior modelling and may present an additional route for nanodiamond production.

Recovery Campaign P173 at GSI

The experimental set-up of the recovery experiment is illustrated in Figure 1. A step pulse is driven into the sample to achieve conditions of ~150 GPa and ~5000 K. The Velocity Interferometer System for Any Reflector (VISAR) is used to characterise the shocked state. For recovery shots, the sample consists of 125 µm polystyrene (PS) with a 100 nm coating on the laser side to reflect laser-pre-pulses. The high speed camera HPVX-2 (Shimadzu Corp., Japan) was combined with a backlighter to observe the dynamics of the ejecta cloud after shock break-out. These particles have velocities between 5-20 km/s and are collected in various catcher systems.

It is known that around 60% of the carbon atoms in polystyrene have formed diamond crystallites in a size range between 4-100 nm [4]. The total expected diamond amount in this experiment is 14.2 µg at maximum, which is distributed in the catcher volume. The small size, high impact velocity and little total amount of diamonds makes it challenging to prove their survival of the hypervelocity impact event.

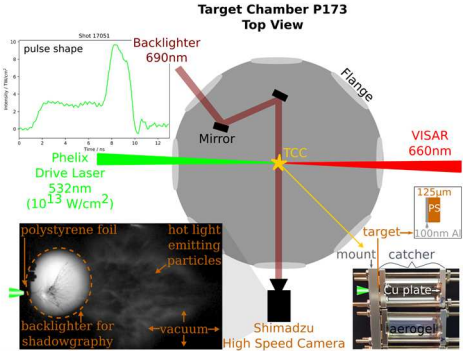

Figure 1: Set-up of recovery experiment P173 at the Z6 endstation at GSI.

On-site Raman measurements were conducted with an excitation wavelength of 473 nm. Figure 2 shows a reference spectrum of a pristine polystyrene foil in black that does not exhibit a peak in the vicinity of the diamond line at 1330 cm^{-1}. The catcher consists of a fused quartz cylinder and a plate, where the glass plate is subject to examination. An optical microscope picture of it with the corresponding measurement points is displayed in Figure 2. The spectra show the characteristic graphite D (1350 cm^{-1}) and G band (1580 cm^{-1}), which means that polystyrene was at least transferred into graphite. Nanodiamonds from detonation synthesis are known to be encapsulated by graphitic layers, which likely applies to our crystallites too. Further analysis to identify diamond structures is under way.

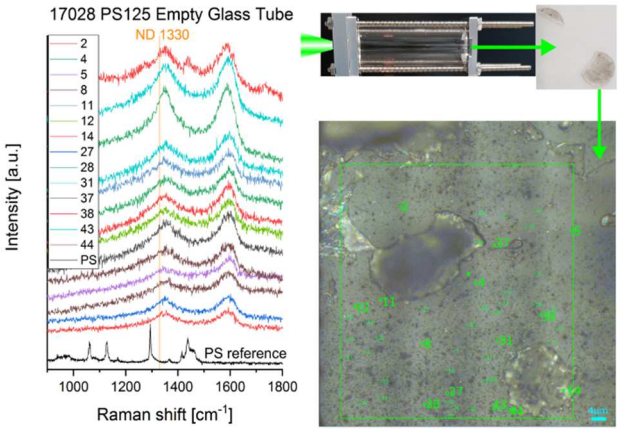

Figure 2: Raman spectra from a glass plate capturing the ejecta from shock-compressed polystyrene and the reference spectrum of a pristine polystyrene foil (black).

References

[1] Kraus, D., et al. Nat Commun. 7.1 (2016): 1-6.
[2] Kraus, D., et al., Nat Astron. 1.9 (2017): 606.
[3] Kraus, D., et al., PoP 25.5 (2018): 056313.
[4] Schuster, A. K., et al., PRB 101.5 (2020): 054301.

On-line detection of radioactive fission isotopes produced by laser-accelerated protons

P. Boller[1,2,*], A.Zylstra[3], P. Neumayer[1,4], L. Bernstein[3], Ch. Brabetz[1], J. Despotopulos[3], J. Glorius[1], J. Hellmund[1], E. A. Henry[3], J. Hornung[1,5,6], J. Jeet[3], J.Khuyagbaatar[1], L. Lens[1], S. Röder[1,2], Th.Stoehlker[1], A.Yakushev[1], Y. A. Litvinov[1], D. Shaughnessy[3], V. Bagnoud[1,2], Th. Kuehl[1,7], and D.H. G. Schneider[3]

[1]GSI, Darmstadt, Germany; [2]T.U. Darmstadt, [3]Lawrence Livermore National Laboratory, [4]Uni Frankfurt, [5]Helmholtz Institute Jena, [6]FSU Jena, [7]Uni Mainz, *p.boller@gsi.de.

The on-going developments in laser acceleration of protons and light ions, as well as the production of strong bursts of neutrons and multi-MeV photons by secondary processes now provide a basis for novel high flux nuclear physics experiments[1]. In the presented experiment pulses of 200 J at 500 fs duration from the PHELIX laser produced more than 10^{12} protons above 15 MeV in a bunch of sub-nanosecond duration[2,3]. They were used to induce fission in foil targets made of natural uranium.

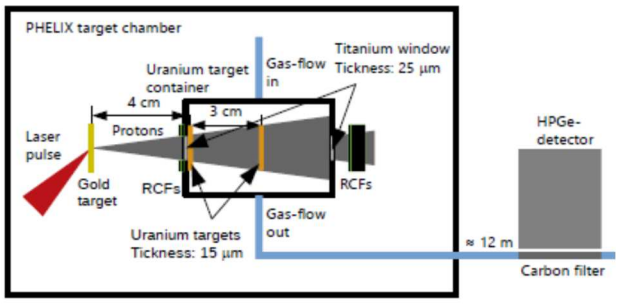

Figure 1: experimental set-up. The produced protons from TNSA enter the uranium target container through a titanium window. RCFs located in front and behind the uranium target container measure the proton spectrum. The fission products are stopped in gas and transported to a HPGe detector outside the PHELIX target chamber.

While the PHELIX target chamber is operated at a vacuum of 10^{-5} mbar, the target container is connected to the gas transport system with a constant gas flow of 500 cm^3 min^{-1} at a pressure of approximately 1 bar. The container has a length of 60mm and a diameter of 40mm. Due to their fission energy the fragments are emitted from a thin layer at the front and back of the target material. Fission fragments are stopped in the gas and transported through a Polytetrafluoroethylene (PTFE) tube with an inner diameter of 4mm, over a distance of 12m to be collected in a carbon filter at room temperature, in front of a HPGe detector system. This method is often practiced for Nuclear Chemistry experiments [31, 32] but not adapted so far together with laser acceleration. The transport distance of several meters is crucial in this case in order to reduce EMP induced background at the HPGE detector to an acceptable level.

The obtained spectra were analyzed and interpreted on the basis of published nuclear data. Isotopes that were identified included 134I, 136I, 137Xe, 138Xe, 139Xe, and 140Cs. Figure 2 depicts spectra recorded at three different times, 27, 65, and 238 seconds, respectively, following the laser pulse. Each spectrum represents an accumulation from the signals of 11 laser shots, each up to the indicated times. These results prove that the new platform is able to support novel research in laser-nuclear research at HED facilities.

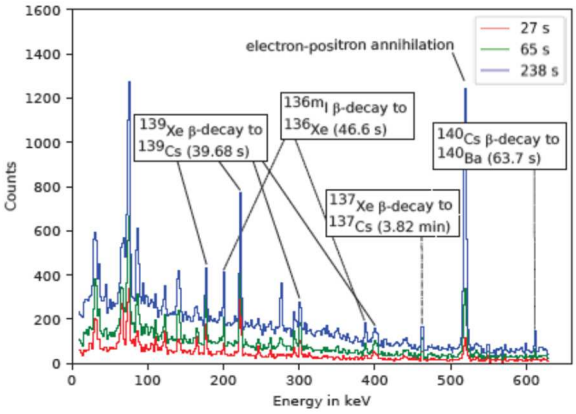

Figure 2: spectra obtained summing up a time window from the laser shot up to 238 second (upper trace) and 27 seconds (lower trace) integrating over 11 shots.

References

[1] Thirolf, P. et al. Acta Phys. Polonica B 42 (2011).
[2] Wagner,F. et al. Phys. Rev. Lett. 116, 205002 (2016).
[3] Hornung,J. et al. Submitted to HPLSE
[4] Schädel, M. & Shaughnessy, D. (Springer, 2013).

* Work within the framework of the EUROfusion Consortium , Euratom research and training program 2014-2018 and 2019-2020 under grant agreement No 633053. J.G and Y.L. acknowledgesupport by the European Research Conceil (ERC) under the European Unions Horizon 2020 research and innovation program(Grant agreement No 682841 ASTRUm").
The experiment was conducted at and supported by the GSI Helmholtzzentrum. U.S. participants weresupported by the U.N.

Wigner crystals in the bubble regime of wakefield acceleration*

Lars Reichwein†[1], *Alexander Pukhov*[1], *and Johannes Thomas*[1]

[1]Institut für Theoretische Physik I, Heinrich-Heine-Universität Düsseldorf, D-40225 Düsseldorf, Germany

Laser-driven plasma wakefield acceleration (LWFA) is of great interest for future acceleration setups, since high particle energies can be achieved at small distances due to the high electric field strengths of more than 100 GV/m that can be applied. The macroscopic structure of the accelerated electron bunch has already been studied i.a. using shadowgraphy. But interesting for applications, such as creating bright sources of short-wavelength radiation, is also its microscopic structure. An ordered structure of the bunch has to be expected as every electron i experiences a focusing wakefield potential $\Psi = (x_i^2 + y_i^2 + \xi_i^2)/8$ and repulsive Coulomb interaction between itself and every other electron. The coordinate $\xi = z - V_0 t$ is co-moving with the bubble at its velocity V_0. Since we consider relativistic electrons, we have to use the retarded Liénard-Wiechert potentials for the description of the electron-electron interaction.

In order to find the equilibrium structure of the electron bunch, we distribute N particles randomly in the bubble volume (or on a slice for 2D simulations) and iteratively minimize the system's energy by shifting the particle positions using steepest descent (see fig. 1). We perform simulations for different longitudinal particle momenta p, plasma wavelengths λ_{pe} and particle numbers N.

In the direction transverse to the bubble's propagation direction we observe the formation of hexagonal lattices with inter-particle distances in the sub-nanometer range. This represents the densest sphere packing in two dimensions and relativistic effects in this direction can mainly be neglected. For the mean inter-particle distance Δr of the electrons in one transverse slice, we can analytically derive scaling laws [1, 2] regarding p and λ_{pe} (and numerically for the N dependency): $\Delta r \propto p^{-1/3} \lambda_{pe}^{2/3} N^{-0.14}$.

In three dimensions we see a different behavior: For small particle numbers all electrons are pushed into a single filament along the ξ-axis as their relativistic motion leads to a distortion of the electromagnetic field structure. Thus, lying in a central chain, where one electron only experiences the forces from particles in front of it, minimizes the system's energy in that case. If the number of electrons in the bunch is increased, not all can fit into the central filament because the external potential gets too strong when being far from its center. The filament therefore starts to twirl up and slowly evades into the x-y-plane. For a sufficiently high number of electrons, this filament seems to "explode" and goes over into a shell-like structure (see fig. 2). Similar to the two-dimensional case we can derive scaling laws for the mean inter-particle distance along the direction of propagation [2]. The electron shells were also observed for conventional circular accelerators, however at a vastly different inter-particle distance. In conclusion, regularly structured electron bunches can be expected in equilibrium.

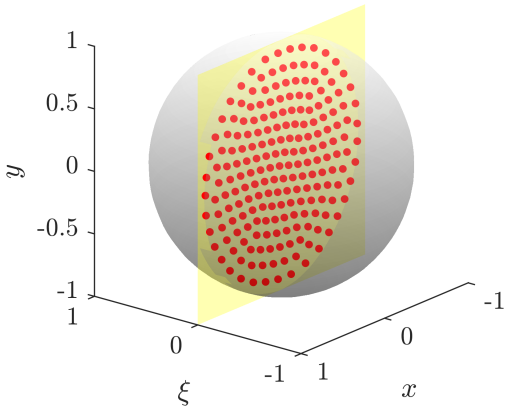

Figure 1: Schematic depiction of a transverse slice (in yellow) of the bubble volume (gray) with a hexagonal lattice consisting of $N = 200$ electrons.

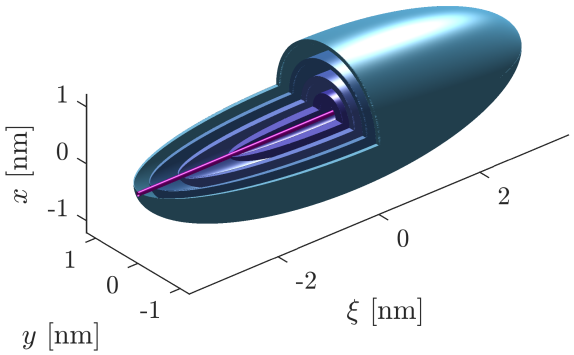

Figure 2: Three-dimensional equilibrium structure for $N = 20\,000$ electrons. The central filament (in magenta) is surrounded by several ellipsoid shells.

References

[1] L. Reichwein, J. Thomas and A. Pukhov, "Two-dimensional structures of electron bunches in relativistic plasma cavities", Phys. Rev. E 98 (2018).

[2] L. Reichwein, J. Thomas and A. Pukhov, "The filamented electron bunch of the bubble regime", arXiv:1903.04858 (2019).

* Work supported by DFG (projects PU 213/6-1 and PU 213/9-1) and BMBF (project 05K19PFA).

† lars.reichwein@hhu.de

Nanostructuring and plasmonics governed by surface plasmon polaritons

P. N. Terekhin*, P. D. Ndione, S. T. Weber and B. Rethfeld

Department of Physics and Research Center OPTIMAS, Technische Universität Kaiserslautern, Erwin-Schrödinger-Strasse 46, 67663 Kaiserslautern, Germany

Self-organized surface structures on metals could be produced by ultrashort laser pulses. This technology has a lot of applications including wetting, medical applications, tribology and others. Thus, it is important to understand the basic governing mechanisms of energy deposition to the irradiated material. Electron density oscillations at the interface between a metal and a dielectric (surface plasmons) coupled to the electromagnetic wave of the incident laser pulse are called surface plasmon polaritons (SPP) [1]. SPP can be excited by prism or grating coupling, surface roughness or a step edge of a sample [1, 2]. It should be mentioned that the complex dielectric functions (CDF) of both media play very important role [1]. The interference of the plasmons wave and the incoming pulse leads to a periodic modulation of the deposited laser energy along the surface of a sample.

The process of the laser energy absorption involving SPP is studied for a silver sample on the basis of an analytical source term [3]. This source term describes the energy absorbed by the electrons of a metal and consists of three terms originated from the interference of the SPP and laser fields, namely: laser-laser, laser-SPP and SPP-SPP.

The energy absorbed by the electrons in dependence on time and lateral distance from a step edge at the interface between Ag and air is shown in Fig.1. We used the following laser parameters: a laser wavelength of 800 nm, pulse duration of 30 fs (full width at half maximum) and the radius of the Gaussian focus of 30 μm centered at the step edge. Fig.1 shows the periodic pattern of the absorbed energy distribution and the SPP propagating along the sample after the laser pulse is gone.

The developed energy source can be used in the TTM model [4] for investigation of the evolution of the electronic and lattice temperatures on large timescales when thermalization between electron and lattice subsystems is approached. Implementation of the derived source term [3] into the combined atomistic-continuum molecular dynamic-TTM model [5] will allow direct comparison with experiments performed at the same temporal and spatial scales. Apart from nanostructuring applications, the present source term can be useful in plasmonics, for example, to describe plasmon-induced hot carriers generation.

The developed approach can be applied for different materials and arbitrary parameters of the laser beams. It can be used for studying properties of the SPP waves and the mechanisms of laser energy absorption under controlled conditions.

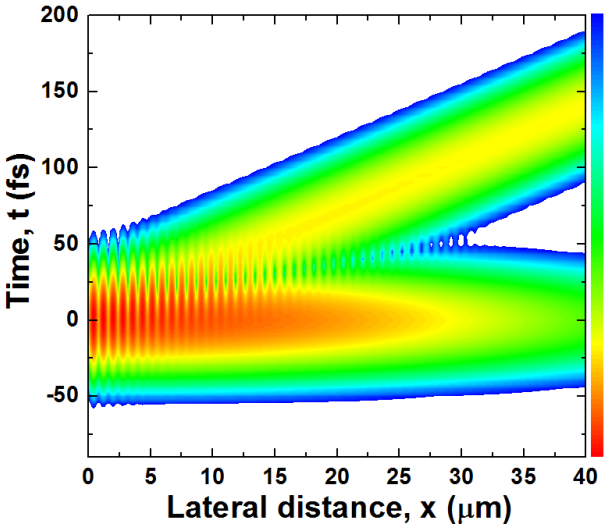

Figure 1. The energy absorbed by the electrons of Ag at laser wavelength 800 nm and pulse duration 30 fs at the surface irradiated at normal incidence. The colour code represents the amplitude of the energy absorption strength up to $25.2 \cdot 10^{18}$ J s^{-1} m^{-3} (red) in logarithmic scale.

References

[1] S. A. Maier, Plasmonics, Fundamentals and Applications (Springer, Berlin) (2007).

[2] A. Klick, S. de la Cruz, C. Lemke, M. Großmann, H. Beyer, J. Fiutowski, H.-G. Rubahn, E.R. Méndez, M. Bauer, Amplitude and phase of surface plasmon polaritons excited at a step edge, Appl. Phys. B 122 (2016) 79.

[3] P. N. Terekhin, O. Benhayoun, S. T. Weber, D. S. Ivanov, M. E. Garcia, B. Rethfelda, Influence of surface plasmon polaritons on laser energy absorption and structuring of surfaces, Appl. Surf. Sci. 512 (2020) 144420.

[4] S. I. Anisimov, B. L. Kapeliovich, T. L. Perel'man, Electron emission from metal surfaces exposed to ultrashort laser pulses, Zh. Eksp. Teor. Fiz. 66 (1974) 776. [Sov. Phys.-JETP 39 (1974) 375].

[5] D. S. Ivanov, V. P. Lipp, A. Blumenstein, F. Kleinwort, V. P. Veiko, E. Yakovlev, V. Roddatis, M. E. Garcia, B. Rethfeld, J. Ihlemann, P. Simon, Experimental and theoretical investigation of periodic nanostructuring of Au with ultrashort UV laser pulses near the damage threshold, Phys. Rev. Appl. 4 (2015) 064006.

#terekhin@physik.uni-kl.de

Application of Geant4 toolkit for modeling of experiments on laser-driven neutron and gamma generation.

A. Skobliakov[1], O. N. Rosmej[2,3], M. Gyrdymov[3], M. M. Günther[2], P. Tavana[3], A. Golubev[1], A. Kantsyrev[1]

[1] NRC "Kurchatov Institute"-ITEP, Moscow, Russia; [2]Helmholtzzentrum GSI, Darmstadt, Germany; [3]IAP, Goethe University Frankfurt, Germany;

High luminous neutron and gamma sources play a very important role in many reserch fields such as higt energy density physics, material science, and astrophysics [1]. Laser-driven neutron generation via (γ, xn) disintegration reactions in high Z materials is one of the possible ways. The threshoulds of such reactions lay in MeV gamma energy region, so that for effective MeV gamma production ulra-relativistic electron beams are neccesery. In experiments at the PHELIX-facility, high current well directed beams of ultra-relativistic electrons were generated when the short laser pulse of 1-2×10^{19} Wcm^{-2} laser intensity interacted with plasma of near critical electron density (NCD). Such kind of plasma was generated by the super-sonic ionization mechanism when a ns pulse was send onto low density polymer aerogels forerunning the main laser pulse [2]. Penetration of well-directed high current electron beams with energies up to 100 MeV in high-Z materials causes MeV-gamma production and photodisintegration reactions. In the experiment, high yield Ta, Cr and Au isotopes as well as neutron yield from the In probes was measured. In order to optimize the setup for the next experimental campaigns the GEANT4 simulations [3] were performed.

Geant4 simulation model

Geant4 Monte-Carlo code includes comprehensive physical processes and databases of particle-matter interactions [3, 4]. The scheme of the model that describes experimental geometry is shown in Fig. 1.

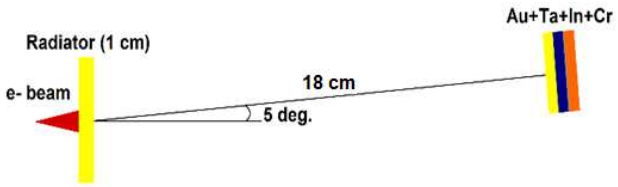

Figure 1. The geometrical model for investigation of the (γ, xn) disintegration reaction yields.

Since Geant4 cannot simulate laser interaction with foam and generation of relativistic electrons, the measured angular and energy distribution of relativistic electrons with the total number of electrons 3 × 10^{11} in the energy range 2 MeV < E < 90 MeV was used (1):

$$\frac{dN}{dE}[MeV^{-1}] = 1.9 \cdot 10^{10} e^{-\frac{E}{7.92}} + 0.54 \cdot 10^{10} e^{-\frac{E}{28.4}} \quad (1)$$

The angular distribution of initial electrons is Gaussian with FWHM 26° and 20 μm initial diameter. In the experiment and in simulations, this electron beam propagates through 1mm thick Au-radiator producing MeV bremsstrahlung radiation. MeV gammas and electrons that escaped the radiator interacted with a stack of high-Z materials placed at 5° to the laser propagation direction at the distance of 15 cm from the laser-foam interaction point. The sample-stack consists of four metal plates: Au (1 mm), Ta (1 mm), In (0. 25 mm) and Cr (1 mm) with dimension 7.5 × 7.5 mm. For the simulation of photonuclear reactions, the ShieldingLEND (Low Energy Nuclear Data) [4] physics list was used. This physics list ensures a high precision cross section data for photonuclear reactions below 20 MeV. For energies higher 20 MeV, one of the standards physics lists was taken into account. The result of simulations that is in a good agreement with experiment is shown in the table.

Isotopes	Yields
180Ta	0.49E+06
196Au	0.54E+06
51Cr	1.02E+05
49Cr	2.20E+03
194Au	0.56E+04
192Au	0.55E+03

Concluding we would like to emphasize that the GEANT4 Monte-Carlo code provides a reliable tool for simulations of photonuclear reactions and can be successfully used for optimization of laser-driven nuclear experiments.

References

[1] Pomerantz I et al, Phys. Rev. Lett. **113** (2014)184801
[2] Rosmej O N et al, New J. Phys. **21** (2019) 043044 (
[3] Geant4 Toolkit http://geant4 userdoc.web.cern.ch. userdoc.web.cern.ch/geant4-userdoc/UsersGuides/ForApplicationDeveloper/fo/BookForApplicationDevelopers.pdf
[4]https://indico.cern.ch/event/781244/contributions/3251933/attachments/1782461/2902499/HadronicPhysics.pdf

* Work supported by grant No. 16 APPA (GSI) funded by the Ministry of Science and Higher Education of the Russian Federation.
#Aleksei *Skobliakov* [dinalt220@yandex.com]

Superionic states produced by nonthermal melting in laser spots

R.A. Voronkov[1,#], N. Medvedev[2,3], A.E. Volkov[1,4,5]

[1]Lebedev Physical Institute of the Russian Academy of Sciences, Moscow, Russia; [2]Institute of Physics, Czech Academy of Sciences, Prague, Czech Republic; [3]Institute of Plasma Physics, Czech Academy of Sciences, Prague, Czech Republic; [4]Joint Institute for Nuclear Research, Dubna, Russia; [5]National Research Centre "Kurchatov Institute", Moscow, Russia;

Superionic matter is a state exhibiting fluid and solid behaviors at the same time. It was recently discovered and confirmed experimentally in water and water-based mixtures [1] under high pressures, typical for interiors of giant planets or generated by means of laser pulses [1].

High-intensity femtosecond laser irradiation excites electronic system of solids [2]. It causes sharp changes in the electronic properties and in the atomic potential energy surface in a target [3]. These changes may induce an instability of the target lattice manifesting itself in melting even without significant atomic heating – so-called nonthermal melting [4].

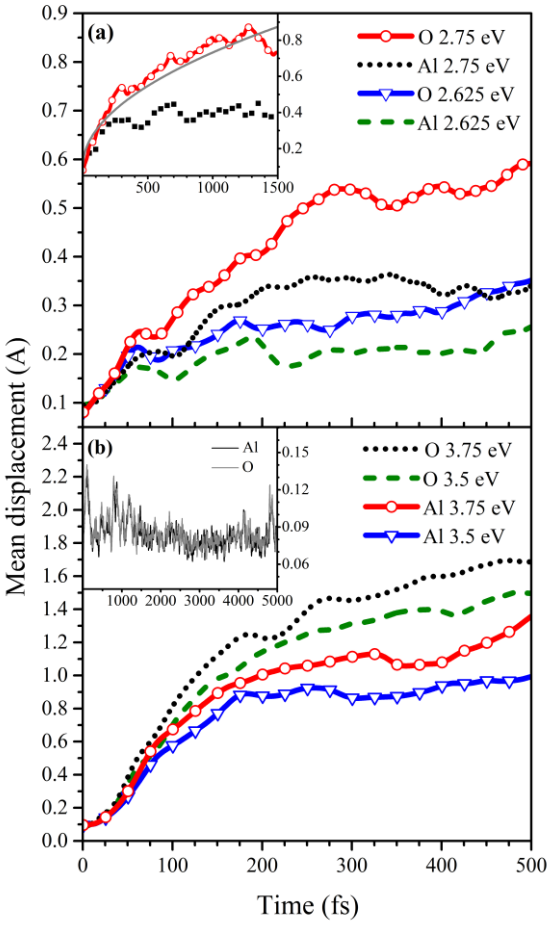

Figure 1. Mean atomic displacements in Al_2O_3 at (a) T_e = 2.625 eV and T_e = 2.75 eV, (b) T_e = 3.5 eV and T_e = 3.75 eV. Inset in panel (a) shows displacements at T_e = 2.75 eV in a longer time interval; solid line is $\sim\sqrt{t}$ indicating diffusive behavior. Inset in panel (b) shows stability of the semi-disordered phase at room temperature and 400 GPa pressure at the picosecond timescale.

roman.a.voronkov@gmail.com

We applied Quantum Espresso simulation package [5], based on the density functional theory molecular dynamics, to study an effect of the elevated electronic temperature on nonthermal structure instability in Al2O3 [6].

We found that at an elevated electronic temperature above Te = 2.75 eV (corresponding to the deposited dose D = 1.4 eV/atom, or Ne = 4.8% electrons are in the conduction band), semiconducting superionic phase forms with the liquid oxygen but crystalline aluminum sublattices (see Figure 1) [6]. Cooling the electronic system with simultaneous application of pressure above 400 GPa freezes this superionic phase into a novel class of materials of a mixed amorphous-crystalline insulator state, with the disordered oxygen and ordered aluminum subsystems [6].

At Te ~ 3.25 eV (D = 2.3 eV/atom, Ne = 6.8%) the band gap collapses, forming a metallic superionic state of alumina. It indicates that a superionic-superionic phase transition can be produced and studied. When the electronic temperature reaches Te ~ 3.75 eV (D = 3.5 eV/atom, Ne = 8.8%), aluminum sublattice disorders manifesting total amorphization of Al2O3 [6].

Results obtained in [6] showed that the superionic state is not limited to water-based systems, but can be produced in other compounds. This state is not unique but can be insulating, semiconducting, or metallic. It can be produced not only by pressure, but via nonthermal phase transition, thus opening up new possibilities of research and production of this exotic state [6].

References

[1] M. Millot, F. Coppari, J. R. Rygg, et al., Nature **569**, 251 (2019).
[2] J. C. H. Spence, Struct. Dyn. **4**, 044027 (2017).
[3] V. Tkachenko, et al., Phys. Rev. B **93**, 144101 (2016).
[4] P. Stampfli and K. H. Bennemann, Phys. Rev. B **42**, 7163 (1990).
[5] P. Giannozzi, S. Baroni, N. Bonini, et al., J. Phys. Condens. Matter **21**, 395502 (2009).
[6] R. A. Voronkov, N. Medvedev, A. E. Volkov, Phys. Status Solidi – Rapid Res. Lett. **14**, 1900641 (2020).

5 Fusion Related Issues of Plasma Physics

A new approach to inertial fusion energy

M. Roth[1,2], G. Korn[1,3], M. von der Linden[1], P. Shabalin[1] and K-G Schlesinger[1].
[1]Marvel Fusion GmbH, München, Germany; [2]TU Darmstadt, Germany, [3]ELI-Beamlines, Dolní Břežany, Czech Republ

Situation

The quest for sustainable energy to fight global climate change has to include baseload power plants operating reliable and without the emission of CO_2. Moreover, as fossil fuels have to be replaced, at the same time large parts of the world's population enter the industrial age, we need new technologically advanced approaches to satisfy global energy needs. Among the two principal pathways to Fusion, magnetic confinement fusion and inertial confinement fusion, significant progress has been made not only in understanding the physics, but also in new available technology that allows for new approaches to fusion energy. This is also reflected in the rapidly growing number of privately funded enterprises taking on the quest for clean, sustainable fusion energy, for the first time fusion based on fast ignition is approached by a start-up company

Marvel Fusion Approach

The current approach to inertial confinement fusion involves indirectly driven targets that are supposed to ignite in the self-inflicted central hotspot due to the coalescence of individual shockwaves. This requires a highly symmetrical implosion, without the onset of hydrodynamic instabilities, while at the same time accelerate the fuel to very high in-flight velocities (of about 350 km/s, which requires at least $2x10^{12}$g acceleration) and keeping it as cold as possible.

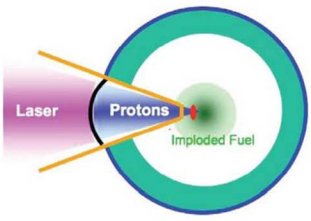

Marvel Fusion's approach will be the separation of compression and subsequent heating and ignition by introducing the fast ignition approach, based on the concept of proton fast ignition (PFI).

By separation of compression and heating, the fast ignition approach largely reduces the requirements on symmetry compression and at the same time results in a much higher gain. This, together with the reduction of the size of the driving laser system, opens up point designs for power plants with respect to cost and baseload electrical power that cannot be achieved by other approaches. Marvel Fusion relies in two decades of research in fast ignition using ultra-intense lasers, the detailed work of scientists from 11 countries on a possible initial point design, and the rapid development of high-energy short-pulse laser systems.
Acknowledging the experience over the last decades on different approaches for the Fast Ignitor concept, Marvel Fusion has decided to aim for laser-driven protons as the preferred ignition beam. PFI has been proposed since the discovery of intense laser driven proton beans from ultra-intense high-energy laser systems in 1999 at the Lawrence Livermore National Laboratory. For the last two decades experiments at different laser systems have explored the prospect of PFI. All the experiments, even though on a subscale, have clearly demonstrated the prospect of this scheme. Conversion efficiency of laser light into useful proton energy, the focus ability of laser driven proton beams to spot size required for fast ignition, the interaction with the guiding cone in a combined experiment have all led to the confidence that PFI will work. It benefits from the research on capsule compression in the broader FI and ICF community, using direct or indirect drive. In fact, PFI leverages the capability for fuel assembly $\sim$1 g cm^{-2} and >400 g cm^{-3} demonstrated on the National Ignition Facility.Progress in this field has been limited, because of non-scientific reasons. Large-scale fusion programs have been linked to non-civilian applications and therefore have so far largely followed the indirectly driven approach with a central hot spot ignition. Short pulse lasers have become operational at high repetition rate and superior beam quality, but all fusion research facilities still operate on flash-lamp driven laser systems design in the 1980's and provide a few experiments a day at best.
Consequently, we start building a test facility within the next three years, while we will conduct experiments at existing facilities in order to fast track remaining physics questions. Our facility will combine multi kJ, shaped, ns drive beams with kJ-class ps ignition beams operating at a shot a minute repetition rate. As soon as the first laser systems will be installed in our own facility we will start experiments at the designed repetition rate to address physics, optimize the reaction and explore advanced fuel concepts. This will allow to answer fundamental questions with high statistics significance in a time orders of magnitude faster than every other existing approach so far. In addition, we will demonstrate reliable operation, target insertion, and investigate optics damage and power management as well as we will address questions on data mining, automatic analysis, and machine learning.
It is important for Marvel Fusion also to explore advanced fuels that are capable of minimizing the number of neutrons released in the fusion process, as well as minimizing the energy of the released neutrons in order to protect the first wall and the reactor chamber. This will also serve to minimize nuclear activation of reactor components and the subsequent storage requirement for components from the reactor itself. Here the fast ignition approach is unique compared to all other existing pathways to fusion energy.
To summarize, we believe that it is time to speed up the quest for fusion energy by using the experience of our science community and the drive of a privately funded start-up company.

Experimental scheme for investigation of stopping and fusion reactions initiated by laser-accelerated proton beams in a dense boron plasma

Jieru Ren[1] , Yongtao Zhao[1*], Wenqing Wei[1], Xing Xu[1], Zhigang Deng[2], Shaoyi Wang[2], Quanping Fang[2], Bubo Ma[1], Shuai Yin[1], Xing Wang[1], Benzheng Chen[1], Jianhua Feng[1], Rui Cheng[3], Dieter H.H. Hoffmann[1], Weimin Zhou[2], Leifeng Cao[2],

[1] MOE Key Laboratory for Nonequilibrium Synthesis and Modulation of Condensed Matter, School of Science, Xi'an Jiaotong University, Xi'an 710049, China
[2]Laser Fusion Research Center, Chinese Academy of Engineering Physics, Mianyang, 621000, China
[3] Institute of Modern Physics, Chinese Academy of Sciences, Lanzhou,730070, China

By irradiating a thin foil with ultrahigh-intensity lasers, multi-MeV ions with unprecedentedly high intensity (10 $^{19\text{-}20}$cm^{-3}) in ps time scale can be generated through various accelerating mechanisms. Such ion beams opened up new perspectives for many fields of research and application, such as ion fast ignition, ion driven high energy density matter and aneutronic nuclear reactions. During the interaction of such high-intensity ion beam with dense plasma, complicated, nonlinear behaviors are expected to emerge, while are far more to be understood.

Recently, proton-boron reaction rates initiated by laser-accelerated proton beams in a laser-produced boron plasma are reported to be higher than those reported previously [1]. Varied energy loss in plasma are resorted for explanations [2]. In our previous studies, unusually high degree of intense laser-accelerated proton beam stopping in dense ionized matter was demonstrated in comparison with the current-widely used models describing individual ion stopping in matter [3,4]. Supported by Particle-in-Cell simulation, the enhancement of the stopping is supposed to be caused by the beam-driven strong decelerating electric field approaching 1 GV/m. Here we propose an experimental scheme to study the stopping and fusion reactions initiated by laser-accelerated proton beams in a dense boron plasma. This scenario on one hand allows for correlate study of stopping and nuclear reaction processes, and on the other hand enables to visualize the beam-driven strong fields in the plasma.

The experiment will be carried out in October of the year 2020 at the XG-III laser facility of Laser Fusion Research Center in Mianyang. The experimental setup is shown in Fig. 1. The dense plasma is generated through heating a boron-doping Tri-Cellulose Acetate foam with ns laser-driven hohlraum radiation. In this way, ~mm scale, uniform, ns-long living plasma can be generated. The ps laser is focused on a thin foil to generate intense proton beams with Target Normal Sheath Acceleration (TNSA) mechanism. The energies of the protons passing through the plasma are measured with a Thompson Parabola Spectrometer (TPS). The TPS is designed to have two channels. This allows for measuring the unperturbed/initial ions spectra simultaneously as references for energy loss analysis. The fs laser-accelerated protons are used to image the decelerating fields which is predicted to be present in the plasma when the ps laser-accelerated proton beam passing through the plasma. The probing protons are diagnosed by RCF stacks. In addition, another two-channel TPS is mounted to measure the fs laser-accelerated ion energy loss in the plasma.

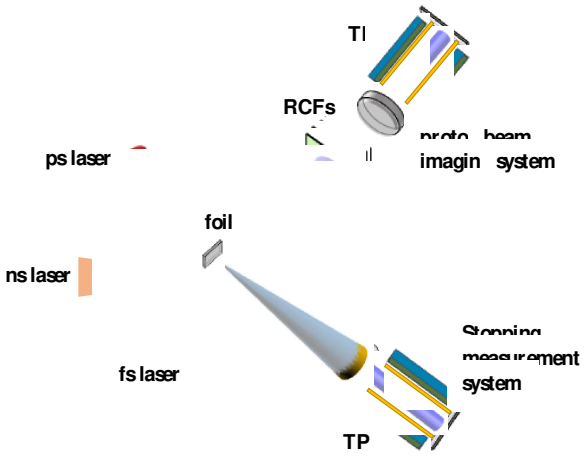

Fig.1. Experimental Setup

References

[1] C. Labaune, C. Baccou, S. Depierreux et al., Nature Communications ature Communications 4,1 (2013).

[2] Yihang Zhang, Zhe Zhang, Baojun Zhu et al., arXiv:2002.03190, 2020.

[3]Y Zhao, W Liu, X Wang et al., GSI-2018-2 REPORT: News and Reports from High Energy Density generated by Heavy Ion and Laser Beams, page 35, 2018.

[4]Jieru Ren, Zhigang Deng, Wei Qi et al., arXiv:2002.01331, 2020.

* zhaoyongtao@xjtu.edu.cn

About Thermal and Non-thermal Ignition of Nuclear Fusion Reactions

H. Hora[1,2*], J. Krasa[3], D.H.H. Hoffmann[4,5], S. Eliezer[6], N. Nissim[6], J. Kirchhoff[2], W. McKenzie[2], G. Kirchhoff[2], P. Lalousis[7], G.H. Miley[8], D. Margarone[3], A. Picciotto[9], L. Giuffrida[3], P.G.A. Cirrone[10], G. Korn[3], B. Liu[11,12], M. Ho[13]

[1]University of NSW, Sydney, Australia; [2]HB11 Energy Pty.Ltd. Freshwater, Sydney, Australia; [3]Institute of Physics, Czech Academy of Science, Prague, Czech Republic; [4] IKP, TU Darmstadt, Germany, [5]Xian Joao Tong Unviersity Xian, China; [6]SOREQ Research Center, Yavne, Israel; [7]Inst. Electronic Structure and Lasers, FORTH Heraklion, Greece; [8]Dept. Nucl. Plasma & Radiol., Engineering University of Illinois, USA; [9]Fondazione Bruno Kessler, Trento, Italy; [10]INFN Instituto Nazionale de Fisica Nucleare, Catania, Italy; [11]Hebei Key Laboratory of Compact Fusion, Langfang, China; [12]ENN Science and Technology Development Co., Ltd., Langfang, China; [13]ANSTO, Kirrawee 2223, Australia

In her inauguration speech 1st December 2019 in Portugal the President of the European Commission, Dr. Ursula von der Leyen, mentioned that one of her two priorities is the decarbonisation of energy generation not as a catastrophe but as a problem of *existential survival*. The attempt to use renewables is acknowledged but for reaching low carbon it is of an impossibly monstrous amound. Apart from the expected doubling of energy demand within the next 30 years it is of such a gigantic volume that this can never be fully reached by present measures.. Thanks to Lord Rutherford and Otto Hahn we have to focus on nuclear energy for generators of electricity based on ten milion times higher energy per reaction than chemical energy as from carbon. Fission of uranium under extreme control produces now more than 10% of all electricity but the exclusion of dangerous nuclear radiation or catastrophic accidents cannot be excluded by 100%.

What remains is nuclear fusion from the energy by joining together very light nuclei to heaviers. This is the energy source of myriades of the stars. The more than million times higher nucelar reaction energy than from burning carbon needs then ignition temperatures of many million degrees Celsius. The sun burns hydrogen into helium at 15 million degrees. To repeat this in power stations is tried since 60 years but „...Fusion always seems to be 30 years away“, see J.M. Windridge in [1].

A radical change of this situation is now neverless open thanks to getting rid of the temperatures above of the million degrees temperaures by using the just reached ultra-extreme CPA (Chirped Pulse Amplification) laser pulses for LASER BORON FUSION without the problems of dangeous nuclear radiation.

The equation of motion for the force density **f** in high-temperature plasmas is given by hydrodynamics for nuclear fusion

$$\mathbf{f} = -\nabla p + \mathbf{f}_{NL} \quad (1)$$

consists of a first term with the gas dynamic pressure p given by the density and the thermal equilibrium temperature T. This is in the range below eV (electronvolt = 8135 °C) as chemical energy when burning coal, but is at about ten million times higher for nuclear energy. For ignition, this range is of many dozens of million degree Celsius °C and was well reached with magnetic plasma confinement in tokamaks or stellarators or in aimed billion degrees in reverse field tri-alpha-energy configurations or in laser driven spherical compression with lasers of nanosecond pulses, but for too short times than needed for building a reactor for generating electricity.

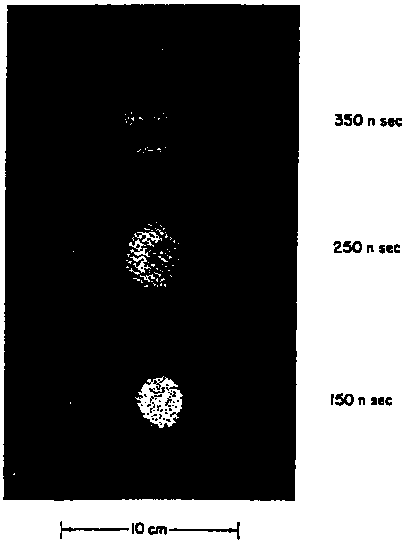

Fig. 1. Side-on framing camera picture of a plasma produced from an aluminum sphere of 80 µm radius at the time indicated after irradiation from the left hand side by a 30 ns ruby laser pulse focused to 0.4 mm diameter at the mentioned times after irradiation. The second frame shows the outer part of a rapidly expanding half-moon-like plasma and an inner spherical thermally expanding part [5]

*h.hora@unsw.edu.au

Apart from the first term with the thermal pressure p in Eq.(1), the presence of electric and magnetic fields and plasma-optical responses can generate the non-thermal electromagnetic nonlinear force $\mathbf{f}_{NL}$. This could directly be seen in the experiments by Sucov et al. [2] at laser interaction in Figure 1 resulting first in the non-transient equation of motion Eq. (10) with Maxwell's plasma stress tensor needing additional nonlinear terms in Schlüters earlier formulation seen from momentum conservation [3]. Finally for the general transient case clarifying six controversal solutions, the Lorentz and gauge invariant Eq. (6b) [4] was deriveed.

Evaluating about 500 pictures like Fig. 1 for different laser pulse energies, pulse durations and sphere diameters showed the central plasma thermally expanding with temperaures around 20 eV fully following the expected thermal plasma propeerty of the heated sphere taking the varying energy depending on the cases of the interacting laser energy of the cross section of values of about 90%.

The maximum energy of the ions in the half-moons were in the range up to 5 keV showing a non-thermal behaviour [5]. This definitely could not be from bremsstrahlung in the corresponding range of 20 MeV tempeature. Very detailled hydrodynamic computation of plane geometry condition of deuterium plasma at 10^{17} W/cm^2 laser intensity up to the critical density during 1.5 ps laser irradiation showed a plasma block acceleration of 10^{20} cm/s^2 [6]. This ultrahigh acceleration against the direction of the laser beam was measured from blue Doppler-shifted spectral lines by Sauerbrey [7] using CPA laser pulses [8] for which discovery the 2018 Physics Nobel Prize was awarded to Donna Strickland and Gerard Mourou. The nonlinear force driven acceleration [7] was about 100,000 times higher than thermal acceleration by the world's largest NIF laser.

One highlight of non-thermal energy density by nonlinear force conditions against the thermal energy density with plasma temperaures of hundred Million ^{o}C is the measururement by Sven Steinke where 18nm thin diamond films absorbed 99% energy of laser pulses and produces an energy density of 6.55×10^{12} J/cm^3 [9]. This is much higher than the hundred million degrees of thermal equilibrium ignition especially for the very low gains of hydrogen H with the boron isotope 11 (HB11 reaction) that is primarily environmnatally clean without radioacitvity. This supports the design (Fig. 16 of [11]) and is the basis for an absolutely clean, safe, low-cost and abundant electricity generator.

References

[1] Miley G.H. and H. Hora. Fusion Science and Technology. 75 (2019) 575

[2] Sucov EW, Pack JL, Phelps AV and Engelhardt AG. Physics of Fluids 10, (1967) 2035

[3] Hora, H., (1969) Physics of Fluids 12, (1969) 182

[4] Hora H., The transient electrodynamic forces at laser-plasma-interaction. Physics of Fluids. 28 (1985) 3705

[5] Hora H., Experimental results of free targets. Laser Interaction and Related Plasma Phenomena, Plenum Press, NewYork NY Vol.1, 1971,p. 273

[6] Hora H., *Physics of Laser Driven Plasmas*,Wiley Press, NewYork 1981, Fig 10.18 a&b

[7] Sauerbrey R. Acceleration of femtosecond laser produced plasmas. Physics of Plasmas 3, (1996) 4712-4716.

[8] Strickland D. and Mourou G. (1985) Optics Communications., 56, 2019

[9] Steinke S., Hening A., Schnürer M., Sokolnik T., Nickles P.V., Jung D., Kiefer D., Hörlein R.,Schreiber J., Tajima T., Yan XQ, Hegelich M., Meyer-ter-Vehn J., Sandner W., and Habs D. Laser an Paricle Beams 28 (2010) 215

[10] Hora H., G.H. Miley, S. Eliezer and H. Nissim. High Energy Density Physics 35 (2020) 100739

[11] Hora Heinrich, Georg Korn, Lorenzo Giuffrida, Daniele Margarone, A. Picciotto, Josef Krasa, Karel Jungwirth, Jiri Ullschmied, Paraskevas Lalousis, Shalom Eliezer, George H. Miley, Stavros Moustaizis and Gérard Mourou. Laser and Particle Beams 33 (2015) 607

Possible explanations of PXTD-measured reaction histories

Zixiang Yan[1] *and Wei Kang*[*1]

[1]HEDPS, Center for Applied Physics and Technology, Peking University, Beijing 100871, China

Recently, Sio *et al.* have obtained DT and D^3He nuclear reaction history data and concluded the existing of the separation of fuel-ion species during strong shock propagation [1]. However, separation of different species can only happen on the scale of the length of the mean free path under strong shock, which is about several angstroms in this experiment. Whether the separation really happens, or whether another physical process can be found to explain the experimental data, awaits further experimental demonstration and a detailed theoretical explanation from other aspects as well.

Non-equilibrium effect on yields near the shock front

The assumption of thermal equilibrium is often used in the calculations of cross section and average activity [2], which means the fuel-ion species satisfiy maxwell distribution. However, considering the thermal non-equilibrium properties across the shock front [3], the averaged reactivities here should be calculated using the bimodal distribution rather than the Maxwell one. Taken DT reaction as an example, the average activity is calculated using the following equation,

$$< \sigma v >= \int \sigma(v) v f(v) dv \tag{1}$$

which can be calculated via Monte Carlo method. In three dimensions, we shall have

$$f(v) \equiv f(\sqrt{v_x^2 + v_y^2 + v_z^2}) = f_0(v_x) f_0(v_y) f_0(v_z) \tag{2}$$

The bimodal approximation is considered to be a better description of the distribution near the shock front [2],

$$f_0(v', z) = (1 - \alpha(z)) f_1(v') + \alpha(z) f_2(v') \tag{3}$$

The distributions of temperature and density near the shock front are fitted based on our previous work [4], with the parameters given in Sio's work [1]. The result shows only a little enhancement on the average reactivity of DT reaction according to the non-equilibrium effect, which is also observed in the case of D^3He reaction.

Difference on the peak times of T_i and η

The ion temperature T_i can be roughly backstepped from the ratio of the yields of DT and D^3He reactions, and fitted with an a gaussian form which is displayed in Fig. 1(a) with the blue line. The compression ratio η verse time is also assumed to be a gaussian form while fuel ratio remains unchanged. However, the peak time is assumed to be different from that of T_i, which can be seen in Fig. 1(a) with the red line.

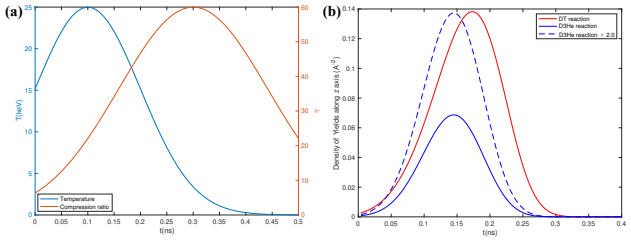

Figure 1: (a) The ion temperature and compression ratio verse time, both of which are fitted with a gaussian form. Here, $t = 0$ is set to be $0.6\ ns$ in real time, which is about the beginning of the reactions; (b) The density of yields along z axis verse time. The blue dashed line is the density of yields twice that of the D^3He reaction.

The result is shown in Fig. 1(b). With the assumption of no separation of the species due to the unchanged fuel ratio, the same phenomenon, i.e., both the beginning and the ending of D^3He reaction are earlier than that of DT reaction, can still be observed in our result.

Our work provides a new possible explanation accounting for the difference of the peak times of PXTD-measured reaction histories displayed in Sio's work.

References

[1] H. Sio *et al.*, "Observations of Multiple Nuclear Reaction Histories and Fuel-Ion Species Dynamics in Shock-Driven Inertial Confinement Fusion Implosions", Physical Review Letters 122(2019) 035001.

[2] H. S. Bosch and G. M. Hale, "Improved formulas for fusion cross-sections and thermal reactivities", Nuclear Fusion 32(1992) 611.

[3] V. V. Zhakhovskii, K. Nishihara and S. I. Anisimov, "Shock wave structure in dense gases", Journal of Experimental and Theoretical Physics Letters 66(1997) 99.

[4] H. Liu *et al.*, "Molecular dynamics simulations of microscopic structure of ultra strong shock waves in dense helium", Frontiers of Physics 11(2016) 115206.

* weikang@pku.edu.cn

Inner screening corrections to the Debye interaction in hot / dense plasmas in the vicinity of the bound - free transitions Paper for the GSI Scientific Report*

C. Deutsch[1], G. Naouri[1], N.A. Tahir[2]

[1]LPGP, UPS, Universite Paris - Saclay, 91405 - ORSAY, France; [2] Helmholtzzentrum GSI, Darmstadt, Gerrmany

lt seems that the plasma physics community is presently experiencing a continuous and steadily increasing reassment of the basic concept, pillars of our discipline.

A few salient examples among many, focus on deep and refined reexamination of the Debye screening length altogether with a deep mathematical interpretation of the nonlinear Landau damping [1-4].

Boltzmann-Maxwell equilibria are also under a scrutiny through non-extensive statistical physics [5] featuring non-Maxwellian distributions.

These revisitations lead to the introduction of novel perspectives in the whole field of plasma physics, they are often motivated by theoretical breakthroughs in other disciplines.

In this context, we do intend to give a specific attention to the remaining Debye bound states in strongly ionized hot/dense plasmas with ion charge $1 \leq z \leq 6$.

Considering those hydrogenic levels in the usual temperature Saha-distribution, we then focus on pressure effects, and highlighting the apriori messy intrication of excited Debye orbitals.

As well documented, in contradistinction to the Coulomb spectrum, Debye bound states are finite in number, and the lowest ones could be well approximated as nondegenerate Coulombic. So, a typical electron-ion orbital may be allocated the appromixate average extention (a. u.) [6]:

$$r_{n\ell} = \sqrt{\frac{\langle n\ell | r^2 | n\ell \rangle}{\langle n\ell | n\ell \rangle}} a_o = \frac{1}{2Z} \{3n^2 - \ell(\ell+1)\}, \quad (1)$$

with the Bohrradius $a_0 = 5.29.10^{-9}$ cm already demonstrating a possible inclusion of small orbitals within those endowed with a larger main quantum number, an effect particulary conspicious for $\ell = n-1$.

At this functure, it appears fruitful to make contact with a methodology developed in condensed matter physics.

Here, we allude to the systematic embedding of bound orbitals featuring long range interactions between dislocations [7,8], monitored by a 2D Coulomb interaction [9-11].

In this regard, we emphasize hot/dense plasmas with a Debye length (n_e, electron density)

$$D = \left(\frac{k_B T}{4\pi e^2 (n_e + Z^2 n_z + (Z-1)^2 n_{z-1})} \right)^{1/2} \quad (2)$$

Where n_e = density of fully stripped ions with charge Z, n_{z-1} = density of hydrogenic ions with charge Z -1 and mass m_i.

For the sake of simplicity we restrict ourselves to a 3-component system consisting of electrons, bare ions of nuclear charge Z in Saha equilibrium with hydrogenic ions of total charge Z-1.

These plasmas share an electron plasma parameter

$$\Lambda_e = \frac{\beta e^2}{D_e} = \frac{2.43 \times 10^{-4} n_e (cm^{-3})^{1/2}}{T(^\circ K)^{3/2}} \quad (3)$$

with D_e, electron restriction of Eq.(2).

Then, the extension (1) of the lowest bound orbitals are contrasted in Table I to mean interparticle distance R_o and electron thermal wavelength λ.

The r_{nl} data are plotted in order of increasing excitation (1s, 2s, 2p, 3s, etc....). The average spatial extension of higher orbitals is clearly larger than D and R_0.

lt should also be noticed that enhanced r_{nl} goes hand in hand with large orbiting time Z_{nl}, fulfilling according to the correspondence principle.

$$\zeta_{nl} \frac{Ze^2}{2\pi r_{nl}} = n\hbar \quad , \quad (4)$$

for a pure Coulombic interaction($D \rightarrow \infty$), while providing a lower bond to corresponding Debye 6_{nl} nl. We now stress the view, that electron-ion bound pairs can be seen

as electric dipoles innerly screening the Debye interaction within the biggest dipoles containing them, while simultaneously experiencing the influence of less extended dipoles included by them.

One can picture this ordering of embedded electric dipoles as an analogue to the familiar Russian puppets (Babouchkas) thus mimicking their apparently inextricable entanglement.

As a prelude to the systematics of the dipole embedding process, it is of interest to pay attention to the D-Dependence of an ion-electron dipole bound in a Debye potential. Figs. 1 a,b picture the probability of presence $r^2R^2_{nl}(r)$ of the electron around its bounding ion. $R_{nl}(r)$ denotes the usual Debey and radial wave function restric-

TABLE I

Relevant Lengths (in a_o/Z) in Dense Hydrogenic Plasma with Plasma Parameter Λ_e=0.7
(Number of Particles in Debye Sphere 0.23)

$\chi_e = 4.09 \times 10^{-5}\left(\frac{\Lambda_e}{D}\right)^{1/2}$	D	Z=1 R_o	Z=1 r_{nl}	Z=2 R_o	Z=2 r_{nl}	Z=3 R_o	Z=3 r_{nl}	Z=4 R_o	Z=4 r_{nl}	Z=5 R_o	Z=5 r_{nl}	Z=6 R_o	Z=6 r_{nl}	nl
2.86 x 10-4	4	4.556	1.577	4.555	1.577	4.554	1.577	4.554	1.577	4.553	1.577	4.553	1.577	1s
			12.370		12.582		12.718		12.813		12.883		12.937	2s
3.575 x 10-4	5	5.395	1.550	5.2557	1.550	5.176	1.550	5.124	1.555	5.088	1.555	5.061	1.555	1s
			8.6660		8.706		8.735		8.755		8.769		8.780	2s
			8.69834		9.139		9.241		9.312		9.366		9.407	2p

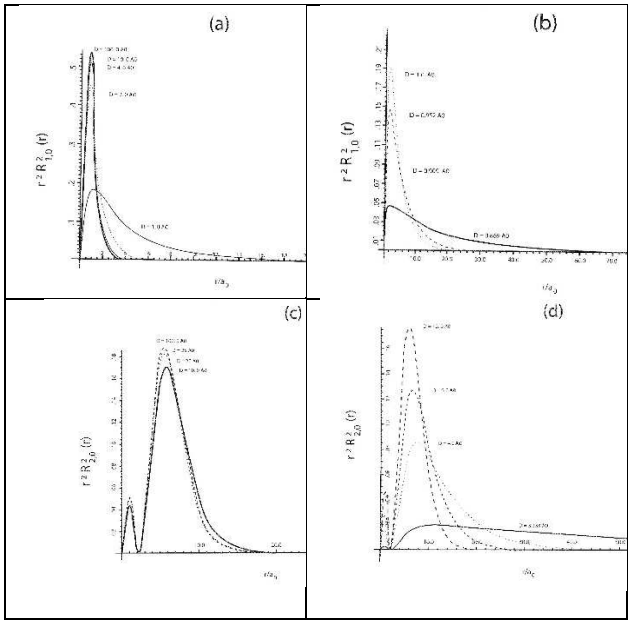

Figs. 1: Orbitals 15 and 25 in a 3-component hydrogen plasma with T = 8.62 eV and Ne= 2.24 x 10^{23} cm^{-3} ; (a) 1s with D = 100 ->1 aa, (b) 15 with D = 1 -> 0.869 a0 , (c) 25 with =100->10 aa and (d) 25 with D = 103.333 ao

ted to low-lying orbits, 1s and 2s in a pretty correlated hydrogen (Z=1) plasma with T=8.618 eV (10^5 °K) and n_e = 2.24x10^{23} cm^{-3} Corresponding Fermi temperature T_F = 13.462 eV features
a typical case of partial degeneracy- strongly coupled plasma, allowing for a vivid illustration of the progressive disappearance of bound orbitals through enhanced delocalisation when strong coupling and concommittent partial electron degeneracy increase [11].

Those pictures highlight conspicuously swift bound - free transitions of the remaining 1s and 2s bound states (Figs.1 b,d) when the screening length D decays even by a very small amount.

Delocalisation is then signalled by the rather impressive wave function flattening. Those data got derived from the classical onces.

References

[1] G.I. Ivadiotis, On the generalized formulation of Debye shielding in plasmas, Phys. Plas- mas 26, 050701, (2019)

[2] Y.L Liu and CL.Li A generalized Debye - Huckel the Theory of electrolyte solutions. AIP Advances cp 2019, 015214 (2019)

[3] R.K Janev, S. Zhang and J. Wang, Review of quantum collision dynamics in Debye plas- mas 1, 237 (2016)

[4] C.Villani, Particles systems and nonlinear Landau damping, Phys. plasmas 21, 030901 (2014)

[5] See for instance J.A.S, Linar, R, Sliva and J Santos, Plasma oscillations and nonextensive statistics, Phys.Rev. E61, 3260 (2000)

[6] H.A. Bethe and E.E.Salpeter, Quantum Mechanics of one and two-electron atoms, Roset- ta Publ, plenum Press, NY 1977

[7] V.L Berezinskii, Destruction of long-range order in 10 and 20 systems possessing a continuous symmetry group. II Quantum systems Sov.Phys. JETP34, 61O (1972)

[8] V.N Ryzhov, E.E. Tareyeva, Yu D. Fomin and E.N. Tsiok, Berezinskii - Kosterlitz - Thouless transition and D melting, Phys.USP.60,857 (2017)

[9] J.M.Kosterlitz and D.J. Thouless, Ordering, metastability and phase transitions in 20 systems,J.Phys. C6,1181(1973)

[1O] K.G.Wilson, The renomalization group and critical phenomena Rev.Mod.Phys. 55,583(1983)

[11] C.Oeutsch and M. Lavaud, Equilibrium properties of a 20 Coulomb Phys.ReV.A9,2598

Authors List

T. Abel	5	R. Doron	10
A. Ageev	14	A. Drozdovsky	25
Nafees Ahmad	34	S. Drozdovsky	25
J. Amann	29	T. Eberl	5
S. Ananiev	6	U. Eisenbarth	40
S. Aumüller	21	S. Eliezer	49
V. Bagnoud	39,40,41	A. Eychmüller	40
A. Benad	40	A,Ya. Faenov	11
L. Bernstein	41	K. Falk	5
K. Blaum	21	Quanping Fang	8,48
A. Blazevic	9, 13,40	Jianhua Feng	8,24,48
A Bogdanov	25	M. Fröhlich	3
B. F. Bohlender	17	R. Gavrilin	3,25
P. Boller	39,41	L. Geiger	1
N. Borisenko	32	D. O. Gericke	40
L. Bozyk	21	L. Giuffrida	49
C. Brabetz	9,39,40,41	J. Glorius	41
M. Bussmann	19	I.E. Golovkin	27
Leifeng Cao	8,48	A. Golubev	44
Benzheng Chen	8,24,30,48	S. A. Gorbunov	20
Rui Cheng	8,48	M. Gordimov	32
P. Christ	3	S. Götte	40
P.G.A. Cirrone	49	A. Grum-Grzhimailo	11
K. Cistakov	3	K. Gubskiy	6
Bo Cui	8	M. M. Günther	44
M. Cvejic	10	M. Gyrdymov	18
X. del Arco	29	M. Gyrdymov	44
Zhigang Deng	8,48	R. Hampf	23
A. Denker	9	V. Hannen	19
C. Deutsch	52	N. J.Hartley	40
J. Despotopulos	41	D. Hartnagel	5

J. Hellmund	41	S. Klammes	19
E. A. Henry	41	B .Klemmed	40
F. Heppner	3	R. Kodama	11
M. Hesse	5	G. Korn	47,49
P. Hilz	33	G. Kourkafas	9
M. Ho	49	E. Kozlova	32
C. Hock	3	S. Kozub	14
D.H.H. Hoffmann	24,30,48,49	J. Krasa	49
H. Hora	49	D. Kraus	40
J. Hornung	39,41	E. Kroupp	10
F. Horst	32	Th. Kühl	19,39,41
A. Hyland	1	Punit Kumar	34
M. Iberler	4, 3, 17	A. Kuznetsov	6
Y. Inubushi	11	J. A. L'huillier	29
M. Ishino	11	L. Laghchioua	3
J. Jacoby	4,3, 17, 18,32	P .Lalousis	49
J.Jeet	41	X .Le	26
A. Kalchuk	14	L. Lens	41
Wei Kang	51	A. Litvinov	41
A. Kantsyrev	25,44	Wei Liu	8,24
H. Karadas	1	B. Liu	49
E. Kashtanov	14	I. Lomonosov	16
K .Katagiri	11	J. Lütgert	40
T.Kawachi	11	Bubo Ma	8,24,48
T.Kazieva	6	X.Ma	19
F. G.Keabou	29	Zs.Major	1,39
A.Kharchenko	14	S.S. Makarov	11
A. Khurchiev	3	D. Mann	3
J. Khuyagbaatar	41	D. Margarone	49
D. Kiefer	19	Y. Maron	10
V. Kim	16	T. Matsuoka	11
J. Kirchhoff	49	W. McKenzie	49
G. Kirchhoff	49	N. Medvedev	28,45

T.A. Mehlhorn	27	Jieru Ren	8,24,30,48
M. Metternich	1	B. Rethfeld	29,43
A. Michel	17	D. Riley	1
A. Mikhaylyuk	6	S. Röder	41
D. Mikitchuk	10	O. Rosmej	3, 18,32,44
G.H Miley	49	M. Roth	5,47
V. Mintsev	16	I. Roudskoy	25
K. Miyanishi	11	H. Ruhl	33
V. Mochalova	7	A. A. Rukhadze	37
A. Müller-Münster	3	S.P. Sadykova	37
G. Naouri	52	S. Sander	5
H.Nazary	1	P. Sasorov	25
P. D. Ndione	43	S. Savin	3,25
S. Neff	13	M. Schäfer	29
P. Neumayer	1, 3, 9,41	G. Schaumann	5
D. Nikolaev	16	K.-G. Schlesinger	47
M. Nishikino	11	D.H.G. Schneider	41
N. Nissim	49	U. Schramm	19
A. Orlov	14	D. Schumacher	1,40
N. Ozaki	11	A.K. Schuster	40
V. Panyushkin	25	P. Shabalin	47
V. Pauw	33	D. Shaughnessy	41
A. Picciott	49	M. Siebold	19
T.A. Pikuz	11	Shiv Singh	34
S.A. Pikuz	11	I. Skobelev	11
V. Pirog	6	A. Skobliakov	44
Alexander Pukhov	42	M. Šmíd	5
Wei Qi	8	A. Sokolov	32
I. Rack	40	P. Spiller	19, 21
T .Radon	32	Th. Stöhlker	19,41
D. Reemts	40	M. Stoliarov	14
Lars Reichwein	42	N.A. Tahir	52
G.E. Remnev	26	K.A. Tanaka	11

Y. Tange	11	S.T .Weber	43
P. Tavana	44	Wenqing Wei	48
A. Tebartz	5	W. Wen	19
P.N. Terekhin	29,43	J. Wieser	23
Johannes Thomas	42	D. Winters	19
L. Tkachenko	14	D. Wu	30
T. Togashi	11	Xing Xu	26,48
M. E. Toimil Molares	40	M. Yabashi	11
M. Tomut	40	T. Yabuuchi	11
K. Tono	11	A. Yakushev	41
G. Torosyan	29	Zixiang Yan	51
A. Ulrich	23	Shuai Yin	8,24,26,48
A. Utkin	7	N. Zahn	32
D. Varentsov	3	S.Zähter	18
A. Vlasov	14	M. Zepf	39
K. Voigt	40	S. Zhang	26
A E. Volkov	20,28,45	M. Zhang	40
M. von der Linden	47	Yongtao Zhao	8,24,30,48
J. Vorberger	40	Xingming Zhou	8
R.A. Voronkov	45	Weimin Zhou	8
Th. Walther	19	Weimin Zhou	48
Xing Wang	8,24,48	Y. Zobus	39
Shaoyi Wang	8,48	A. Zylstra	41

List of Contributing Institutes

ANSTO
Kirrawee 2223, Australia

Beihang University
37 Xueyuan Road, Haidian District
Beijing, 100083, China

Center for Applied Physics
and Technology
Peking University, Beijing, 100871, China

ELI-Beamlines
Za Radnicí 835
252 41 Dolní Břežany, Czech Republic

ENN Science and Technology
Development Co., Ltd.
Langfang 065001, China

European Synchrotron Radiation
Facility (ESRF)
71 Avenue des Martyrs
38000 Grenoble, France

Excitech GmbH
Branterei 33, 26419 Schortens
Germany

Facility for Ion and Antiproton
Research (FAIR)
64291 Darmstadt, Germany

Fondazione Bruno Kessler,
Micro-Nano Facility,
Via Sommarive, 18
38123 Povo, Trento, Italy

Forschungszentrum Jülich
Wilhelm-Johnen-Straße
52428 Jülich, Germany

Friedrich-Schiller-Universität Jena
Inst. für Optik und Quantenelektronik
Abbe Center of Photonics
07743 Jena, Germany

GSI Helmholtzzentrum für
Schwerionenforschung GmbH
64291 rmstadt, Germany

HB11 Energy Pty. Ltd.
Freshwater, Sydney 2096, Australia

Hebei Key Laboratory of Compact Fusion
Langfang 065001, China

Heinrich-Heine-Universität Düsseldorf
Institut für Theoretische Physik I
40225 Düsseldorf, Germany

Helmholtzzentrum Berlin
Hahn-Meitner-Platz 1
14109 Berlin, Germany

Helmholtz-Zentrum
Dresden-Rossendorf e.V.
Bautzener Landstr. 4,
01328 Dresden, Germany

Helmholtz-Institut Jena
Fröbelstieg 3, 07743
Jena, Germany

Horia Hulubei National Institute for R&D
in Physics and Nuclear Engineering
Strada Reactorului 30,
Bucharest - Măgurele, Romania

IHEP – Institute for High Energy Physics,
NRC 'Kurchatov Institute",
Protvino142281, Moscow Region, Russia

INFN-Laboratori Nazionali del Sud
Via Santa Sofia, 62
95125 Catania CT, Italy

IMP - Institute of Modern Physics
Lanzhou 730000, China

Inst. Electronic Structure and Lasers,
FORTH Heraklion
Heraklion, Crete GR - 711 10, Greece

Institute of Physics,
Institute of Plasma Physics
Academy of Science,
Na Slovance 2 18221 Prague,
Czech Republic

Institute of Problems of Chemical Physics (IPCP), RAS
142432 Chernogolovka, Russia

JASRI and RIKEN Spring-8 Center
1-1-1 Kouto, Sayo-gun
Hyogo 679-5148, Japan

Joint Institute for High Temperatures, RAS
Moscow 125412, Russia

Johannes Gutenberg Universität Mainz
Fachbereich Physik, Mathematik und Informatik
Staudingerweg 7
55128 Mainz

Johann-Wolfang-Goethe-Universität
Institut für Angewandte Physik,
Frankfurt, Germany

Joint Institute of Nuclear Research
Moscow region, Joliot-Curie St. 6
141980 Dubna, Russia

Justus Liebig Universität
Ludwigstraße 23
35390 Gießen, Germany

Kansai Photon Science Institute
Kizugawa, Kyoto 619-0215, Japan

Keldysh Institute of Applied Mathematics - RAS
Moscow 125047, Russia

Laser Fusion Research Center,
Academy of Engineering Physics,
Mianyang, Sichuan, China

Lawrence Livermore National Laboratory
Livermore, CA 94550, USA

Lebedev Physical Institute, RAS
Leninskij Prospekt, 53
119991 Moscow, Russia

Leibniz-Rechenzentrum, LMU München
Boltzmannstraße 1
85748 Garching, Germany

L.P.G.P., CNRS
Université Paris Sud
91405 Orsay, France

Ludwig-Maxemilians-Universität
Fakultät für Physik
Am Coulombwall 1
85748 Garching, Germany

Marvel Fusion GmbH
Blumenstrasse 28
80331 München, Germany

Moscow Engineering Physics Institute (MEPhI), Nat. Research Nucl. Univ.
Moscow 115409, Russia

Moscow State University
Faculty of Physics
Moscow 119991, Russia

NRC “Kurchatov Institute” - ITEP
Moscow 117259, Russia

National Research Center - ‘Kurchatov Institute’,Kurchatov Sq. 1
123182 Moscow, Russia

Osaka University:
Open and Transdisciplinary Research,
Graduate School of Engineering,
Institute of Laser Engineering
2-6 Yamadaoka
Suita, Osaka 565-0871, Japan

Photonik-Zentrum Kaiserslautern e.V.
Research Center OPTIMAS
67663 Kaiserslautern, Germany

Prism Computational Sciences, Inc,
Madison, WI, 455 Science Dr. 140
Madison, WI 53711, USA

Prokhorov General Physics Institute, RAS
Vavilov st., 38 Moscow 117942, Russia

Queens University Belfast
School of Mathematics and Physics,
7-9 College Park E
Belfast BT7 1PS, UK

Skobeltsyn Institute of Nuclear Physics,
MSU, Leninskie gory, GSP-1
Moscow 119991, Russia

SOREQ - Nuclear Research Centre
81800 Yavne, Israel

Technische Universität Darmstadt
Institut für Kernphysik (IKP)
64289 Darmstadt, Germany

Technische Universität Dresden
Fakultät Physik
01062 Dresden, Germany

Technische Universität Kaiserslautern,
Fachbereich Physik und Landes-
forschungszentrum OPTIMAS
67663 Kaiserslautern, Germany

Technische Universität München,
Physik Department E12
85748 Garching, Germany

Universität Heidelberg
Institut für Physik
Im Neuenheimer Feld 226
69120 Heidelberg, Germany

University of Michigan,
Beaverton, Oregon, USA

University of Lucknow
Department of Physics
Lucknow-226007, India

University of Illinois
Dept. Nucl. Plasma & Radiol. Eng.
216 Talbot Laboratory, MC-234
04 South Wright Street
Urbana, IL 6180, USA

University of Peking
Haidian, Beijing 100871, China

University of New South Wales
Dept. of Theoretical Physics
Sydney, NSW 2052, Australia

University of Warwick
Centre for Fusion, Space- and
Astrophysics, Physics Depart.
Coventry CV4 7A1, UK

Weizmann Institute of Science
Rehovot 7610001, Israel

Westfälische Wilhelms-Universität
Münster, Schlossplatz 2
48149 Münster, Germany

Xi'an Jiaotong University
School of Science,
MOE
Xi'an, 710049, Shaanxi, China

Zhejiang University
Institute for Fusion Theory and
Simulation, Department of Physics
Hangzhou 310058, China